Investigation of deformed nuclei in Interacting Boson Models

A thesis submitted for the degree
of Doctor of Philosophy of
the Australian National University

Siu Cheung Li

May 14, 1996

The work contained in this thesis is my own original research, produced in collaboration with my supervisor – Dr S. Kuyucak. Any material taken from other references is explicitly acknowledged as such.

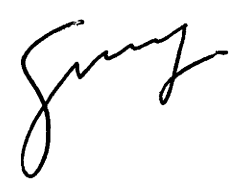

S. C. Li

Acknowledgements

I would first like to thank my supervisor, Dr S. Kuyucak, for the generous guidance and discussions that he has provided throughout the period of my research. I would also like to extend thanks to Dr B. A. Robson, and Dr W. S. Woolcock for their invaluable help and encouragement. Thanks should also go the Prof. J. F. Liu, who during his time in the department provided support which I benefited immensely. At last, I would like to express my gratitude to my wife, Clara, for her patience and support during all my painful moments, and to all members of my family, especially to my father and grandfather who passed away when I was pursuing my study in Australia.

Abstract

The *sdg* interacting boson model (IBM) is applied to the studies of high-spin states, asymmetric deformation and anharmonic effects in deformed nuclei. The previous code for numerical diagonalisation in the *sdg*-IBM has recently been modified for running on supercomputers. This modified code is used to study the accuracy of various truncation schemes employed in *sdg*-IBM calculations. The results from the study of convergence properties of some key physical quantities suggest that diagonalisation of the *sdg*-IBM Hamiltonians in a truncated model space with the maximum number of g bosons $\approx N/3$, will give a reliable description of the low-lying states. For the study of high-spin states, the $1/N$ expansion solutions for the ground, γ- and $\gamma\gamma$-bands in the interacting boson models are extended to higher orders by using computer algebra. The analytic results are compared with those obtained from an exact diagonalisation of the Hamiltonian and are shown to be very accurate. The extended formulae are used for systematic studies of high-spin states in the *sd* and *sdg* boson models with emphasis on the spin dependence of the moment of inertia and $E2$ transitions. It is found that the d-boson energy plays a crucial role in description of the high-order terms in the moment of inertia. The results are applied to the study of nuclei in both deformed and superdeformed regions, where the need for the g bosons is especially acute. An investigation on the triaxiality and anharmonicity is carried out by using the Hamiltonian with parametrisation adopted for the deformed nuclei. The γ-degree of freedom in the *sdg*-IBM, which serves as a measure of asymmetric deformation, is generated by the $O(5)\oplus O(9)$ transformation. The results indicate that there is no stable triaxial shape for the ground band, and the $E_{\gamma\gamma}/E_{\gamma}$ ratio ranges only from 1.9 to 2.2.

Contents

CHAPTER 1

Introduction

1.1 Review of the interacting boson model (IBM)

The description of a wide variety of collective phenomena exhibited by atomic nuclei is one of the most challenging problems in nuclear physics. Since the inception of the interacting boson model [1] (IBM), a new paradigm in treating many-body nuclear systems has been created. The IBM, which serves as a bridge between the shell model [2, 3] and the geometrical model [4], has been drawing a great deal of attention for more than two decades. The idea of describing collective phenomena in nuclear physics by means of spectrum-generating algebra dates back to the late 50's. The first algebraic model in nuclear structure was the SU(3) model proposed in 1958 by J. P. Elliott [5–7]. This model was used to demonstrate how collective features, such as rotational bands, could be obtained from an independent-particle shell model treatment. Within the framework of such a model, an additional two-body interaction of the quadrupole type is added to the single-particle harmonic oscillator well to remove some of the degeneracy. The SU(3) classification is useful in shell-model calculations where the residual interaction is reasonably well represented by a quadrupole force and the remaining portion of the residual interaction can be treated as a perturbation. Thus its applicability is limited to the *sd*-shell region where the SU(3) symmetry is still approximately preserved. In shells which are well above the *sd* region the symmetry is strongly broken by the spin-orbit interaction, so that extensions and refinements of the model are needed [8–13].

In the 70's, an attempt to unify the description of the various aspects of the

collective nuclear properties of medium and heavy even-even nuclei was made by Iachello and Arima [14]. Their model was known as the Interacting Boson Model. The idea was to replace the large number of single-particle fermion degrees of freedom by a few collective boson degrees of freedom [15]. Due to the strong interaction between pairs of protons (and neutrons), these bosons are supposed to be correlated fermion pairs outside of the closed shells. In the simplest version of the model, particles or holes in the valence shell are coupled together forming pairs with angular momentum $L = 0$ denoted by a scalar boson, s, and with angular momentum $L = 2$ denoted by a five-component quadrupole boson, d_μ. The counting of bosons is done with respect to the nearest closed shell, i.e. the number of bosons is considered as the number of particle pairs if less than half of the shell is filled, and as the number of hole pairs otherwise. Such a rule of counting stems from the Pauli principle and hence the fermionic origins of the collective bosons [16]. These boson states when expressed in second quantized form, generate a set of creation and annihilation operators. With the restriction that the number of bosons in the nuclear system is conserved, the 36 bilinear products of the operators form a closed algebra of the compact U(6) group, i.e. the unitary Lie group in 6 dimensions. As a consequence, many of the characteristic features of the IBM can be derived analytically by group-theoretical methods. Perhaps the most elegant feature of the model is its richness in group structure. There are three dynamical symmetries when different group reduction schemes of U(6) are employed. These symmetry limits are known as U(5), SU(3) and O(6), which have their geometrical realisations as the spherical vibrator, deformed rotor and γ-unstable deformed rotor, respectively [1]. The algebraic Hamiltonian governing the interaction between bosons consists of only one- and two-body terms which conserve both the total number of bosons and rotational invariance. To simplify calculation and to gain more physical insight on the choice of Hamiltonian, a popular parametrisation known as the consistent Q formalism (CQF) has been introduced by Warner and Casten [17]. With this simple choice of parameters, one can have a clear picture of the phase transitions between the symmetry limits. A more detailed discussion on the choice of Hamiltonian will be

presented in Chapter 2.

1.2 Connection of IBM with other models

The interacting boson model as written in second quantized algebraic language is rather abstract and does not possess an immediate physical picture associated with it as does the Bohr-Mottelson model [4]. The three dynamical symmetry limits do provide some sort of geometrical insight into the model, however they are broken strongly in most nuclei of interest and thus are not very illuminating. To obtain physical intuition in algebraic models is crucial, especially when one wants to search for criteria and guidance in modelling the Hamiltonian. This shortcoming has been overcome by the geometrical realisations of the IBM and its extensions through either classical analysis [18] or the intrinsic state formalism [1, 19–24]. In fact, it has been shown that the interacting boson model basically can be regarded as the algebraic representation [20] or second quantization of the geometrical model, and their key difference mainly stems from the finiteness of boson number in the IBM.

The intrinsic state for the ground state can be interpreted as a condensate of N intrinsic bosons [20],

$$|N, \alpha_\mu\rangle = (s^\dagger + \sum_\mu \alpha_\mu d^\dagger_\mu)^N |0\rangle, \tag{1.1}$$

where $\alpha_\mu (\mu = \pm 2, \pm 1, 0)$ are the five classical (collective) complex mean-fields which bear similarity with the variables in the geometrical model. For static problems, due to the symmetries of the system [25], those complex mean-fields can be reduced to two real variables β and γ which relate to the quadrupole deformation and triaxiality of the system respectively. The intrinsic state now takes the form [20]

$$|N, \beta, \gamma\rangle = [s^\dagger + \beta \cos\gamma d^\dagger_0 + \frac{1}{\sqrt{2}} \beta \sin\gamma (d^\dagger_2 + d^\dagger_{-2})]^N |0\rangle. \tag{1.2}$$

Alternatively, the γ degree of freedom can be generated by performing an appropriate O(5) transformation on the axially symmetric ground state of the boson system. This technique can be generalised easily to a system of bosons with higher spins and a detailed discussion of that will be presented in Chapter 6. One of the salient features of the intrinsic state is its over-completeness [20]. As a consequence, the

use of variational calculus to derive physical quantities becomes viable. In fact, the intrinsic state formalism forms the basis for performing the $1/N$ expansion [26] for the matrix elements of various observables.

Over the years, considerable effort has been devoted to linking the boson models microscopically with the shell model which is regarded as the fundamental model in nuclear structure. In fact, the interplay between single-particle and collective degrees of freedom is one of the most intriguing problems in many-body systems. However, the mapping of many-fermion systems to bosonic ones had already been known long before the introduction of IBM [27]. The gist of most of the boson realisation schemes is to find a smaller boson space with a manageable size, and a set of boson images of the Hamiltonian and transition operators in the boson system that can reproduce the basic low-energy dynamics of the original fermion system. In most of such studies, the first step is to identify and restrict the fermion space that can capture the essential physics of the many-body system. The construction of the fermion space is based upon the residual nucleon-nucleon interaction adopted. One of the most popular approaches which emphasises the pairing-type interaction between identical nucleons was proposed by Otsuka, Arima and Iachello [28] and is widely known as the OAI mapping. In this approach, the fermion space, which is constructed from the generalised seniority scheme, is truncated by keeping only the correlated fermion S and D pairs with angular momentum $L = 0$ and $L = 2$ respectively. This spherical basis works well with nuclei near closed shells. In general, the fermion-pair operators constructed in this way, do not form a closed algebra under commutation in the truncated space. In this case, the boson realisation can be done by mapping the s and d bosons with the corresponding S and D fermion pairs and insisting that the matrix elements of boson operators reproduce exactly the matrix elements of their fermion counterparts. Since no quasiparticle transformation is involved, the boson number N is conserved and can be identified as the number of valence correlated nucleon pairs. The above mapping technique has the virtue that it preserves the effects of the Pauli principle in the boson system. For deformed nuclei, one can adopt a deformed basis to maximise the long range two-body quadrupole interaction. In

this case, the fermion space is constructed from the scheme based on the Nilsson + BCS model with particle number projection [29]. There are many other approaches which differ in their truncation schemes adopted for the fermion or boson space and also their ways of mapping between them. Although there has been considerable success in establishing the microscopic foundation of the interacting boson model, further work is required for a fully self-consistent microscopic derivation.

1.3 Inadequacy of IBM

The interacting boson model has been shown to be a powerful tool in providing a systematic description of the properties of even-even nuclei and a uniform treatment of low-lying band structures over extended mass regions [16]. Despite its simplicity and success, extension of the standard *sd*-model is necessary. The shortcomings of the model are most apparent in the deformed rare-earth region where both microscopics [30] and phenomenology indicate that the pair truncation to the *sd* space is too severe. Here we briefly summarise some of its inadequacies.

i) Premature falloff in B($E2$) strengths: Due to the finiteness of boson number in the system, the *sd*-model predicts that the ground band terminates at $L = 2N$ and a reduction in collectivity is expected in high-spin states. As a result, the yrast B($E2$) values are expected to fall off relative to rotor values and vanish at maximum spin. However, some remarkable data were provided recently in the actinide region where the energy levels and B($E2$) of the ground band were measured up to spin $L = 30$, 28 and 30 for ^{232}Th, ^{234}U, and ^{236}U (see Chapter 5), respectively, without any sign of boson cut-off effect (^{232}Th, ^{234}U, and ^{236}U have $N = 12$, 13 and 14 bosons, hence the ground band are expected to terminate at $L = 24$, 26 and 28 respectively in the *sd*-model).

ii) Inadequacy in the descriptions of hexadecapole band structures: The existence of the 3^+ and 4^+ vibrational bands [31–34] in many nuclear spectra and the strong $E4$ excitations of 4^+ states provide a distinct signature that they are hexadecapole phonon excitations. These hexadecapole bands clearly lie beyond the *sd* model space. Furthermore, the $E4(0_1^+ \rightarrow 4^+)$ transition strengths for some nuclei obtained

from electron and proton scattering experiments [35–40], are comparable with the in-band $E4$ strength of the ground band. The hexadecapole operator given in the *sd*-IBM is certainly not flexible enough to account for the experimental data [41].
iii) Ground band moment of inertia problem: As criticised by Bohr and Mottelson, the model fails to account for the spin-dependent terms in the energy [42]. The $L \cdot L$ term in the Hamiltonian, which accounts for most of the missing moment of inertia, does not have any dynamical content. In addition, this term is not flexible enough to describe high-spin data. As most deformed nuclei deviate very much from the rigid rotor, the $L \cdot L$ term is inadequate to reproduce the higher-order terms in the $L(L+1)$ expansion of the moment of inertia. Recently, a Hamiltonian with a more general spin-dependence has been introduced [43]. Within this Hamiltonian, a spin-dependent coefficient, $1/(1 + fL \cdot L)$, has been included in the dipole and quadrupole interactions. Although this denominator form of coupling constant does ameliorate the situation, it is physically not easy to comprehend.
iv) Absence of stable triaxial shapes: Since some nuclei have long been thought to have triaxial shapes [16], the incapability of modelling a stable triaxial shape in the standard *sd*-IBM has raised concern. To obtain leading order triaxial shapes, one can introduce symmetry-breaking cubic terms [44–46] into the Hamiltonian. Though such terms can be motivated as effective interactions generated from the renormalisation of higher spin bosons, they were chosen in an ad-hoc fashion. It is therefore more appealing to study directly the effect of higher spin bosons on shape deformations.
v) Absence of large anharmonic effects: The *sd*-IBM is inadequate for accommodating the large anharmonicities (ranging from 1.5 to 2.5) which are claimed to be observed in some proposed double-γ bands. A clue offered by recent geometrical model calculations, suggests that anharmonicity may be linked with triaxiality which is beyond the scope of the standard *sd*-model. On the other hand, there have been arguments that some of the observed 4^+ bands are in fact of hexadecapole character [32]. Thus there is a need for an extended model which can treat both the quadrupole double-phonon and hexadecapole bands on an equal footing.

1.4 Hexadecapole degree of freedom in IBM

The first two points mentioned in the Section 1.3 are kinematical in origin and can be attributed to the lack of collectivity in the *sd*-model caused by the severe truncation of the model space. It can be ameliorated by simply including the g bosons, thus the cut-off spin is changed from $2N$ to $4N$ and all falloffs in B$E(2)$ are pushed to higher spins. In addition, more phonon bands such as β', γ', 1^+, 3^+ and 4^+ emerge from the SU(3) representations, providing a proper framework for describing hexadecapole band structures. From the microscopic point of view, the original truncation to the *sd* space was motivated by the fact that these pairs come lowest in energy in a shell-model calculation. However, according to the microscopic studies carried out in the past decade, there are strong reasons favouring the inclusion of g bosons. It has been found that the inclusion of G-pairs is necessary and sufficient [47] for a proper description of physical observables such as binding energies. Similar studies carried out by using the deformed basis [48–50], concluded that the S and D pairs alone cannot exhaust the intrinsic wavefunctions and the effects of G pairs must be included explicitly, at least for the treatment of high-spin states. Thus, microscopic analysis has established a solid foundation for pursuing the *sdg*-IBM.

In regard to the ground band moment of inertia problem, there have been conjectures [42] that the spin-dependence of excitation energies may be attributed to the g-boson effects. In addition, the hexadecapole degree of freedom in the *sdg*-IBM, provides a better way of modelling triaxial shapes in nuclei. In comparison with the cubic three-body interaction mentioned in Section 1.3, the hexadecapole two-body force is physically more appealing. Recently, it has been shown that with appropriately chosen two-body quadrupole and hexadecapole interactions, one can generate an asymmetric energy surface which is γ-soft [25]. Such a Hamiltonian is useful in the description of triaxiality in transitional nuclei. It will be interesting to see whether the hexadecapole interaction can produce a similar effect on deformed nuclei. Furthermore, regarding the issue of anharmonicity in deformed nuclei, the *sdg*-IBM provides a unified approach to the study of both the $\gamma\gamma$- and the hexadecapole, 4^+ bands. Thus, in the light of phenomenological and microscopic studies,

the *sdg*-IBM should provide a more complete picture of nuclear collective behaviour.

1.5 Solution techniques in boson models

The *sdg*-IBM does not share many of the simplifying features of the *sd*-IBM which made the latter so popular over the last two decades. First of all, the representations in some symmetry limits of the dynamical group U(15) are not associated with actual spectra. For instance, the ground bands of the SU(5), SU(6) and O(15) limits of the parent group U(15) have the spin sequence (0, 4, 8,..) which cannot be used in nuclear spectroscopy. In addition, due to the large basis space, exact numerical diagonalisation of the *sdg*-IBM Hamiltonians is not possible for most deformed nuclei. As a result, progress with *sdg*-IBM calculations has been rather slow, and due to the various truncation schemes involved, a satisfactory description of both low-lying band structures and high-spin states in deformed nuclei is still missing. Here we summarise and comment on some of the techniques used in the literature.

Numerical approaches

(i) Truncation in the SU(3) basis: In this method, the model space is truncated to low-lying SU(3) representations with a Hamiltonian consisting of various SU(3) tensor operators. The matrix elements are evaluated through group theoretical techniques and the Hamiltonian is diagonalised in the truncated space. This scheme has been successfully applied to ^{168}Er [51]. However, this choice of Hamiltonian does not share the usual physical picture associated with the CQF quadrupole Hamiltonian.

(ii) Coupling of one g boson to the *sd*-core ($n_g \leq 1$): The diagonalisation of the Hamiltonian is carried in the basis space with configurations, $\{(sd)^N, (sd)^{N-1}g\}$. This approach was motivated by the fact that the use of a large g-boson energy can induce only a small expectation value for the g-boson number ($\langle n_g \rangle \ll 1$). However, with such large ε_g, the applicability of this approximation scheme is limited to those nuclei where the coupling between the g and sd bosons is relatively weak. The situation gets even worse in the case of superdeformed nuclei where recent studies suggest that the g bosons are strongly coupled to the *sd*-core [52–55]. Furthermore, with $n_g \leq 1$, the truncated space is unable to describe accurately the high-spin data

in deformed nuclei.

(iii) Coupling of $n_{g\,\max}$ g bosons ($n_g \leq n_{g\,\max}$): The configuration space is extended to include up to $n_{g\,\max}$ g bosons, and for which a new computer code, *super*-SDGBOSON [56] has been developed. This scheme can alleviate the situation mentioned above. However, due to the basis space involved, numerical diagonalisation is still not possible for $N > 14$.

Analytic approaches

(iv) SU(3) limit: For deformed nuclei, the SU(3) symmetry in the *sdg*-IBM is strongly broken by both the large g-boson energy, ε_g and the quadrupole interaction with a q-scaling factor (refer to Chapter 2) ranging from $0.5 - 0.7$. Therefore, the group-theoretical approach [57,58] serves to provide a qualitative picture of nuclear spectra only.

v) Hartree-Bose and Tamm-Dancoff approximations [59]: Using this approximation, only the leading order results in N for the ground and single-phonon band energies are evaluated. Therefore, they only provide qualitative descriptions of low-lying band structures and are not accurate enough for the analysis of experimental data.

vi) $1/N$ expansion [26]: This technique is based on the angular momentum projected mean field theory. It gives an accurate extrapolation from the SU(3) limit, and presumably provides a feasible alternative for a realistic description of high-spin states in the *sdg*-IBM. With the recent development in computer algebra, the task of evaluating the matrix elements up to the order $1/N^6$ [60], which is crucial for accurate descriptions of high-spin states [60–62], has been completed. However, beyond the single-phonon bands, the evaluation of band-mixing effects becomes very complicated.

1.6 Outline of the thesis

This thesis is divided into seven chapters. In Chapter 2, the consistent Q formalism in the *sd*-model and its extensions to the *sdg*-IBM are discussed. In addition, various parametrisation schemes for the *sdg*-Hamiltonian are presented. In Chapter 3, the recent developments in numerical diagonalisation and the reliabil-

ity of various truncation schemes for the *sdg*-model space are discussed. Chapter 4 presents the $1/N$ formalism for both the ground and γ-bands. In Chapter 5, systematic studies on the predictions of the *sd*- and *sdg*-models are reported. In the light of the $1/N$ formulae, the moment of inertia problem is addressed. In particular, the effects of one-body energies on the spin-dependence of moment of inertia are discussed. Furthermore, the $1/N$ results are applied to the study of high-spin states in deformed and superdeformed nuclei. In Chapter 6, the possibility of generating stable triaxial shapes and large anharmonic effects in deformed nuclei is explored. Finally, Chapter 7 contains the summary and conclusion of the whole investigation.

CHAPTER 2

Choice of Hamiltonian

2.1 Hamiltonian for the *sd*-model

In the *sd*-IBM, the Hamiltonian can generally be expressed as combinations of the creation and annihilation operators, $s, s^\dagger, d_\mu$, and $d^\dagger_\mu$ under the condition that both the rotational invariance and hermiticity are to be preserved. To reduce the complexity, one can limit the Hamiltonian to one consisting of only one- and two-body interactions so that it also conserves the total number of bosons. With these constraints, a general Hamiltonian consisting of six free parameters, can be written in the form of a multipole expansion,

$$H = \varepsilon_d \hat{n}_d + \kappa_1 L \cdot L - \kappa_2 Q \cdot Q - \kappa_3 T_3 \cdot T_3 - \kappa_4 T_4 \cdot T_4, \tag{2.1}$$

where

$$\begin{aligned} &\hat{n}_d = d^\dagger \cdot \tilde{d} = \sum_\mu d^\dagger_\mu d_\mu, \qquad && L_\mu = \sqrt{10}[d^\dagger \times \tilde{d}]^1_\mu, \\ &Q_\mu = [s^\dagger \times \tilde{d} + d^\dagger \times \tilde{s}]^2_\mu + \chi[d^\dagger \times \tilde{d}]^2_\mu, \\ &T_{3\mu} = [d^\dagger \times \tilde{d}]^3_\mu, && T_{4\mu} = [d^\dagger \times \tilde{d}]^4_\mu, \end{aligned} \tag{2.2}$$

and

$$\tilde{s} = s, \qquad \tilde{d}_\mu = (-1)^\mu d_{-\mu}. \tag{2.3}$$

The tensor and scalar products of two irreducible tensor operators are defined as

$$[T_j \times T_l]^k_\mu = \sum_{m_j m_l} \langle j m_j l m_l | k \mu \rangle T_{j m_j} T_{l m_l}, \tag{2.4}$$

and

$$T_k \cdot U_k = \sum_{\mu}(-1)^{\mu} T_{k\mu} U_{k-\mu}. \tag{2.5}$$

The $L \cdot L$ term in eq. (2.1) is always diagonal and simply gives a contribution to the rigid moment of inertia. In other word, it has no effect on state wavefunctions and therefore has no dynamical content. The $T_3 \cdot T_3$ is a Casimir operator common to both the U(5) and O(6) group chains. In most applications, it has been found

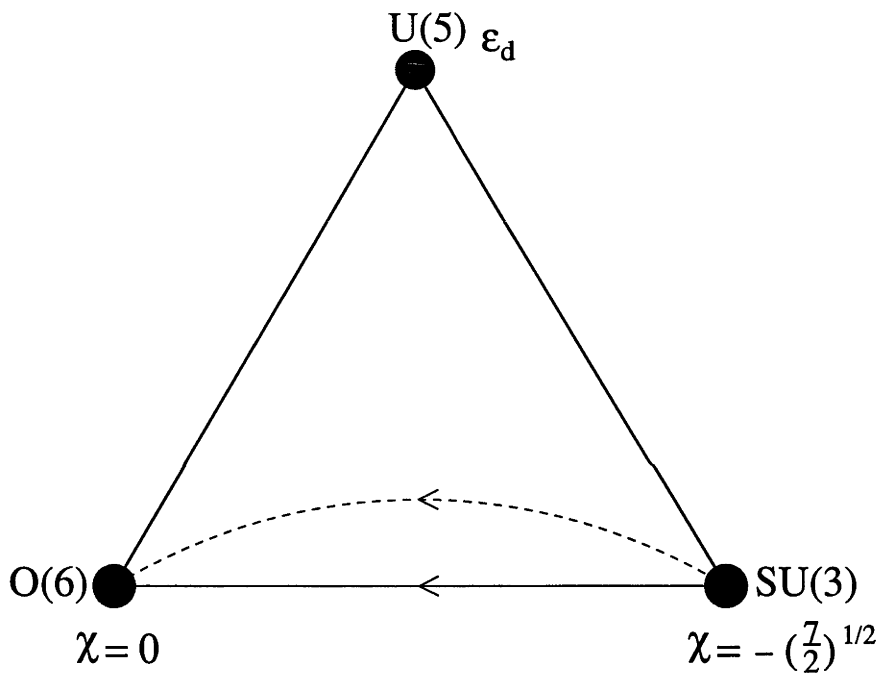

Figure 2.1: Symmetry triangle of the IBM indicating the three symmetry limits on each of the vertices and the transition legs between symmetries. ε_d and χ are defined in the text. The dotted line represents a deformed edge with a finite d-boson energy.

that usually one or two terms in the multipole expansion suffice to get a good description of the low-lying collective properties. For example, in deformed nuclei, the quadrupole force plays a dominant role. Therefore, in realistic calculation, the Hamiltonian can be simplified as

$$H = \varepsilon_d \hat{n}_d + \kappa_1 L \cdot L - \kappa_2 Q \cdot Q. \tag{2.6}$$

For consistency, the same quadrupole operator is used in the $E2$ transition operator, i.e. $T(E2) = e_2 Q$, as in the Hamiltonian, where e_2 is the effective charge. The above choice of parametrisation (with $\varepsilon_d = 0$) is known as the consistent-Q formalism (CQF) [16]. At zero ε_d, χ serves as a free parameter which reproduces the SU(3) and O(6) symmetries when $\chi = -\sqrt{7}/2$ and 0 respectively. In reality, most of the nuclei have spectra showing behaviour deviating from the three symmetry limits. In terms of the Casten triangle (Figure 2.1), the canonical way of breaking the symmetries is to move along the three edges of the triangle. In the description of high-spin states in deformed nuclei (discussed in Chapter 5), one needs to employ the d-boson energy to solve the moment of inertia problem. In this case, one needs to break the symmetry by proceeding along a deformed edge as shown in Figure 2.1. Of course, a more complete description of deformed nuclei, including high-spin states and hexadecapole bands, requires extension of the model space to the *sdg* bosons.

2.2 Hamiltonian for the *sdg*-IBM

A minimal extension of the CQF Hamiltonian, to the *sdg*-IBM can be achieved by including the g-boson energy term, $\varepsilon_g \hat{n}_g$, and modifying the quadrupole operator eq. (2.2) to the form

$$Q_\mu = [s^\dagger \tilde{d} + d^\dagger \tilde{s}]^{(2)}_\mu + q_{22}[d^\dagger \tilde{d}]^{(2)}_\mu + q_{24}[d^\dagger \tilde{g} + g^\dagger \tilde{d}]^{(2)}_\mu + q_{44}[g^\dagger \tilde{g}]^{(2)}_\mu. \tag{2.7}$$

As a result, we have

$$H = \epsilon_g \hat{n}_g - \kappa_2 Q \cdot Q. \tag{2.8}$$

We shall refer to this minimal extension as the CQF hamiltonian below. A study of high-spin states in the *sdg*-IBM using the CQF Hamiltonian, which will be presented in Chapter 5, indicates that the energy surface remains too rigid and inclusion of the d-boson energy term, $\varepsilon_d \hat{n}_d$, is essential to reproduce the spin dependence of the moment of inertia and of the $E2$ transitions in the ground band [60]. The success of this pairing plus quadrupole type of Hamiltonian, however, does not extend to the side bands which are more sensitive to interference from the hexadecapole interaction. Thus, for a comprehensive description of deformed nuclei, one needs to

employ the Hamiltonian

$$H = \varepsilon_d \hat{n}_d + \epsilon_g \hat{n}_g - \kappa_2 Q \cdot Q - \kappa_4 T_4 \cdot T_4, \tag{2.9}$$

where the hexadecapole operator is given by

$$T_{4\mu} = [s^\dagger \tilde{g} + g^\dagger \tilde{s}]^{(4)}_\mu + h_{22}[d^\dagger \tilde{d}]^{(4)}_\mu + h_{24}[d^\dagger \tilde{g} + g^\dagger \tilde{d}]^{(4)}_\mu + h_{44}[g^\dagger \tilde{g}]^{(4)}_\mu. \tag{2.10}$$

Note that, we have deliberately left out the dipole interaction in eq. (2.8) as it is found to be at the root of the rigid moment of inertia problem in the IBM. This Hamiltonian contains 10 parameters, namely, the one-body energies ε_d and ε_g, the multipole interaction strengths κ_2 and κ_4, and the quadrupole and hexadecapole parameters q_{jl} and h_{jl}. In a systematic study covering many nuclei, it is desirable to have a smaller set of free parameters. To achieve this goal, we adopt a similar strategy as in a previous study of deformed nuclei [63]. The quadrupole parameters $\{q_{22}, q_{24}, q_{44}\}$ are scaled from their SU(3) values with a single factor q as suggested by microscopics [28] in which the relevant fermion single-particle orbits are mapped onto an equivalent single shell. In short, q_{jl} can be written as

$$(q_{22}, q_{24}, q_{44}) = (q, q, q) \times \mathrm{SU(3)}, \tag{2.11}$$

where the SU(3) values of q_{22}, q_{24} and q_{44} are $-11\sqrt{10}/28$, $9/7$ and $-3\sqrt{55}/14$, respectively [64]. Alternatively, one can scale q_{jl} as

$$(q_{22}, q_{24}, q_{44}) = (q, 1, q) \times \mathrm{SU(3)}. \tag{2.12}$$

This scaling has been used in previous studies of deformed nuclei [63]. The hexadecapole parameters, h_{jl}, can be determined by a similar scaling strategy or mapped from the quadrupole parameters, q_{jl} [63]. The former refers to using the same quadrupole scaling factor for the SU(3) hexadecapole operator which is transformed according to the $(\lambda, \mu) = (2, 2)$ irreducible representation. The corresponding SU(3) values for h_{22}, h_{24} and h_{44} are $19\sqrt{5}/28$, $-5\sqrt{11}/14$ and $3\sqrt{143}/28$ respectively [64]. The second way is to determine the hexadecapole parameters h_{jl} from those of q_{jl} by imposing some conditions on the multipole operators. To obtain the leading order

solution of the $1/N$ expansion for any two-body multipole interaction is equivalent to solving the eigen-mode condition, namely

$$[Q_0, b^\dagger] = \lambda b^\dagger, \qquad [T_{40}, b'^\dagger] = \lambda' b'^\dagger, \tag{2.13}$$

where λ, λ' are the eigenvalues, and $b^\dagger|0\rangle, b'^\dagger|0\rangle$ can be interpreted as the eigenstates of the quadrupole and hexadecapole operators, respectively. The sought after condition will be more apparent when the above relations are expressed as

$$\sum_l \bar{q}_{jl} x_j = \lambda x_l, \qquad \sum_l \bar{h}_{jl} x'_j = \lambda' x'_l, \tag{2.14}$$

where $\bar{q}_{jl} = \langle j0l0|20\rangle q_{jl}$ and $\bar{h}_{jl} = \langle j0l0|40\rangle h_{jl}$. To determine h_{jl} from q_{jl}, one can simply impose the condition that $x_j = x'_j$. In this case, the quadrupole and hexadecapole operators share the same eigenstates. Such a condition can be incorporated in a simple commutation relation, $[\bar{\mathbf{h}}, \bar{\mathbf{q}}] = 0$ [63], where $\bar{\mathbf{q}}$ and $\bar{\mathbf{h}}$ are the two symmetric matrices,

$$\bar{\mathbf{q}} = \begin{pmatrix} 0 & 1 & 0 \\ 1 & \bar{q}_{22} & \bar{q}_{24} \\ 0 & \bar{q}_{42} & \bar{q}_{44} \end{pmatrix}, \qquad \bar{\mathbf{h}} = \begin{pmatrix} 0 & 0 & 1 \\ 0 & \bar{h}_{22} & \bar{h}_{24} \\ 1 & \bar{h}_{42} & \bar{h}_{44} \end{pmatrix}. \tag{2.15}$$

This commutation relation ensures that the quadrupole and the hexadecapole mean fields are coherent. Thus it leads to a set of three linear equations, giving the prescription for h_{jl} as

$$\bar{h}_{22} = \bar{q}_{24}, \;\; \bar{h}_{24} = \bar{q}_{44}, \;\; \bar{h}_{44} = \bar{q}_{24} + (\bar{q}_{44}^2 - \bar{q}_{22}\bar{q}_{44} - 1)/\bar{q}_{24} \,. \tag{2.16}$$

This reduction of parameters from 10 to 5 is obtained at the expense of a detailed description of the quadrupole and hexadecapole operators. Since information, especially on the latter, is rather patchy, this will not cause any problems except in a few isolated cases. The four choices of parametrisations for the quadrupole and hexadecapole interactions can be summarised as

P(1): $(q,q,q)\times$SU(3) for Q with T_4 mapped by eq. (2.16),

P(2): $(q,1,q)\times$SU(3) with T_4 mapped by eq. (2.16),

P(3): $(q,q,q)\times$SU(3) for both Q and T_4,

P(4): $(q,1,q)\times$SU(3) for both Q and T_4.

In the calculation of $E2$ and $E4$ transitions, we shall use the consistent operators, $\mathrm{T}(E2) = e_2 Q$, $\mathrm{T}(E4) = e_4 T_4$, so that, apart from the effective charges e_2 and e_4, no new parameters are introduced.

In concluding this section, we present an alternative parametrisation of the Hamiltonian eq. (2.9) which is more convenient in the implementation of the $1/N$ expansion formulas. In regard to the leading order in $1/N$ expansion, the matrix elements of the one- and two-body interactions are proportional to N^2 and N respectively. This involves factoring out the energy scale and the leading order N dependence from the energy expressions. Since the quadrupole interaction is dominant, it is desirable to factor out the energy scale, κ_2, and the leading order N^2 dependence from the energy expressions. A suitable choice for such a set of dimensionless parameters is given by

$$\eta_l = \varepsilon_l / N\kappa_2, \quad \zeta_4 = \kappa_4/\kappa_2, \tag{2.17}$$

where $l = 0, 2, 4$ correspond to the subscripts s, d, g.

CHAPTER 3

Exact diagonalisation technique

As mentioned earlier, there is an extensive set of experimental data indicating the necessity of including the g-boson degree of freedom in IBM calculations. With this extension of the model space, diagonalisation becomes a formidable task. A computer code which can diagonalise arbitrary *sdg*-IBM Hamiltonians in full space has been available for some time [65], but due to excessive memory requirements it had only limited applications to transitional nuclei [66] which have $N \leq 10$. Recently this code has been modified to run on supercomputers improving its applicability [56]. Nevertheless, exact diagonalisation for deformed nuclei with boson number greater than ten remains elusive, and truncation of the model space is still necessary. In the following sections, recent developments in numerical diagonalisation and the effects of various truncation schemes on the computation of physical quantities will be discussed.

3.1 Basis states

One of the attractive features of the *sd*-IBM is its simplicity, namely that the model space is relatively small in size so that the model Hamiltonian can be diagonalised exactly. For example, in Table 3.1, it is shown that for most nuclei, the number of basis states with this model is less than a thousand. However, with introduction of the g-boson degree of freedom, the enormous growth in size of the model space becomes an intriguing problem. As seen in Table 3.1, the number of states in the *sd*-model grows at a rate of N^3 while that in the *sdg*-model grows at a rate of N^8. The number of basis states that can be handled by supercomputers such as

the VP2200 at ANU is about 10^5. Therefore, to make the problem tractable, various approximation schemes have been devised, such as the truncation of the model space by restricting the maximum number of g bosons to one [67–69]. As seen from Table 3.1, the basis size is remarkably reduced by this truncation. However, such a severe truncation creates problems of convergence in some physical observables; a problem which will be addressed in Section 3.3.

Table 3.1: The variation of number of states with the number of bosons. The first row ($n_{g\,\mathrm{max}} = 0$) and the last row ($n_{g\,\mathrm{max}} = N$) show the the full basis sizes in the *sd*- and *sdg*- models respectively.

	The number of states with $M = 0$				
$n_{g\,\mathrm{max}}$	$N = 8$	10	12	14	16
0	105	203	358	588	915
1	633	1353	2254	4410	7123
2	2.08×10^3	4.91×10^3	9.94×10^3	1.81×10^4	3.03×10^4
4	8.37×10^3	2.49×10^4	5.92×10^4	1.21×10^5	2.23×10^5
6	1.53×10^4	5.89×10^4	1.69×10^5	3.98×10^5	8.13×10^5
N	1.75×10^4	9.21×10^4	3.99×10^5	1.48×10^6	4.86×10^6

To facilitate the algebraic manipulation of matrix elements, the m-scheme [70] is adopted in the following investigation. By choosing those states with zero magnetic quantum number, M, this scheme can be used to eliminate all the degeneracy due to rotational invariance. In addition, the m-scheme can be used to generate states with particular spins. For example, by setting M to the desired spin L, one can construct a basis containing states with spins higher than or equal to L.

Before devoting effort to the study of diagonalising large matrices, it is worth discussing some techniques in storing basis states during computation. In a fermion system, each state constructed from the m-scheme can be specified conveniently by the bit pattern of an integer [71] and all the annihilation and creation operations can be reduced to simple bit-wise operations between integers. Similarly, with a slight modification, one can specify each state of our boson system by a simple bit pattern [65], i.e. all the information concerning the distribution of N bosons among

n quantum states is 'packed' in a 4-byte integer. In the *sdg*-IBM, this 32-bit (or 4-byte) representation (see Appendix A) can accommodate a maximum of 18 bosons which is sufficient for the study of deformed nuclei. Starting with a condensate of N s-bosons, $|(s)^N\rangle$, all the other states can be generated by just shifting the bosons successively to the d- and g-orbitals, thus the integers associated with the basis states are automatically arranged in descending order. This kind of ordering is of crucial importance if searching techniques such as binary search are to be employed in the identification of states. However, in this 32-bit representation, the manipulations of creation and annihilation operators with basis states cannot be performed in a simple bit-wise fashion as in the case of fermion systems. To evaluate the matrix elements, it is necessary to 'unpack' the integer into 15 occupation numbers for the algebraic operations, and after that the numbers are to be repacked again [65]. The 'packing' and 'unpacking' procedures consume a large fraction of CPU time during each calculation. To overcome this difficulty, a less compact 64-bit representation (see Appendix A) has been devised and written in a vectorised form for the supercomputer VP2200 [56] without the need to carry out these 'packing' and 'unpacking' procedures. In this modified code, instead of employing the inherently 'unvectorisable' binary search algorithm which makes use of the numeric ordering of the basis states, a two-dimensional map is constructed to locate each basis state. The number of operations required in the latter method is independent of the size of the basis, and far fewer than that of the binary search technique (at most, $n + 1$ steps are needed for 2^n states). This kind of mapping technique increases substantially the percentage of vectorisation and improves the efficiency of the code.

3.2 Sparse matrix technique

Here we discuss some techniques in exact numerical diagonalisation. In fact, the use of the term 'exact diagonalisation' in the *sdg*-IBM is in some sense misleading, since the matrices are so large that it is rarely possible to fully diagonalise them to obtain all the eigenvalues and eigenvectors. Instead, one generally uses matrix techniques to obtain just the low-lying energies and wavefunctions. Full diagonalisation

is not possible because this requires storage of the full matrix, that is N_m^2 variables where N_m is the dimensionality of the model space. If N_m is sufficiently large this will exceed the memory of any available computer. Note that a single eigenvector only requires N_m variables to be stored, which is far less. We therefore require a method that will generate the low-lying states with a memory requirement of order N_m rather than N_m^2. This means that the matrix must be stored in a 'sparse' format, where one keeps only the non-zero elements, plus information as to where they are located. Since the Hamiltonian connects of order N states with any given state, the matrix of H is indeed very sparse and requires a storage of order NN_m, which is still far less than N_m^2. It may also be possible to generate the matrix sufficiently fast that it can be regenerated at each iteration, rather than stored. Of all sparse matrix techniques, the Lanczos algorithm [71, 72] seems to be the most efficient. In this algorithm, one starts with some initial guess, say $|x_1\rangle$. This guess may be chosen at random or it may be chosen with a particular symmetry. Acting with H on $|x_1\rangle$ gives a new state, $|x_2\rangle'$. Since $|x_2\rangle'$ in general, is not orthogonal to $|x_1\rangle$, one needs to define a new orthonormalised state $|x_2\rangle$ given by

$$H|x_1\rangle = a_1|x_1\rangle + b_1|x_2\rangle, \tag{3.1}$$

where $\langle x_1|x_2\rangle = 0$. Acting with H on $|x_2\rangle$ gives $|x_3\rangle'$, then $|x_3\rangle'$ is orthogonalised with respect to the previous states, so that one gets $|x_3\rangle$ where

$$H|x_2\rangle = b_1|x_1\rangle + a_1|x_2\rangle + b_2|x_3\rangle. \tag{3.2}$$

Note that the coefficients a_i and b_i form the diagonal and off-diagonal elements of H in a new orthogonal basis. Since H is symmetric in any orthogonal basis, the coefficient of $|x_2\rangle$ in eq. (3.1) must equal the coefficient of $|x_1\rangle$ in eq. (3.2). The method continues iteratively, i.e. one generates a state $|x_{p+1}\rangle' = H|x_p\rangle$ and then orthogonalises it to the previous generated states. In this process, we are generating a representation of the Hamiltonian in a new orthogonal basis in which it is still

symmetric. The matrix has the form

$$\begin{pmatrix} a_1 & b_1 & 0 & 0 & 0 & \cdot & \cdot & \cdot & 0 \\ b_1 & a_2 & b_2 & 0 & 0 & \cdot & \cdot & \cdot & 0 \\ 0 & b_2 & a_3 & b_3 & 0 & \cdot & \cdot & \cdot & 0 \\ 0 & 0 & b_3 & a_4 & b_4 & \cdot & \cdot & \cdot & 0 \\ \cdot & \cdot & \cdot & \cdot & \cdot & \cdot & \cdot & \cdot & \cdot \\ \cdot & \cdot & \cdot & \cdot & \cdot & \cdot & \cdot & \cdot & \cdot \\ 0 & 0 & 0 & 0 & 0 & 0 & b_{p-2} & a_{p-1} & b_{p-1} \\ 0 & 0 & 0 & 0 & 0 & 0 & 0 & b_{p-1} & a_p \end{pmatrix}.$$

This corresponds to diagonalising the Hamiltonian in a subspace of dimension p, rather than in the full space. Following the Lanczos procedure, we can generate a complete set of orthonormal states in which the hamiltonian matrix is tri-diagonal, from any given n-boson state. In fact, the final results are insensitive to the choice of the initial state [71]. Such a transformation makes the matrix easy to store and diagonalise. For the most bound states of the system, one needs to carry out only a relatively small number of iterations as only a small subset of the Lanczos vectors is needed for diagonalisation to be achieved. Thus the Lanczos method can be regarded as an algorithm for generating an optimal subset of the model space for the descriptions of the low-lying states of the system. One of the shortcomings of Lanczos method is the need to carry out the re-orthogonalisation procedure as mentioned in [71]. However, such a procedure can readily be vectorised and the computation can be performed on a super computer such as the Fujitsu VP2200 with extremely high efficiency. In fact, orthogonalisation between two states can be carried out by simple vector operations in a vector processor. The convergence of *sdg*-IBM calculations with the number of Lanczos iterations is generally very fast. To illustrate this fact, we use a typical deformed Hamiltonian consisting of a single quadrupole interaction and one-body forces given in eq. (2.9), with $q = 0.5$, $\kappa_2 = -20$MeV, $\kappa_4 = 0$,$\eta_d = 1.5$, $\eta_g = 4.5$, and $N = 10$. Figure 3.1 shows that the γ and β bands converge in less than 100 iterations. However, for the odd-spin states and hexadecapole phonon bands, the convergence is relatively slow until the number of Lanczos iterations exceeds about 300.

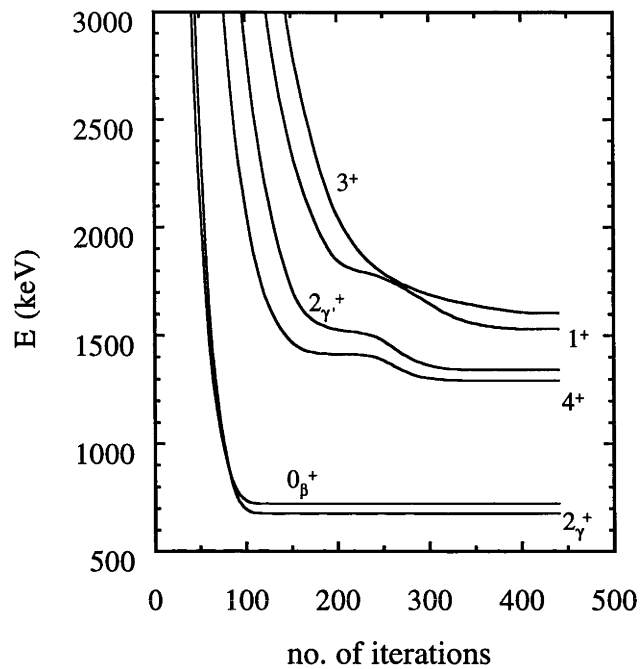

Figure 3.1: Convergence of various excited band energies in terms of the number of Lanczos iterations. The full basis space ($n_{g\,\mathrm{max}} = N$) was used in the calculations.

3.3 Convergence study

In this section, we discuss the results of using the modified code to study the accuracy of various truncated space calculations in the *sdg*-IBM. The truncation scheme used in Ref. [67] is based on the assumption that, by using a large ε_g (ranging from $1 - 1.5$ MeV), the coupling to g bosons is so weak that the expectation values, $\langle n_g \rangle$, of the low-lying states should be far less than one. However, there is no a priori reason that this assumption will still be valid if more g bosons are allowed in the calculations. We have carried out a study of the numerical diagonalisation of a system of 10 bosons with a generalised truncation scheme in which $n_{g\,\mathrm{max}}$ is varied from 1 to 10. We use the consistent-Q formalism with the parametrisation defined in Section 3.2. Here it is useful to highlight some general results. The $\langle n_g \rangle$ of g, γ, and β bands are not affected too much by varying $n_{g\,\mathrm{max}}$, but this is not the case

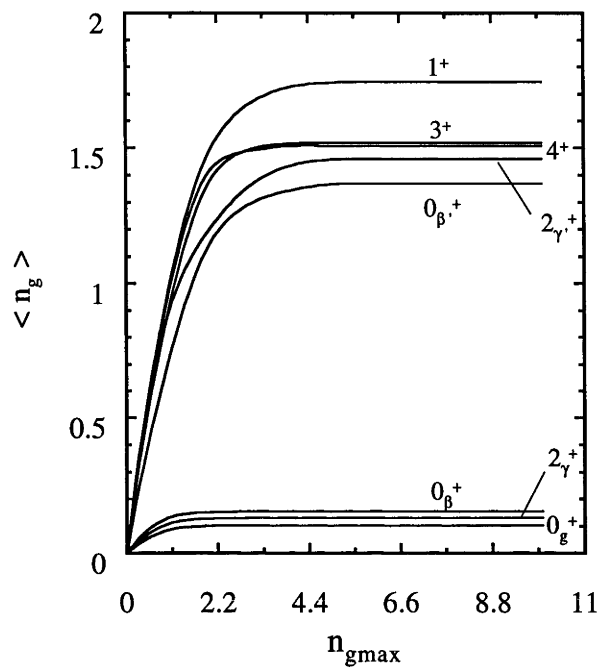

Figure 3.2: The expectation value of the g-boson number in various excitation bands.

for K^π bands as shown in Figure 3.2. When more g bosons are allowed, $\langle n_g \rangle$ grows until saturation occurs roughly at $n_{g\,\mathrm{max}}$ equal to $N/3$. All the expectation values of g-boson number converge to values larger than one. This indicates that these K^π bands are largely characterised by their g-boson nature. These bands appear only in the U(15) representations, and for $K^\pi = 1^+, 3^+$ and 4^+ bands, they are made up by exciting a g boson in the intrinsic frame. Hence their wave-functions are extremely sensitive to the variation in $n_{g\,\mathrm{max}}$. Moreover, they are relatively more high-lying in the energy spectrum, so excitations of more g bosons are favourable.

In Figures 3.3 - 3.4, the convergence properties of some key observables as a function of $n_{g\,\mathrm{max}}$ are illustrated. In Figure 3.3, the effect of truncation on the low-lying band structure is shown for (a) band excitation energies, (b) $E2$ transitions, and (c) $E4$ transitions. The $n_{g\,\mathrm{max}} = 1$ calculations are off by about 10 - 20% (mostly overestimated but underestimated in a few cases), and hence they are not

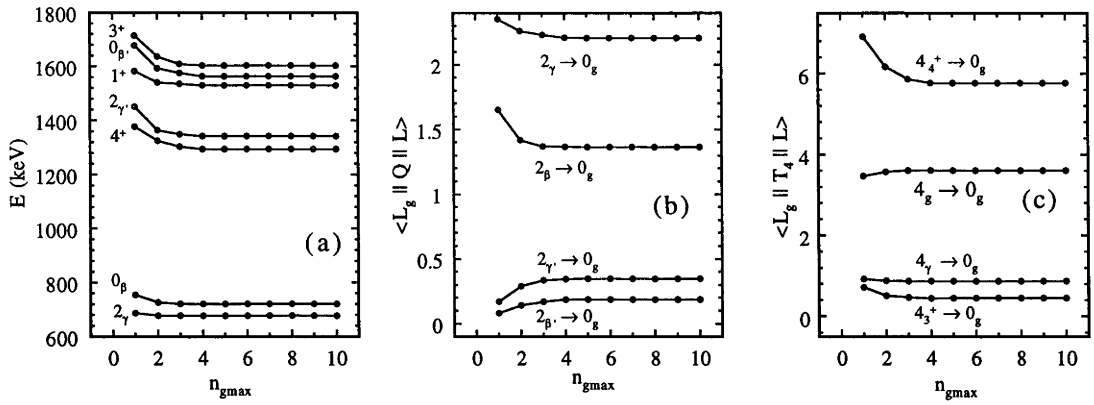

Figure 3.3: Effect of the basis space truncation on (a) band excitation energies (b) $E2$ transitions, and (c) $E4$ transitions. The maximum number of g bosons, $n_{g\,\mathrm{max}}$, allowed in the basis space is increased from 1 to the maximum of $N = 10$. Parameters of the *sdg*-IBM Hamiltonian are given in the text.

very reliable. As expected, the hexadecapole bands take longer to converge compared to the β and γ bands, the worst case being the β' band. Nevertheless, convergence to accuracy of a few percent is obtained in almost all cases for $n_{g\,\mathrm{max}} = 3$. In Figure 3.4, a similar study is presented for the high-spin states in the ground band: (a) excitation energies, and (b) $E2$ transitions. At spins $L \sim 2N$, the $n_{g\,\mathrm{max}} = 1$ calculations are off by about 20 - 30% which will get even worse with increasing spin. On the other hand, the $n_{g\,\mathrm{max}} = 3$ results provide a reasonably accurate picture up to spins $L \sim 2N$. Beyond that, g bosons start dominating the wave functions, and any truncation is likely to lead to substantial errors. The above results suggest that diagonalisation of the *sdg*-IBM Hamiltonians in a model space truncated to $n_{g\,\mathrm{max}} = N/3$ bosons will give a reliable description of states with spins $L < 2N$. This extends the applicability of the *super*-SDGBOSON code to $N = 14$ which covers roughly half of the deformed nuclei. However, one must be cautious that the validity of the above truncation scheme rests very much upon the relative strength of the intrinsic g-boson energy and the parametrisation used. For example, it fails in superdeformed nuclei where the coupling to g bosons is very strong (

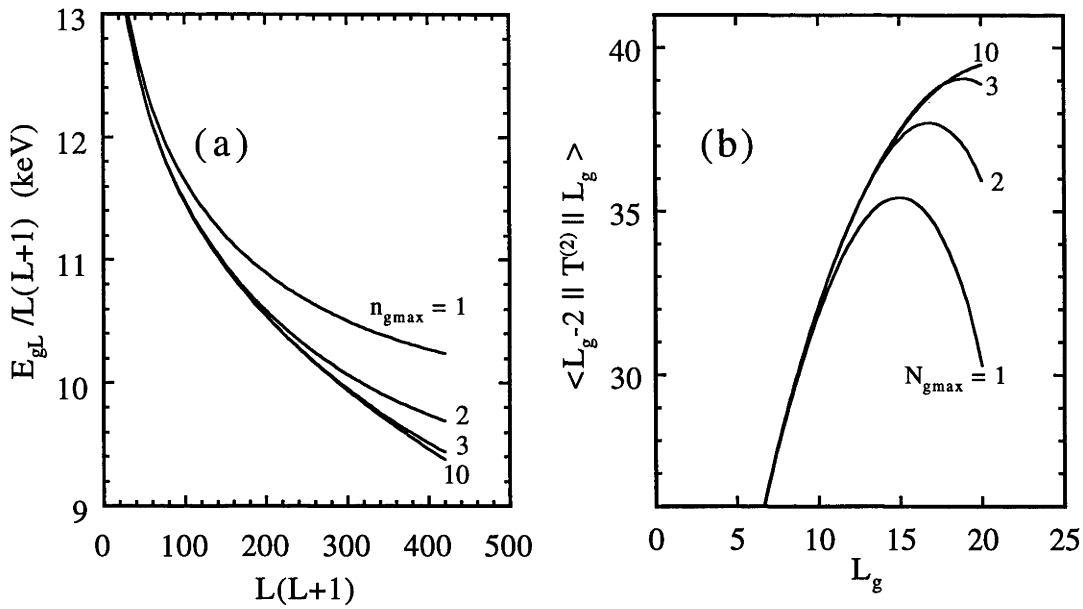

Figure 3.4: Effect of the basis space truncation on the ground band (a) excitation energies, and (b) $E2$ transitions.

$\varepsilon_g = 0$) [55, 60]. After all, it should be emphasised that these computations are expensive, time consuming, and certainly not the best way to deal with the *sdg*-IBM problems. In Chapter 4, the $1/N$ expansion formalism which circumvents the shortcomings of numerical diagonalisation will be introduced.

CHAPTER 4

$1/N$ expansion formalism

The $1/N$ expansion formalism [26] was developed as a response to difficulties in performing calculations in the *sdg*-IBM due to the inadequacy of group theoretical techniques and the large basis space problem in numerical diagonalisation. It is based on angular momentum projected mean field theory and leads to analytic expressions for various physical quantities of interest. Initially, the $1/N$ calculations were carried out to order $1/N^2$ which is quite sufficient for a good description of low-lying spectra. An accurate description of high-spin states, on the other hand, requires the inclusion of terms up to order $1/N^6$ which are not suitable for hand calculation. This difficulty has been overcome by using computer algebra [60]. In the following sections, the extended calculations and the results for the excited bands and the electromagnetic transitions will be presented.

4.1 Coherent states

One of the ingredients of the formalism is the choice of intrinsic states for various rotational bands. These intrinsic states generate a set of collective coordinates x_{lm}, providing a geometric representation for the model which is inherently algebraic in nature. Due to symmetry properties, there are only five independent mean fields in the *sdg*-IBM. We consider a general formulation of the IBM and introduce the boson creation and annihilation operators $b^\dagger_{lm}, b_{lm}$, where $l = 0, 2, 4, \cdots, p$ correspond to $s, d, g, \cdots$ bosons. For convenience, the subscript m is suppressed when it is zero.

The ground band can be written as a condensate of N intrinsic bosons as

$$|\phi_g\rangle = (N!)^{(-1/2)}(\sum_{lm} x_{lm} b^\dagger_{lm})^N |0\rangle. \quad (4.1)$$

Since the above intrinsic state is over-complete, it contains all the non-axial components which highly increase the complexity in performing the angular momentum projection algebra. Moreover, in the light of variational calculus, to locate the global minimum of a five dimensional energy surface is not an easy task. Since the contribution from the non-axial components ($K^\pi \neq 0$) to the ground band is small and most deformed nuclei have axial shapes, it is legitimate to confine the calculation in the subspace having axial symmetry. Thus, the ground band intrinsic state becomes

$$|\phi_g\rangle = |N, \mathbf{x}\rangle + \frac{1}{\sqrt{N(N-1)}} \sum_{m\neq 0} \xi_m b^\dagger_{-m} b^\dagger_m |N-2, \mathbf{x}\rangle \quad + \cdots \quad , \quad (4.2)$$

where $|N, \mathbf{x}\rangle = (N!)^{(-1/2)}(b^\dagger)^N|0\rangle$. The second and higher-order terms in eq. (4.2), representing the mixing with other $K^\pi \neq 0^+$ bands, contribute at $1/N^2$ or higher level. Thus they can be neglected. This approximation can be justified when one compares the $1/N$ expansion results with those obtained from exact diagonalisation which will be shown later. Similarly, the intrinsic states for the single-phonon bands are obtained from the ground band [26] by acting with the other intrinsic boson operators $b^\dagger_m = \sum_l x_{lm} b^\dagger_{lm}$. These prescribed states are orthogonal in the intrinsic frame, but such orthogonality is not guaranteed after angular momentum projection has been carried out. As a result, higher order terms are needed in the intrinsic states to ensure the orthogonality with all other bands. For the γ-band, we have

$$|\phi_\gamma\rangle = b^\dagger_2 |N, \mathbf{x}\rangle + \frac{1}{\sqrt{N-1}} \xi_\gamma (b^\dagger_1)^2 |N-2, \mathbf{x}\rangle \quad + \cdots \quad , \quad (4.3)$$

where ξ_γ is obtained from the orthogonality between the γ- and ground bands. Here $b^\dagger_1|N-1, \mathbf{x}\rangle$ is the $K^\pi = 1^+$ spurious state which results from the breaking of rotational symmetry in the intrinsic frame. This spurious state can be generated by a finite rotation of the ground band [26], and the corresponding mean fields of this spurious intrinsic boson operator can be derived directly from those of the ground band [26]. Thus, the orthogonality term in the γ-band does not introduce any additional degree of freedom into the system.

4.2 Angular momentum projection

Because of the breaking of rotational symmetry, the evaluation of matrix elements in the intrinsic frame is correct only to the leading order in N. In order to obtain accurate results, one has to restore the broken symmetry by performing angular momentum projection. In this case, the energy of a state with particular angular momentum can be obtained by minimising the quantity

$$\langle \hat{H} \rangle_L = E_{K,L} = \frac{\langle \phi_K | P^{L\dagger}_{KK} \hat{H} P^L_{KK} | \phi_K \rangle}{\langle \phi_K | P^{L\dagger}_{KK} P^L_{KK} | \phi_K \rangle} \tag{4.4}$$

where $P^{L\dagger}_{KK}$ [26] is the projection operator defined as

$$P^L_{MK} = \frac{2L+1}{8\pi^2} \int d(\Omega) D^{L*}_{MK}(\Omega) R(\Omega), \tag{4.5}$$

where $D^{L*}_{MK}(\Omega)$, $R(\Omega)$ and Ω are the Wigner-D matrices, rotation operator and Eulerian angle, respectively. Eq. (4.2) can be written in an explicit form,

$$\langle \hat{H} \rangle_L = \frac{2L+1}{2N!\mathcal{N}(\phi_K, L)} \int d\beta \sin\beta \, d^L_{KK}(\beta) \langle \phi_K | \hat{H} e^{-i\beta L_y} | \phi_K \rangle, \tag{4.6}$$

where $\mathcal{N}(\phi_K, L)$ is the normalisation of intrinsic state after projection. Given the prescription for the intrinsic state and the Hamiltonian, the angular momentum projected matrix elements given in eq. (4.6) can be evaluated simply by manipulating the boson algebra.

4.3 Ground band

We consider a general formulation of the IBM as this allows an elegant derivation of the $1/N$ formulae by fully exploiting the angular momentum algebra. In order to keep the variational problem to a manageable size, the intrinsic state for the ground band is chosen as

$$|\phi_g\rangle = (N!)^{-1/2} (b^\dagger)^N |0\rangle, \quad b^\dagger = \sum_l x_l b^\dagger_{l0}, \tag{4.7}$$

where x_l are the normalised boson mean fields, i.e. $\mathbf{x} \cdot \mathbf{x} = 1$, $\mathbf{x} = (x_0, x_2, x_4, \ldots)$. In the classical limit of the IBM, the mean fields are associated with the deformation

parameters of the system [20]. For a given Hamiltonian H, they are determined from $\langle H\rangle_L$ by variation after projection (VAP).

The Hamiltonians in eqs. (2.6, 2.9) can be written in the generalised form as

$$H = \sum_l \varepsilon_l \hat{n}_l - \sum_{k=0}^{2l_{\max}} \kappa_k T^{(k)} \cdot T^{(k)}, \quad \hat{n}_l = \sum_\mu b^\dagger_{l\mu} b_{l\mu}, \quad T^{(k)} = \sum_{jl} t_{kjl} [b^\dagger_j \tilde{b}_l]^{(k)}, \tag{4.8}$$

where the parameters have the obvious correspondence, $\varepsilon_2 = \varepsilon_d$, $\varepsilon_4 = \varepsilon_g$, $t_{2jl} = q_{jl}$, $t_{4jl} = h_{jl}$. This general form has the advantage that, to evaluate the expectation value of H, one needs to perform the calculation for a generic number operator $\hat{n}_l$ and a multipole interaction $T^{(k)} \cdot T^{(k)}$. The expectation value of a scalar operator $\hat{O}$ in the ground band, with angular momentum projection, is given by

$$\langle \hat{O}\rangle_L = \frac{2L+1}{2N!\mathcal{N}(\phi_g, L)} \int d\beta \sin\beta \, d^L_{00}(\beta) \langle 0| b^N \hat{O} e^{-i\beta L_y} (b^\dagger)^N |0\rangle. \tag{4.9}$$

Here, the normalisation, $\mathcal{N}(\phi_g, L)$, follows from eq. (4.9) upon substituting the identity operator for $\hat{O}$. Algebraic manipulations in eq. (4.9) are most easily carried out by the techniques discussed in Appendix B. For the number operator, one obtains

$$\langle \hat{n}_l\rangle_L = \frac{N x_l^2}{F(N,L)} \sum_I \langle L0l00|I0\rangle^2 F(N-1, I), \tag{4.10}$$

where $F(N, L)$ denotes the reduced normalisation integral

$$F(N, L) = \mathcal{N}(\phi_g, L)/(2L+1). \tag{4.11}$$

Eq. (4.10) is exact and highlights the essential role played by the normalisation integral. In the original papers [26], a Gaussian approximation was used in the evaluation of $F(N, L)$. This approximation limited the accuracy of the matrix elements (m.e.) to order $1/N^2$ as mentioned in Ref. [73,74]. This difficulty has been overcome recently using the computer algebra software Mathematica [75]. By exploiting the symmetries of the boson system, the normalisation integral is cast into a system of linear equations which is solved with the help of Mathematica [76]. The result is a double expansion in $1/N$ and $\bar{L} = L(L+1)$ given by

$$F(N, L) = \frac{2}{aN} \sum_{n=0} \frac{(-1)^n}{n!(aN)^n} \sum_{m=0}^{n} \alpha_{nm} \bar{L}^m. \tag{4.12}$$

The coefficients α_{nm} in eq. (4.12) are given in terms of polynomials of the moments of x_l^2,

$$a_n = \sum_l \bar{l}^{n+1} x_l^2, \tag{4.13}$$

and a is defined as $a \equiv a_0$. A list of α_{nm} up to the eighth order is given in Appendix C. The knowledge of $F(N, L)$, in principle, allows evaluation of the m.e. to arbitrary orders in $1/N$. As will be seen from the discussion of the applications, a correct description of moment of inertia at high-spins requires inclusion of terms of order $\bar{L}^3/N^6$. Evaluation of eq. (4.10) to such high orders is too difficult to perform by hand but becomes manageable using computer algebra.

Before presenting the final results, it is useful to comment on the general form of the m.e. of a k-body operator $\hat{O}$, and to illustrate the concept of layers in the $1/N$ expansion

$$\begin{aligned}
\langle \hat{O} \rangle_L &= N^k \sum_{n,m} \frac{O_{nm}}{(aN)^m} \Big(\frac{\bar{L}}{a^2N^2}\Big)^n \\
&= N^k \Big\{ O_{00} + \frac{O_{01}}{aN} + \frac{O_{02}}{(aN)^2} + \frac{O_{03}}{(aN)^3} \; + \; \cdots \\
&\quad + \frac{\bar{L}}{a^2N^2} \Big(O_{10} \; + \; \frac{O_{11}}{aN} + \frac{O_{12}}{(aN)^2} \; + \; \cdots \Big) \\
&\quad + \Big(\frac{\bar{L}}{a^2N^2}\Big)^2 \Big(O_{20} \; + \; \frac{O_{21}}{aN} \; + \; \cdots \Big) \\
&\quad + \Big(\frac{\bar{L}}{a^2N^2}\Big)^3 \Big(O_{30} \; + \; \cdots \Big) + \cdots \Big\}.
\end{aligned} \tag{4.14}$$

The expansion coefficients O_{nm} in eq. (4.14) involve various quadratic forms of the mean fields x_l corresponding to the single-boson m.e. of $\hat{O}$ and its moments. The explicit form is given to facilitate the illustration of layers. Notice that the i coefficients O_{nm} in the i'th column have $n + m = i - 1$ constant, and are referred as the layer "$i - 1$". The leading term in eq. (4.14) thus forms the zeroth layer. This name is appropriate since calculations in the intrinsic frame give the same result independent of projection. In simple terms, the layer in an expansion is given by the maximum power of $\bar{L}$. There is a close connection between the layers in the m.e. given in eq. (4.14) and the normalisation coefficients α_{nm} in eq. (4.12), as to calculate the m.e. up to the i'th layer, one needs to know the coefficients

$\{\alpha_{nn}, \alpha_{nn-1}, \ldots, \alpha_{nn-i+1}, n = 1, 2i\}$. This is very useful in higher order calculations as it restricts the number of terms in the expansion, cutting down the amount of algebra. To make this point clear, we note that eq. (4.14) shows all the terms in the third layer whereas a complete calculation to order $1/N^6$ would require 6 more terms belonging to the fourth, fifth and sixth layers. As can be seen from eq. (4.15) below, the complexity of the coefficients O_{nm} increases "exponentially" with layers, and each of the extra terms would lead to expressions pages long. From a practical point of view, such accuracy is never required. The only $1/N^6$ term of any consequence is $\bar{L}^3/N^6$ which is included in the third layer. The rest are completely negligible. Hence the use of layers is a more sensible approach than a complete calculation to a given order in $1/N$.

With these considerations, we present the result of the Mathematica evaluation of the one-body m.e. in eq. (4.10) to the third layer

$$
\begin{aligned}
\langle \hat{n}_l \rangle_L = N x_l^2 \Big\{ & 1 + \frac{1}{aN}\Big(a - \bar{l}\Big) + \frac{1}{(aN)^2}\Big(-a + a_1/2 + (1 - a_1/a)\bar{l} + \bar{l}^2/2\Big) \\
& + \frac{1}{(aN)^3}\Big(a + 2a^2 - 7a_1/3 - aa_1 + 5a_1^2/4a - a_2/3 \\
& \quad + (-1 - 2a + 2a_1 + 7a_1/2a - 5a_1^2/2a^2 + a_2/2a)\bar{l} \\
& \quad + (-7/6 - a + 5a_1/4a)\bar{l}^2 - \bar{l}^3/6\Big) \\
& + \frac{\bar{L}}{(aN)^2}\Big[(-a + \bar{l}) + \frac{1}{aN}\Big(2a + 2a^2 - 2a_1 + (-2 - 2a + 3a_1/a)\bar{l} - \bar{l}^2\Big) \\
& \quad + \frac{1}{(aN)^2}\Big(-3a - 12a^2 - 4a^3 + 21a_1/2 + 11aa_1 - 15a_1^2/2a + 3a_2/2 \\
& \quad\quad + (3 + 12a + 4a^2 - 33a_1/2 - 14a_1/a + 25a_1^2/2a^2 - 2a_2/a)\bar{l} \\
& \quad\quad + (7/2 + 11a/2 - 5a_1/a)\bar{l}^2 + \bar{l}^3/2\Big)\Big] \\
& + \frac{\bar{L}^2}{2(aN)^4}\Big[(-a - 2a^2 + 3a_1/2 + (1 + 2a - 2a_1/a)\bar{l} + \bar{l}^2/2) \\
& \quad + \frac{1}{aN}\Big(4a + 21a^2 + 14a^3 - 16a_1 - 51aa_1/2 + 13a_1^2/a - 2a_2 \\
& \quad\quad + (-4 - 21a - 14a^2 + 34a_1 + 20a_1/a - 39a_1^2/2a^2 + 5a_2/2a)\bar{l} \\
& \quad\quad + (-4 - 17a/2 + 13a_1/2a)\bar{l}^2 - \bar{l}^3/2\Big)\Big] \\
& + \frac{\bar{L}^3}{3(aN)^6}\Big[-a - 6a^2 - 6a^3 + 25a_1/6 + 9aa_1 - 15a_1^2/4a + 5a_2/12 \\
& \quad\quad + (1 + 6a + 6a^2 - 45a_1/4 - 5a_1/a + 21a_1^2/4a^2 - a_2/2a)\bar{l}
\end{aligned}
$$

$$+(5/6+9a/4-3a_1/2a)\bar{l}^2+\bar{l}^3/12\Big]\Big\}, \tag{4.15}$$

where a_n is defined in eq. (4.13). Eq. (4.15) can be checked against two results that i) it satisfies the number conservation, i.e. $\sum_l \langle \hat{n}_l \rangle_L = N$, and ii) it reproduces the analytic formulae available in the SU(3) limit [1].

A similar calculation for the multipole interaction yields the intermediate result

$$\begin{aligned}\langle T^{(k)} \cdot T^{(k)} \rangle_L = \frac{N(2k+1)}{F(N,L)} \Big\{ & \sum_{jl} \frac{(t_{kjl}x_l)^2}{2l+1} \sum_I \langle L0l0|I0\rangle^2 F(N-1,I) \\ & +(N-1) \sum_{jlj'l'J} t_{kjl}t_{kj'l'}x_j x_l x_{j'} x_{l'} \langle j0j'0|J0\rangle \langle l0l'0|J0\rangle \\ & \times \begin{Bmatrix} j & j' & J \\ l' & l & k \end{Bmatrix} \sum_I \langle L0J0|I0\rangle^2 F(N-2,I) \Big\}. \end{aligned} \tag{4.16}$$

Again this is exact and can be evaluated to any order using Mathematica. The third layer result is given by

$$\begin{aligned}\langle T^{(k)} \cdot T^{(k)} \rangle_L = N^2 \Big\{ & U_k + \frac{1}{aN}\Big(aU_k - U_{k1} + aC_k\Big) \\ & +\frac{1}{(aN)^2}\Big((-2a+a_1)U_k + (1-a-a_1/a)U_{k1} + U_{k2}/2 + a^2C_k - aC_{k1}\Big) \\ & +\frac{1}{(aN)^3}\Big((2a+2a^2-14a_1/3-aa_1+5a_1^2/2a-2a_2/3)U_k \\ & \quad +(-1+a-a_1/2+7a_1/2a-5a_1^2/2a^2+a_2/2a)U_{k1} \\ & \quad +(-7/6+5a_1/4a)U_{k2} - U_{k3}/6 \\ & \quad +(-a^2+aa_1/2)C_k + (a-a_1)C_{k1} + aC_{k2}/2\Big) \\ & +\frac{\bar{L}}{(aN)^2}\Big[-2aU_k + U_{k1} \\ & +\frac{1}{aN}\Big((4a+2a^2-4a_1)U_k + (-2+a+3a_1/a)U_{k1} - U_{k2} - a^2C_k + aC_{k1}\Big) \\ & +\frac{1}{(aN)^2}\Big((-6a-16a^2-4a^3+21a_1+15aa_1-15a_1^2/a+3a_2)U_k \\ & \quad +(3+2a-2a^2-4a_1-14a_1/a+25a_1^2/2a^2-2a_2/a)U_{k1} \\ & \quad +(7/2+2a-5a_1/a)U_{k2} + U_{k3}/2 \\ & \quad +(2a^2+2a^3-2aa_1)C_k + (-2a-2a^2+3a_1)C_{k1} - aC_{k2}\Big)\Big] \\ & +\frac{\bar{L}^2}{2(aN)^4}\Big[(-2a-2a^2+3a_1)U_k + (1-2a_1/a)U_{k1} + U_{k2}/2 \\ & +\frac{1}{aN}\Big((8a+30a^2+14a^3-32a_1-37aa_1+26a_1^2/a-4a_2)U_k \end{aligned}$$

$$
\begin{aligned}
&+(-4-8a+2a^2+29a_1/2+20a_1/a-39a_1^2/2a^2+5a_2/2a)U_{k1}\\
&+(-4-9a/2+13a_1/2a)U_{k2}-U_{k3}/2\\
&+(-a^2-2a^3+3aa_1/2)C_k+(a+2a^2-2a_1)C_{k1}+aC_{k2}/2\Big)\Big]\\
&+\frac{\bar{L}^3}{3(aN)^6}\Big[(-8a-36a^2-24a^3+100a_1/3+54aa_1-30a_1^2/a+10a_2/3)U_k\\
&+(4+12a-24a_1-20a_1/a+21a_1^2/a^2-2a_2/a)U_{k1}\\
&+(10/3+6a-6a_1/a)U_{k2}+U_{k3}/3\Big]\Big\}. \qquad (4.17)
\end{aligned}
$$

Here the quadratic forms C_{kn} arise from normal ordering and simulate an effective one-body term as

$$C_{kn}=(2k+1)\sum_{jl}\bar{l}^n(t_{kjl}x_l)^2/(2l+1), \qquad (4.18)$$

while U_{kn} represent the genuine two-boson interaction

$$U_{kn}=\sum_{jlj'l'I}\bar{I}^n\langle j0j'0|I0\rangle\langle l0l'0|I0\rangle\begin{Bmatrix} j & j' & I\\ l' & l & k\end{Bmatrix}t_{kjl}t_{kj'l'}x_jx_lx_{j'}x_{l'}. \qquad (4.19)$$

For a given multipole, these sums can be evaluated in closed form using Mathematica. For the quadrupole and hexadecapole interactions, the first four terms needed in eq. (4.17) are given by

$$
\begin{aligned}
U_2&=A^2,\\
U_{21}&=(2A_1-3A)A,\\
U_{22}&=(2A_2-24A_1+18A)A+(A_{11}-A_2+7A_1)A_1+(A_{11}-A_2)^2/12,\\
U_{23}&=(2A_3-36A_2-18A_{11}+240A_1-144A)A\\
&\quad+(3A_{21}-3A_3+56A_2+16A_{11}-194A_1)A_1/2\\
&\quad+(11A_{11}^2+14A_{11}A_2-25A_2^2)/12+(A_3-A_{21})(A_2-A_{11})/4,\\
U_4&=B^2,\\
U_{41}&=(2B_1-10B)B/2,\\
U_{42}&=4B_1^2+(2B_{11}-40B_1+20B)B+(B_2-B_{11}-20B_1+180B)^2/180,\\
U_{43}&=(2B_3-120B_2-60B_{11}+2480B_1-4400B)B\\
&\quad+(3B_{21}-3B_3+224B_2+58B_{11}-2756B_1/3)B_1/9,\\
&\quad+(8B_{11}^2+14B_{11}B_2-11B_2^2)/45+(B_3-B_{21})(B_2-B_{11})/60. \qquad (4.20)
\end{aligned}
$$

The quadratic forms A_{mn} and B_{mn} in eq. (4.20) are defined as

$$A_{mn} = \sum_{jl} \bar{j}^m \bar{l}^n \langle j0l0|20\rangle t_{2jl} x_j x_l, \qquad B_{mn} = \sum_{jl} \bar{j}^m \bar{l}^n \langle j0l0|40\rangle t_{4jl} x_j x_l, \tag{4.21}$$

and correspond to various moments of the single-boson m.e. of the quadrupole and hexadecapole operators. Note that the zero subscripts are suppressed for convenience. The quadrupole m.e. given by eqs. (4.17 - 4.20) reproduces the well known Casimir eigenvalues in the SU(3) limit, hence also passes the SU(3) test.

The analytic expressions presented above are already rather long. If for any reason, the next layer results should be required, the expressions would grow to pages in length, and the analytical $1/N$ calculations might not be very practical. In such cases, numerical evaluation of the m.e. given in eqs. (4.10, 4.16), as described in Appendix D, may be preferable. Although this would increase the computation time appreciably, it has the advantage that the calculations are done exactly to all orders in $1/N$.

Variation after projection

The energy expression derived in Section 4.3 is rather lengthy, and in discussing the variational problem, it will be more convenient to express it in a compact form. Thus, using the parametrisation in eq. (2.17), we rewrite the ground band energy as

$$E_{gL} = N^2 \kappa_2 \sum_{n,m} \frac{E_{nm}}{N^m} \left(\frac{\bar{L}}{N^2}\right)^n, \tag{4.22}$$

where the coefficients E_{nm} can be read off from eqs. (4.15-4.21). For example the leading order is given by

$$E_{00} = \sum_l \eta_l \frac{x_l^2}{\mathbf{x}\cdot\mathbf{x}} - \left(\frac{A}{\mathbf{x}\cdot\mathbf{x}}\right)^2 - \zeta_4 \left(\frac{B}{\mathbf{x}\cdot\mathbf{x}}\right)^2, \tag{4.23}$$

with A and B defined in eq. (4.21), and we have restored the normalisation factors $\mathbf{x}\cdot\mathbf{x}$ as a precursor to variation. The minimum of the ground energy is obtained from

$$\partial E_{gL}/\partial x_l = 0, \quad l = 0, 2, 4, \ldots, \tag{4.24}$$

which can be solved algebraically using the ansatz

$$\mathbf{x} = \sum_{n,m} \frac{\mathbf{x}_{nm}}{N^m} \Big(\frac{\bar{L}}{N^2}\Big)^n. \tag{4.25}$$

The use of layers again simplifies solution of the variational equations. For the leading order (zeroth layer), one has the usual Hartree-Bose equations

$$\left.\frac{\partial E_{00}}{\partial x_l}\right|_{\mathbf{x}_{00}} = 0, \tag{4.26}$$

which are a system of coupled non-linear equations, and they are solved numerically by iteration [77]. Having determined $\mathbf{x}_{00}$, the first layer mean fields $\mathbf{x}_{01}$ and $\mathbf{x}_{10}$ are then obtained by solving the respective sets of equations

$$\begin{aligned} \left.\frac{\partial E_{00}}{\partial x_l}\right|_{\mathbf{x}_{00}+\mathbf{x}_{01}/N} &= -\frac{1}{N}\left.\frac{\partial E_{01}}{\partial x_l}\right|_{\mathbf{x}_{00}}, \\ \left.\frac{\partial E_{00}}{\partial x_l}\right|_{\mathbf{x}_{00}+\mathbf{x}_{10}\bar{L}/N^2} &= -\frac{\bar{L}}{N^2}\left.\frac{\partial E_{10}}{\partial x_l}\right|_{\mathbf{x}_{00}}. \end{aligned} \tag{4.27}$$

Upon substituting the mean fields in derivatives in eq. (4.27), the leading order vanishes by virtue of the Hartree-Bose eqs. (4.26), and the next order leads to sets of linear equations for $\mathbf{x}_{01}$ and $\mathbf{x}_{10}$, that can be easily solved using Mathematica. The Hartree-Bose condition also ensures that when the first layer mean fields are substituted in the energy expression, the correction to the first layer exactly vanishes. As a result, they only contribute to the second and higher layers [77]. This holds in general for all layers. Thus for the third layer expansion considered here, one needs at most the second layer mean fields $\mathbf{x}_{02}$, $\mathbf{x}_{11}$ and $\mathbf{x}_{20}$ which are obtained from

$$\begin{aligned} \left.\frac{\partial E_{00}}{\partial x_l}\right|_{\mathbf{x}_{00}+\mathbf{x}_{01}/N+\mathbf{x}_{02}/N^2} &= -\frac{1}{N}\left.\frac{\partial E_{01}}{\partial x_l}\right|_{\mathbf{x}_{00}+\mathbf{x}_{01}/N} - \frac{1}{N}\left.\frac{\partial E_{02}}{\partial x_l}\right|_{\mathbf{x}_{00}}, \\ \left.\frac{\partial E_{00}}{\partial x_l}\right|_{\mathbf{x}_{00}+\mathbf{x}_{10}\bar{L}/N^2+\mathbf{x}_{20}\bar{L}^2/N^4} &= -\frac{\bar{L}}{N^2}\left.\frac{\partial E_{10}}{\partial x_l}\right|_{\mathbf{x}_{00}+\mathbf{x}_{10}\bar{L}/N^2} - \frac{\bar{L}^2}{N^4}\left.\frac{\partial E_{20}}{\partial x_l}\right|_{\mathbf{x}_{00}}, \\ \left.\frac{\partial E_{00}}{\partial x_l}\right|_{\mathbf{x}_{00}+\mathbf{x}_{01}/N+\mathbf{x}_{10}\bar{L}/N^2+\mathbf{x}_{11}\bar{L}/N^3} &= -\frac{1}{N}\left.\frac{\partial E_{01}}{\partial x_l}\right|_{\mathbf{x}_{00}+\mathbf{x}_{10}\bar{L}/N^2} - \frac{\bar{L}}{N^2}\left.\frac{\partial E_{10}}{\partial x_l}\right|_{\mathbf{x}_{00}+\mathbf{x}_{01}/N} \\ &\quad -\frac{\bar{L}}{N^3}\left.\frac{\partial E_{11}}{\partial x_l}\right|_{\mathbf{x}_{00}}. \end{aligned} \tag{4.28}$$

Again these sets of linear equations can be solved using Mathematica. We refrain from presenting these rather bulky results for the first and second layer mean fields

here because, in the absence of analytical solutions for the zeroth layer, they are not very illuminating. Upon substituting eq. (4.25) into eq. (4.22), one obtains the variational corrections introduced by the higher order mean fields in the ground band energies. These lengthy analytic expressions contribute only to the second and higher layers and will not be shown here. All these results, together with other $1/N$ expansion formulae, are nevertheless available in the form of a Fortran code [78]. Finally, if one is interested only in practical applications of the results to high-spin states, one can determine the minimum directly from the energy expression in eq. (4.22) using the numerical simplex method, and thereby avoid the complexities introduced by the higher order terms in the solution of the variational problem.

4.4 Single-phonon bands

Most of the high-spin data, as well as their theoretical analysis, are concentrated on the yrast bands (ground or two-quasiparticle). While relying solely on the yrast data may be tolerated for microscopic models, it could easily lead to misleading results in phenomenological models. For this reason, inclusion of single-phonon bands in the analysis of high-spin data is highly desirable in phenomenological approaches. As will be seen in the applications, there are substantial high-spin data for the γ-bands, which can be singled out among the single-phonon bands in this respect. Therefore, we consider here the γ-band as an example of a single-phonon band calculation. Energy expressions for the other bands can be derived in a similar fashion.

The γ-band intrinsic state is prescribed as

$$|\phi_\gamma\rangle = b_2^\dagger|\phi_g, N-1\rangle + \frac{1}{\sqrt{N-1}}\xi_\gamma(b_1^\dagger)^2|\phi_g, N-2\rangle. \tag{4.29}$$

The higher order terms in eq. (4.3) are ignored since their contributions are small. In this trial state, the mean fields for the ground band are already established in Section 4.3, and those for b_1 are determined from the spurious $K = 1^+$ band as [26],

$$x_{l1} = [\bar{l}/a]^{1/2} x_l. \tag{4.30}$$

Thus, only the γ-band mean fields, x_{l2}, are to be determined by VAP. The coefficient ξ_γ in eq. (4.29) follows from the orthogonality condition $\langle L_\gamma | L_g \rangle = 0$ as

$$\sum_{lI} \langle L2l-2|I0\rangle\langle L0l0|I0\rangle \Big[x_l x_{l2} F(N-1,I) + \xi_\gamma \sum_{jj'} x_j x_{j1} x_{j'} x_{j'1} \langle j0j'0|l0\rangle \langle j1j'1|l2\rangle F(N-2,I) \Big] = 0, \quad (4.31)$$

where F denotes the ground band normalisation in eq. (4.12) for $N-1$ and $N-2$ bosons, and ξ_γ is obtained from the orthogonality between the γ- and ground bands. When VAP is carried out in the SU(3) limit, all the mean fields and ξ_γ coincide exactly with values prescribed in Refs. [22, 23]. The expectation value of a scalar operator $\hat{O}$ in the γ-band (eq. (4.29)) with angular momentum projection, is given by

$$\langle \hat{O} \rangle_{\gamma,L} = \frac{2L+1}{2(N-1)\mathcal{N}(\phi_\gamma, L)} \int d\beta \sin\beta \, d^L_{22}(\beta) \Big\{ \langle 0|b^{N-1} b_2 \hat{O} e^{-i\beta L_y} (b^\dagger)^{N-1} b_2^\dagger |0\rangle + 2\xi_\gamma \langle 0|b^{N-2} b_1^2 \hat{O} e^{-i\beta L_y} (b^\dagger)^{N-1} b_2^\dagger |0\rangle + \xi_\gamma^2 \langle 0|b^{N-2} b_1^2 \hat{O} e^{-i\beta L_y} (b^\dagger)^{N-2} (b_1^\dagger)^2 |0\rangle \Big\}, \quad (4.32)$$

where $\mathcal{N}(\phi_\gamma, L)$, the normalisation for the γ-band, is obtained from eq. (4.32) using the identity operator for $\hat{O}$. The contribution from the orthogonality terms to the band energies are of the order $1/N^2$, and therefore they were ignored in the original papers [26]. In the description of high-spin states, however, these terms make essential contributions and they have to be included in the calculations. Each contraction of the intrinsic boson operators in eq. (4.32) leads to projected single-boson overlaps of the form $x_{lm} x_{lm'} d^l_{mm'}$. The resulting Wigner d-functions are coupled to a final d-function to perform the β integral. This process leads to rather long expressions for the orthogonality terms. In order to reduce their size, we introduce a compact notation for the recoupling coefficients as follows

$$R_2(jmm', lnn'; I) = x_{jm} x_{jm'} x_{ln} x_{ln'} \langle jmln|Im+n\rangle \langle jm'ln'|Im'+n'\rangle,$$

$$R_3(jmm', lnn', k\mu\mu'; I, J) = R_2(jmm', lnn'; I) x_{k\mu} x_{k\mu'} \langle Im+nk\mu|Jm+n+\mu\rangle \langle Im'+n'k\mu'|Jm'+n'+\mu'\rangle,$$

$$R_4(jmm', lnn', k\mu\mu', k'\nu\nu'; I, I', J) = R_2(jmm', lnn'; I) R_2(k\mu\mu', k'\nu\nu'; I')$$

$$\langle Im + nI'\mu + \nu | Jm + n + \mu + \nu \rangle$$
$$\langle Im' + n'I'\mu' + \nu' | Jm' + n' + \mu' + \nu' \rangle. \qquad (4.33)$$

Higher recoupling coefficients (R_5, R_6) are defined similarly. Using this notation, the reduced normalisation for the γ-band, $F_\gamma(N,L) = \mathcal{N}(\phi_\gamma, L)/(2L+1)$, can be written as

$$\begin{aligned}
F_\gamma(N,L) = \sum_{Ij} \langle L2j-2|I0\rangle^2 & \\
\times \Big\{ x_{j2}^2 F(N-1,I) + (N-1) \sum_{ll'} R_2(l'20, l02; j) F(N-2,I) & \\
+ 2\xi_\gamma \Big[2 \sum_{ll'} R_2(l'21, l01; j) F(N-2,I) & \\
+ (N-2) \sum_{kk'll'} R_3(k10, k'10, l02; l', j) F(N-3,I) \Big] & \\
+ \frac{2\xi_\gamma^2}{N-1} \Big[\sum_{ll'} R_2(l'11, l11; j) F(N-2,I) & \\
+ 2(N-2) \sum_{kk'll'} R_3(k10, k'01, l11; l', j) F(N-3,I) & \\
+ \frac{1}{2}(N-2)(N-3) \sum_{kk'k''ll'l''} R_4(k10, k'10, l01, l'01; k'', l'', j) & \\
\times F(N-4,I) \Big] \Big\}. \qquad (4.34)
\end{aligned}$$

Eq. (4.34) expresses the γ-band normalisation in terms of the ground-band normalisation in eq. (4.12), and it can be evaluated to any order in $1/N$ using Mathematica.

The expectation value of the number operator in the γ-band can be calculated similarly, giving

$$\begin{aligned}
\langle \hat{n}_l \rangle_{\gamma,L} = \frac{1}{F_\gamma(N,L)} \sum_{Ij} \langle L2j-2|I0\rangle^2 \Big\{ x_{l2}^2 \delta_{jl} F(N-1,I) & \\
+ (N-1) \sum_{l'} \Big(R_2(l'22, l00; j) + 2R_2(l'20, l02; j) \Big) F(N-2,I) & \\
+ (N-1)(N-2) \sum_{kk'l'} R_3(k20, k'02, l00; l', j) F(N-3,I) & \\
+ 2\xi_\gamma \Big[2 \sum_{l'} \Big(R_2(l'21, l01; j) + R_2(l'01, l21; j) \Big) F(N-2,I) & \\
+ (N-2) \sum_{kk'l'} \Big(2R_3(k21, k'01, l00; l', j) + 2R_3(k20, k'01, l01; l', j) &
\end{aligned}$$

$$
\begin{aligned}
&+R_3(k10,k'10,l02;l',j)\Big)F(N-3,I)\\
&+(N-2)(N-3)\sum_{kk'k''l'l''}R_4(k10,k'10,l'02,l00;k'',l'',j)F(N-4,I)\Big]\\
&+\frac{\xi_\gamma^2}{N-1}\Big[4\sum_{l'}R_2(l'11,l11;j)F(N-2,I)+\\
&+2(N-2)\sum_{kk'l'}\Big(R_3(k11,k'11,l00;l',j)+4R_3(k11,k'10,l01;l',j)\\
&+2R_3(k10,k'01,l11;l',j)\Big)F(N-3,I)\\
&+4(N-2)(N-3)\sum_{kk'k''l'l''}\Big(R_4(k11,k'10,l'01,l00;k'',l'',j)\\
&+R_4(k10,k'10,l'01,l01;k'',l'',j)\Big)F(N-4,I)\\
&+\sum_{kk'k''l'l''j'j''}(N-2)(N-3)(N-4)R_5(k10,k'10,l'01,j'01,l00;k'',l'',j'',j)\\
&\times F(N-5,I)\Big]\Big\}. \qquad (4.35)
\end{aligned}
$$

It can be easily checked that the condition, $\sum_l\langle\hat{n}_l\rangle_{\gamma,L}=N$ is satisfied by the form in eq. (4.35). The expectation value of a general two-body interaction in the γ-band is given by

$$
\begin{aligned}
\langle T^k\cdot T^k\rangle_{\gamma,L}&=\sum_{jl}\frac{2k+1}{2l+1}t_{kjl}^2\langle\hat{n}_l\rangle_{\gamma,L}\\
&+\frac{(N-2)(2k+1)}{F_\gamma(N,L)}\sum_{jlj'l'J}t_{kjl}t_{kj'l'}\begin{Bmatrix}j'&j&J\\l&l'&k\end{Bmatrix}\sum_{iII'}\langle L2I'-2|I0\rangle^2\\
&\times\Big\{(N-1)\Big[\frac{2}{N-2}(P_{2002}+P_{0022})F(N-2,I)\delta_{i0}\\
&+\Big(x_{i2}^2P_{0000}+4x_{i2}x_iP_{2000}\Big)F(N-3,I)\\
&+(N-3)\sum_{kk'}R_2(k20,k'02;i)P_{0000}F(N-4,I)\Big]\\
&+4\xi_\gamma\Big[\frac{2}{N-2}P_{2101}\delta_{i0}F(N-2,I)\\
&+\Big(2x_{i2}x_{i1}P_{0001}+x_{i2}x_iP_{0101}+2x_{i1}x_i(P_{2001}+P_{0021})\Big)F(N-3,I)\\
&+(N-3)\sum_{kk'}\Big(R_2(k21,k'01;i)P_{0000}+2R_2(k20,k'01;i)P_{0001}\\
&+R_2(k10,k'10;i)P_{0002}\Big)F(N-4,I)
\end{aligned}
$$

$$+\frac{1}{2}(N-3)(N-4)\sum_{kk'k''i'} R_3(k10,k'10,i'02;k'',i)P_{0000}F(N-5,I)\Big]$$
$$+\frac{4\xi_\gamma^2}{N-1}\Big[\frac{1}{N-2}P_{1111}F(N-2,I)$$
$$+2\Big(x_{i1}^2(P_{1001}+P_{0011})+2x_{i1}x_iP_{1011}\Big)F(N-3,I)$$
$$+(N-3)\sum_{kk'}\Big(\frac{1}{2}R_2(k11,k'11;i)P_{0000}+4R_2(k11,k'10;i)P_{0001}$$
$$+2R_2(k10,k'01;i)(P_{1001}+P_{0011})+R_2(k10,k'10;i)P_{0101}\Big)F(N-4,I)$$
$$+(N-3)(N-4)\sum_{kk'k''i'}\Big(R_3(k11,k'10,i'01;k'',i)P_{0000}$$
$$+2R_3(k10,k'10,i'01;k'',i)P_{0001}\Big)F(N-5,I)$$
$$+\frac{1}{4}(N-3)(N-4)(N-5)\sum_{kk'k''i'i''l''}R_4(k10,k'10,i'01,i''01;k'',l'',i)$$
$$\times P_{0000}F(N-6,I)\Big]\Big\}. \qquad (4.36)$$

Here we have introduced the compact notation for the two-boson m.e.

$$P_{m'nmn'} = x_{jm}x_{j'm'}x_{ln}x_{l'n'}\langle j'm'jm|Jm+m'\rangle\langle lnl'n'|Jn+n'\rangle$$
$$\langle Jm+m'\,i2-m-m'|I'2\rangle\langle Jn+n'\,i2-n-n'|I'2\rangle. \qquad (4.37)$$

The dummy summation indices j, j', l, l', J, i, I' in P are suppressed for convenience. The first term in eq. (4.36) is the effective one-body term that arises from normal ordering of the boson operators in the multipole interaction, and it is expressed using eq. (4.35).

Eqs. (4.35, 4.36) are the counterparts of eqs. (4.10, 4.16) for the ground band and can be input directly into Mathematica for evaluation. As one can surmise from a cursory comparison of the parent equations, the resulting third layer expressions are pages long as shown in Appendix E. Regarding high-spin states, they are not as accurate as the ground band results, presumably requiring inclusion of even higher order terms. For these reasons, we have opted for a numerical evaluation of eqs. (4.35, 4.36) in the applications. Such a calculation includes all orders in $1/N$, and hence provides more reliable results for the γ-band energies.

4.5 Double-phonon bands

In a similar fashion, one can generalise the above results to the $\gamma\gamma$-band. Here we choose the intrinsic state as

$$|\phi_{\gamma\gamma}\rangle = (b_2^\dagger)^2|N-2,\mathbf{x}\rangle. \tag{4.38}$$

In fact, this simple prescription greatly reduces the complexity in evaluating matrix elements.

The normalisation is then given by

$$\begin{aligned}
F_{\gamma\gamma}(N,L) = &\sum_{Ij}\langle L2j-2|I0\rangle^2 \\
&\times\Big\{\sum_{ll'}2R_2(l'22,l22;j)F(N-2,I) \\
&\quad+4(N-2)\sum_{kk'll'}R_3(k20,k'02,l22;l',j)F(N-3,I) \\
&\quad+(N-2)(N-3)\sum_{kk'k''ll'l''}R_4(k20,k'20,l02,l'02;k'',l'',j) \\
&\qquad\times F(N-4,I)\Big\}.
\end{aligned} \tag{4.39}$$

The leading term in the $1/N$ expansion of the norm comes from $F(N-2,I)$, and the term containing $F(N-4,I)$ does not contribute to the first layer results (see Appendix F). The expectation value of the number operator is given by

$$\begin{aligned}
\langle\hat{n}_l\rangle_{\gamma\gamma,L} = &\frac{1}{F_\gamma(N,L)}\sum_{Ij}\langle L2j-2|I0\rangle^2\Big\{4\sum_{l'}R_2(l'22,l22;j)F(N-2,I)+ \\
&+2(N-2)\sum_{kk'l'}\Big(R_3(k22,k'22,l00;l',j)+4R_3(k22,k'20,l02;l',j) \\
&\quad+2R_3(k20,k'02,l22;l',j)\Big)F(N-3,I) \\
&+4(N-2)(N-3)\sum_{kk'k''l'l''}\Big(R_4(k22,k'20,l'02,l00;k'',l'',j) \\
&\quad+R_4(k20,k'20,l'02,l02;k'',l'',j)\Big)F(N-4,I) \\
&+\sum_{kk'k''l'l''j'j''}(N-2)(N-3)(N-4)R_5(k20,k'20,l'02,j'02,l00;k'',l'',j'',j) \\
&\quad\times F(N-5,I)\Big\}.
\end{aligned} \tag{4.40}$$

Due to the properties of the Clebsch-Gordan coefficients, only three terms in eq. (4.40) survive at the first layer expansion (see Appendix F).

Finally, we have the two-body matrix element

$$
\begin{aligned}
\langle T^k \cdot T^k \rangle_{\gamma\gamma,} = & \sum_{jl} \frac{2k+1}{2l+1} t^2_{kjl} \langle \hat{n}_l \rangle_{\gamma\gamma,L} \\
& + \frac{4(2k+1)}{F_{\gamma\gamma}(N,L)} \sum_{jlj'l'J} t_{kjl} t_{kj'l'} \begin{Bmatrix} j' & j & J \\ l & l' & k \end{Bmatrix} \sum_{iII'} \langle L2I' - 2|I0\rangle^2 \\
& \times \Big\{ P_{2222} F(N-2,I) + 2(N-2)\Big(x^2_{i2}(P_{2002} + P_{0022}) + 2x_{i2}x_i P_{2022} \Big) F(N-3,I) \\
& + (N-2)(N-3) \sum_{kk'} \Big(\frac{1}{2} R_2(k22,k'22;i) P_{0000} + 4R_2(k22,k'20;i) P_{0002} \\
& + 2R_2(k20,k'02;i)(P_{2002} + P_{0022}) + R_2(k20,k'20;i) P_{0202} \Big) F(N-4,I) \\
& + (N-2)(N-3)(N-4) \sum_{kk'k''i'} \Big(R_3(k22,k'20,i'02;k'',i) P_{0000} \\
& + 2R_3(k20,k'20,i'02;k'',i) P_{0002} \Big) F(N-5,I) \\
& + \frac{1}{4}(N-2)(N-3)(N-4)(N-5) \sum_{kk'k''i'i''l''} R_4(k20,k'20,i'02,i''02;k'',l'',i) \\
& \times P_{0000} F(N-6,I) \Big\}. \qquad (4.41)
\end{aligned}
$$

Similarly, only three terms contribute to the first layer expansion of the expectation value of the two-body forces. Here we show the first layer $1/N$ expansion results for the $\gamma\gamma$-band, which will be useful in the study of anharmonic effects presented in Chapter 5. The matrix elements of the one-body and two-body interactions are given by

$$
\begin{aligned}
\langle \hat{n}_l \rangle_{\gamma\gamma,L} &= N x_l^2 \Big\{ 1 + \frac{1}{aN} \Big(-(a+\bar{l}) + 2a x^2_{lk}/x^2_l \Big) + \frac{\bar{L}}{(aN)^2} \Big(\bar{l} - a \Big) \Big\}, \\
\langle T^{(k)} \cdot T^{(k)} \rangle_{\gamma\gamma,L} &= N^2 \Big\{ U_k + \frac{1}{aN} \Big(8aU''_k - 3aU_k - U_{k1} + aC_k \Big) \\
&\quad + \frac{\bar{L}}{(aN)^2} \Big(-2aU_k + U_{k1} \Big) \Big\}, \qquad (4.42)
\end{aligned}
$$

where U''_{kn} is defined as

$$
\begin{aligned}
U''_{kn} &= \frac{(2k+1)}{2} \sum_{jlj'l'I} \bar{I}^n \langle j2j'0|I2\rangle \big(\langle l'0l2|I2\rangle x_{l'} x_{l2} + \langle l'2l0|I2\rangle x_{l'2} x_l \big) \\
&\quad \times \begin{Bmatrix} j & j' & I \\ l' & l & k \end{Bmatrix} t_{kjl} t_{kj'l'} x_{j2} x_{j'}. \qquad (4.43)
\end{aligned}
$$

It is interesting to point out that the ground and $\gamma\gamma$-bands have the same leading order results. In fact, it is true for all other excited bands as well. To test the validity of eq. (4.42), one can substitute the dipole interaction $(L \cdot L)$ and the number operator into the above expressions. In such cases, the two- and one-body matrix elements will be reduced to $\bar{L}$ and N, respectively.

4.6 $E2$ transitions

Description of the yrast $E2$ transitions at high-spins is one of the main aims of this work. Therefore, a brief review of the currently available $1/N$ results for $E2$ m.e. and their extensions to higher orders will be presented. A comprehensive study of the $E2$ transitions among the ground, γ- and β-bands was given previously [79]. The first layer m.e. obtained in Ref. [79] for the yrast $E2$ transitions appears to work rather well even at high-spins [60]. Inclusion of the d-boson energy leads to some deterioration at high-spins, which can be rectified by incorporating the higher order terms in the expansion.

The ground band m.e. of the quadrupole operator is given by

$$\langle L' \parallel Q \parallel L\rangle = \hat{L}[4F(N,L')F(N,L)]^{-1/2}\sum_{M}\langle LM2-M|L'0\rangle \times \int d\beta \sin\beta\, d^{L}_{M0}\langle 0|b^{N}Q_{-M}e^{-i\beta L_y}(b^{\dagger})^{N}|0\rangle, \tag{4.44}$$

where $\hat{L} = [2L+1]^{1/2}$. As before, this can be reduced to the form

$$\langle L' \parallel Q \parallel L\rangle = \frac{\sqrt{5}N\hat{L}\hat{L}'}{[F(N,L')F(N,L)]^{1/2}}\sum_{jlJ} q_{jl}x_j x_l \times\langle j0L'0|J0\rangle\langle L0l0|J0\rangle \begin{Bmatrix} j & L' & J \\ L & l & 2 \end{Bmatrix} F(N-1,J), \tag{4.45}$$

which can be evaluated to any order using Mathematica. However, because of the tensor nature of the $E2$ operator, the resulting third layer expressions are much more complicated than those for the Hamiltonian. In contrast, because there is no variation involved, numerical evaluation of eq. (4.45) is straightforward and is preferred over using the lengthy algebraic forms to evaluate the results presented in the following section.

4.7 Comparison with the exact results

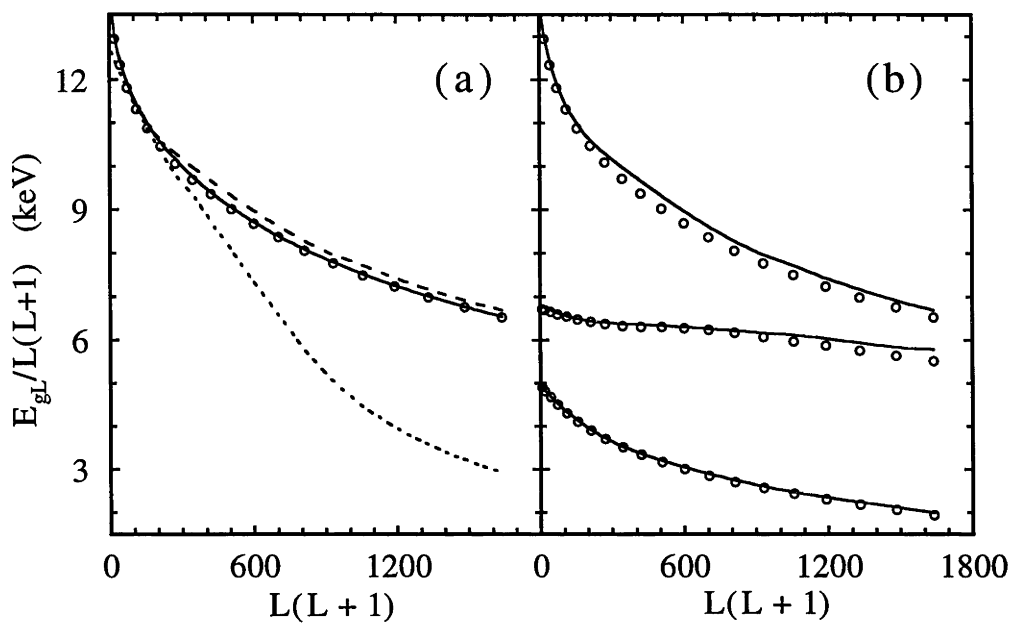

Figure 4.1: Comparison of the ground band energies obtained from the $1/N$ expansion with the exact diagonalisation results (circles). In (a) different lines refer to the second layer calculation (dotted line), the third layer (dashed line), and the numerical one to all orders (solid line). In (b) the lines correspond to the third layer results obtained with $\eta_d = 1.5$, $\eta_g = 4.5$ (top), $\eta_d = 0$, $\eta_g = 4.5$ (middle), and $\eta_d = 0$, $\eta_g = 0$ (bottom).

Before applying the $1/N$ expansion technique to real cases, we compare the expansion results with those obtained from an exact diagonalisation of the Hamiltonian [56]. Of necessity, the boson number is fixed at $N = 10$. The Hamiltonian parameters are as in Section 2.2 ($\kappa_2 = -20$ keV, $\kappa_4 = 0$, $q = 0.5$, $\eta_d = 1.5$, $\eta_g = 4.5$), except where noted. Figure 4.1 contains a comparison of the ground band energies normalised with $\bar{L} = L(L+1)$ so that they all have the same energy scale. In Figure 4.1(a), the convergence of the $1/N$ results obtained with the VAP procedure is illustrated. The second layer $1/N$ results (dotted line) rapidly diverge from the exact energies (circles) for spins $L > 2N$, and hence are not reliable in applications

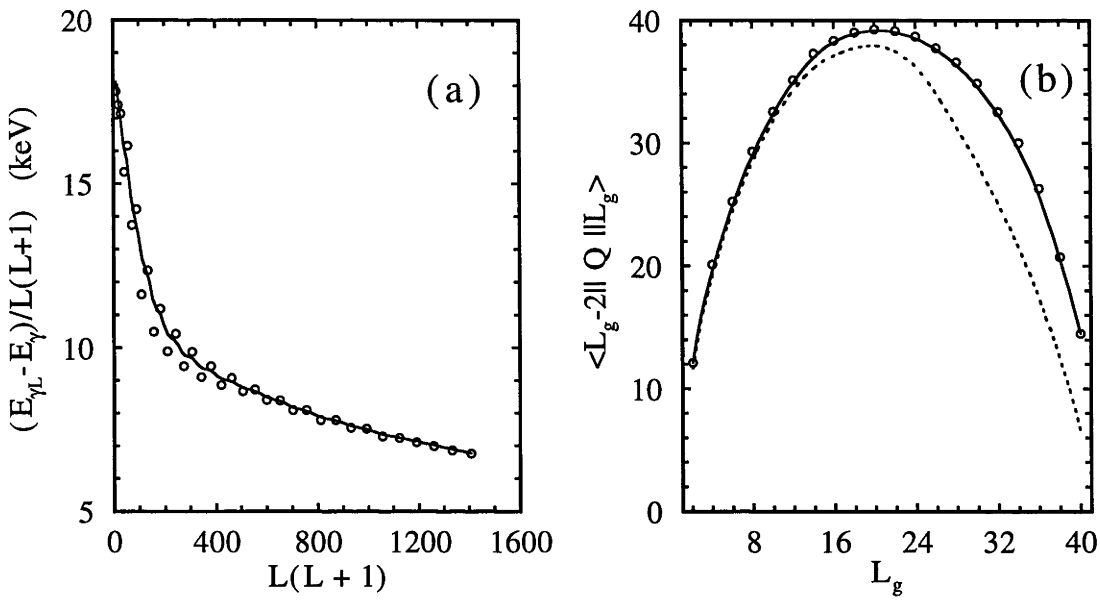

Figure 4.2: (a) Comparison of the γ-band energies obtained from the $1/N$ expansion with the exact diagonalisation results (circles). (b) Comparison of the yrast $E2$ transition m.e. obtained from eq. (5.2) (dashed line) with the exact diagonalisation results (circles). The solid line shows the numerical evaluation of the m.e. to all orders.

to high-spin states. The third layer results (dashed line), on the other hand, track the exact energies within a few percent up to the maximum spin $L = 4N$. Using the numerical technique described in Appendix D, one can evaluate the $1/N$ expansion to all orders (solid line) which exhibits an almost perfect agreement with the exact energies. This study demonstrates that the third layer $1/N$ expansion results are both necessary and sufficient for a reliable description of high-spin sates. In Figure 4.1(b), the effect of the one-body energies on the accuracy of the third layer results is demonstrated. The top line is the same as the one in Figure 4.1(a). The middle and bottom lines compare the exact and $1/N$ results for $\eta_d = 0$, $\eta_g = 4.5$, and $\eta_d = 0$, $\eta_g = 0$, respectively. It is seen that the agreement for a pure quadrupole Hamiltonian is excellent at all spins, while the addition of g-boson energy leads to a few percent deviation at very high-spins. In a typical situation with d-boson energy, this few percent deviation starts occurring at medium high-spins.

In Figure 4.2(a), we present a similar study for the γ-band energies. The average behaviour is well reproduced by the $1/N$ expansion results but staggering is underestimated. This happens because staggering is caused mainly by band mixing between the ground and γ-bands which is not included in the present calculations (note that the odd-spin levels, which are not affected by band mixing, are very well reproduced). We have not attempted to include band mixing effects here because they are strongly suppressed for the larger N values used in deformed nuclei [79], and hence they can be ignored for the purposes of this work. Finally, in Figure 4.2(b), we compare the $1/N$ results for the yrast $E2$ transition m.e. with the exact ones (circles). The dashed line shows the first layer result obtained from eq. (5.2) which is accurate to a few percent for $L < 2N$, but progressively gets worse with increasing spin. The solid line shows the numerical evaluation of eq. (4.45), which is complete to all orders in $1/N$. The agreement with the exact results becomes almost perfect in this case, including the highest spins which are dominated by the g bosons.

CHAPTER 5

A study of high-spin states

In the following sections, we first present a brief study of the effect of the d-boson energy in the sd-model. These results will provide us with better insight in understanding the moment of inertia problem in the IBM. On the other hand, there have been conjectures [42, 79] that inclusion of the g bosons may resolve this problem. Therefore, it is worth carrying out a similar study of the g boson effects in the sdg-IBM with a minimal extension of the Hamiltonian given by eq. (2.8). After that, a detailed systematic study of the sdg-IBM will be presented. This study involves a Hamiltonian consisting of the one-body energies and both the quadrupole and hexadecapole interactions. Application of the $1/N$ results is focused on the high-spin states in rare-earth and actinide nuclei as their description in the IBM has been a source of criticism [42] which has not been adequately addressed previously. To constrain the model parameters properly, both the high-spin data and the low-lying band structures are described simultaneously. Finally, a brief discussion on the applications of the analytic formulae to the study of superdeformed nuclei will be presented. (All the figures are shown at the end of the chapter.)

5.1 Systematic studies

The analytic formulae obtained in Chapter 4 have the advantage that one can easily perform systematic studies of key physical quantities and obtain useful insights on the effects of various parameters. In this section, we present such studies that shed light on the above problems and suggest more appropriate Hamiltonians for the description of deformed nuclei.

To simplify the discussion, we rewrite the ground and γ-band energies as

$$E_{gL} = \lambda_{g1}\bar{L} + \lambda_{g2}\bar{L}^2 + \lambda_{g3}\bar{L}^3, \quad E_{\gamma L} = E_\gamma + \lambda_{\gamma 1}\bar{L} + \lambda_{\gamma 2}\bar{L}^2 + \lambda_{\gamma 3}\bar{L}^3, \tag{5.1}$$

where the coefficients λ_n can be read from the respective energy expressions. eq. (5.1) is the familiar rotational expansion of the level energies used in the geometrical model [4]. The difference between the two models is that in the IBM the coefficients λ_n follow from an underlying Hamiltonian (which is used in describing other properties) whereas in the geometrical model they are directly extracted from the data. The moment of inertia problem raised in Ref. [42] refers to the fact that i) the λ_1 coefficient gets a substantial contribution from the dipole interaction, $L \cdot L$, which has no dynamical content, ii) the λ_2 coefficient is much smaller than the experimental values, and iii) the variation in λ_1 among different bands cannot be described. All three problems are in fact interrelated. Although the second can be resolved by renormalising the moment of inertia at high-spins (e.g. by modifying $L\cdot L \rightarrow L\cdot L/(1+fL\cdot L)$ [43]), such modifications are purely kinematical in origin and do not address the dynamical problem. Further quantities of interest in the study of high-spin states are the yrast $E2$ transitions. For systematics, it is sufficient to consider the first layer $1/N$ expansion result which has the generic form

$$\langle L-2 \parallel T(E2) \parallel L\rangle = e_2 N \hat{L} \langle L0\,20|L-2\,0\rangle [m_1 + m_2 L(L-1)] \tag{5.2}$$

where the coefficients m_n are given in Ref. [79]. The first term in eq. (5.2) gives the familiar rigid-rotor result. The second term is negative and is responsible for the falloffs predicted in $E2$ transitions.

In presenting systematics, it is convenient to use ratios which eliminate the undesired effects of the scale parameters κ_2 and N. The energy scale can be fixed, for example, by fitting κ_2 to the excitation energy of the γ band, E_γ.

sd-model

Here we carry out a systematic study of the predictions for high-spin states in the *sd*-model by using the standard Hamiltonian given by eq. (2.6). Since $L \cdot L$

does not play any role in the dynamics of the system, its effect will not be discussed further (it can be easily restored by changing λ_{g1} to $\lambda_{g1}+\kappa'$). In Figure 5.1(a) - (d), four such quantities as a function of $q=\chi/\chi_{SU3}$ for various values of $\eta_d=\varepsilon_d/N\kappa$ are shown. We comment on their behaviour and contrast them with the experimental data below.

(a) $E_\gamma/N\lambda_{g1}$: This ratio relates the energy scales of the γ and ground bands, and its mismatch with experiment has been a source of criticism [42]. It is around 4-5 in the rare-earth region and increases to 8 - 10 in the actinides. The SU(3) limit ($q=0,\eta_d=0$) is seen to give the maximum value which overestimates the experimental values by a factor of 2 - 4. It decreases rapidly with ε_d and q though, and through a judicious use of these parameters, it should be possible to describe this ratio (and hence the moment of inertia) without using the $L\cdot L$ term.

(b) $N^2\lambda_{g2}/\lambda_{g1}$: This ratio measures the deviation from the rigid rotor behaviour (SU(3) limit) due to the loss of pairing. It ranges from about -0.2 in the rare-earth region to -0.1 in the actinides. Clearly, it cannot be explained by the standard *sd*-IBM Hamiltonians currently in use for deformed nuclei which assume $\eta_d=0$, $q\sim 0.4-0.5$. However, it is quite sensitive to η_d values and the experimental range can be easily attained by including the *d*-boson energy in the Hamiltonian.

(c) $N^4\lambda_{g3}/\lambda_{g1}$: There is some uncertainty in the extraction of this ratio from data, especially in the rare-earth region. In the actinides, it is about 0.01. It depicts even more sensitivity to both q and η_d, and therefore its description should not pose any problems.

(d) N^2m_2/m_1: As there is no boson cutoff effect, experimentally this ratio is consistent with zero. For $\eta_d=0$, it remains rather flat at the SU(3) value which gives the maximum possible effect. Introduction of the one-body energy, however, reduces it substantially, becoming more in line with experiments.

According to the above results, the *d*-boson energy plays a significant role in altering the moment of inertia of the ground band, although for small values ($\eta_d\sim 1$), its effect on low-lying states is negligible and it is not really needed in their description [80]. The above analysis indicates that breaking of the SU(3) limit by

either the pairing interaction [42] or by varying the χ parameter [16] does not lead to a soft enough energy surface which is the main reason for the perceived moment of inertia problem in the *sd*-IBM. The obvious way towards a softer energy surface is to include the *d*-boson energy in the Hamiltonian which is seen to vastly improve the description of the spin-dependent terms in the ground energies and $E2$ transitions.

sdg-**IBM**

The problem of the missing moment of inertia at first was interpreted as due to the insufficient collectivity of the *sd*-boson system. One of the obvious solution is to introduce the *g*-boson degree of freedom into the system. It will be interesting to see how much the *g* boson can help in solving the moment of inertia problem. In the following, we study the *g*-boson effects by using (i) a minimal *sdg*-Hamiltonian (eq. (2.8)) and (ii) a more general Hamiltonian (eq. (2.9)), consisting of the *d*-boson energy and the hexadecapole interaction.

Case (i): Effect of the *g* bosons in a minimal *sdg*-Hamiltonian

The minimal *sdg*-Hamiltonian used in this study, consists of the quadrupole interaction and the *g*-boson energy as shown in eq. (2.8). The dipole interaction is deliberately omitted for the reason mentioned earlier. In order to limit the number of parameters, we choose the (q, q, q) parametrisation defined in Section 2.2. In Figure 5.2, we plot the same ratios that were presented in Figure 5.1 as a function of q for various values of $\eta_g = \varepsilon_g/N\kappa$. Before commenting on specific ratios, we point out some general features. For large η_g, the *g* bosons decouple and the results converge to those of the *sd*-model shown in Figure 5.1. This convergence is apparent from the overlap of lines in Figures 5.2(a) - (b) but requires even larger values of η_g in the case of Figure 5.2(c) - (d). It is harder to pin down realistic values for η_g due to lack of data, nevertheless, we quote the literature values for comparison which range from 3 - 6.

(a) $E_\gamma/N\lambda_{g1}$: The inclusion of *g* bosons increases this ratio which is contrary to the experimental trend. However, for realistic η_g values, this adverse change is too

small to worry about.

(b) $N^2\lambda_{g2}/\lambda_{g1}$: This ratio also increases (in absolute value) which is good but again too small for realistic η_g values to have any impact.

(c) $N^4\lambda_{g3}/\lambda_{g1}$: This ratio shows some sensitivity to the g bosons, however, it is nowhere near the effect of η_d in Figure 5.1(c), and therefore not likely to have much relevance.

(d) N^2m_2/m_1: The boson cutoff was the original reason for the introduction of g bosons and it is clear from this figure why. In the SU(3) limit, this ratio is reduced by a factor of 4 compared to the sd-IBM. Its q and η_g dependence, however, is opposite to that of Figure 5.1(d), and things get worse away from the SU(3) limit. For realistic parameters, the reduction from the sd-IBM result (with $\eta_d = 0$) is less than 40% which is certainly not enough, and one needs the d-boson energy to reduce it further.

The somewhat surprising conclusion of the above systematic study is that introduction of the g bosons, though necessary to describe states with $L > 2N$, hardly improves the dynamics of the boson system. The problems attributed to the sd-IBM are, in fact, due to not having a soft enough energy surface and can only be resolved by including the d-boson energy in the Hamiltonian (and not solely by introduction of g bosons).

Case (ii): Systematic study for a general sdg-Hamiltonian

The above study indicates that, the minimal sdg-IBM Hamiltonian is inadequate and inclusion of the d-boson energy and hexadecapole interaction appears to be necessary to improve the situation in regard to the spin dependence of the moment of inertia and yrast B($E2$) values. In addition, the description of excited bands appears to require the hexadecapole interaction. Since the g-boson energy has a negligible dynamical effect, it is not varied but fixed at $\eta_g = 4.5$ in this study. Similar to the above, we discuss five ratios as a function of q for various values of (i) $\eta_d = \varepsilon_d/N\kappa_2$ and (ii) $\zeta_4 = \kappa_4/\kappa_2$. The parameter q is varied from 0 - 1 which covers the whole range of the quadrupole operator from the γ-unstable to the SU(3)

limit. η_d is varied from 0 - 2 in 10 equal steps, and ζ_4 from 0 - 0.5 in 5 equal steps, which cover the range of values used in the applications. Negative values of ζ_4 on the whole are found to have an adverse effect and hence are not considered. In the η_d systematics study, $\zeta_4 = 0$ is used as its precise value does not have much influence on the results. In the ζ_4 study, however, the choice of η_d does have an impact, and we adopt $\eta_d = 1.5$ which is the average value used in the applications which will be presented later. Below, we comment on the behaviour of each ratio and contrast them with the experimental data. For reference, we note that q assumes values around ~ 0.5 in the rare-earth nuclei and ~ 0.7 in the actinides.

1) $E_\gamma/N\lambda_{g1}$ (Figure 5.3): This ratio decreases with η_d (Figure 5.3(a)), indicating that the d-boson energy has similar effect on both the sd- and sdg-models. Figure 5.3(b) contains a similar study of the effect of the hexadecapole interaction which is seen to be going in the right direction of reducing this ratio, but is too small to have any impact.

2) $N^2\lambda_{g2}/\lambda_{g1}$ (Figure 5.4(a), (b)): The d-boson energy has the effect of softening the rigid rotor. The minimal sdg-Hamiltonian (with $\eta_d = 0$, $\kappa_4 = 0$), gives values an order of magnitude smaller (Figure 5.4(a)) and hence fails to account for the spin dependence of moment of inertia as first pointed out in Ref. [42]. In Figure 5.4(b), the hexadecapole interaction is seen to have a coherent effect in further reducing this ratio away from the rigid rotor limit.

3) $N^2\lambda_{\gamma 2}/\lambda_{\gamma 1}$ (Figure 5.4(c), (d)): An identical study for the γ band indicates broadly similar but somewhat larger effects of the d-boson energy on the behaviour of γ band moment of inertia (Figure 5.4(c)). A softer moment of inertia in the γ band is in line with data in most deformed nuclei though there are a few exceptions as will be seen in the specified applications to be discussed. The hexadecapole interaction has an opposite effect (Figure 5.4(d)) which reduces the difference between the ground and γ band moment of inertia caused by the d-boson energy.

4) $\lambda_{\gamma 1}/\lambda_{g1}$ (Figure 5.5(a), (b)): This ratio compares the moment of inertia of ground and γ-bands. It fluctuates within a band of $\pm 10\%$ across the deformed nuclei. The earlier IBM calculations gave results near one and could not accommodate

such fluctuations. In Figure 5.5(a) - (b), it is shown that inclusion of the d-boson energy can increase this ratio by up to 20 - 30%, while the hexadecapole interaction can reduce it significantly (up to 20 - 30%) thereby covering the whole range of fluctuations.

5) N^2m_2/m_1 (Figure 5.5(c), (d)): From Figure 5.5(c), it is clear that the d-boson energy plays an important role in reducing the boson cutoff effect on the yrast B($E2$) values. The effect of the hexadecapole interaction on this ratio (Figure 5.5(d)) is similar to that displayed in Figure 5.4(b). It is positive but comparatively too small to make a difference.

Another ratio, namely, $N^4\lambda_{g3}/\lambda_{g1}$ is also of interest especially at very high-spins ($L = 20 - 30$) where the cubic term in eq. (5.1) plays an important role [55]. It exhibits a similar dependence on η_d and ζ_4 as $N^2\lambda_{g2}/\lambda_{g1}$ as shown in Figure 5.4(a) - (b) and so is not discussed further.

The d-boson energy has been neglected in most studies of deformed nuclei, presumably due to the success of the CQF (variable χ, $\varepsilon_d = 0$) in explaining the energy and $E2$ transition systematics of low-lying states [16]. In fact, for small values ($\eta_d \sim 1$), its effect on low-lying states is negligible and it is not really needed in their description [80]. The CQF, however, basically leads to a rigid moment of inertia and cannot explain either the known spin dependence or variation among different bands of that quantity. The obvious way to have a softer energy surface is to include the d-boson energy in the Hamiltonian which is seen to vastly improve the description of the spin-dependent terms in the level energies and $E2$ transitions. The hexadecapole interaction performs a similar function but has a much smaller effect, nevertheless, there are variations in the moment of inertia which could not be reproduced without the hexadecapole interaction.

5.2 Applications to deformed nuclei

In the light of the systematic trends discussed above, we carry out fits to the rare-earth nuclei $^{158-162}$Dy, $^{164-168}$Er, $^{168-176}$Yb, $^{170-178}$Hf and the actinides $^{228-232}$Th, $^{234-238}$U [62]. The isotopes chosen are all well deformed rotors with energy ratio

E_4/E_2 close to 3.3. We have excluded those exhibiting backbending as their proper description requires inclusion of two-quasiparticle states in the model space. While we mainly focus on the description of high-spin states, which has not been done before, we also consider a selected set of low-lying bands. This is important in properly constraining the model parameters so that the results obtained are valid in a broader sense and not just for a small subset of observables. The *sdg*-IBM parameters used in the fits are listed in Table 5.1. Each parameter is particularly sensitive to a certain set of observables which simplifies the fitting process. For example, q is determined from interband $E2$ transitions, η_d from the spin dependence of the moment of inertia and E_γ (cf. Figures 5.3, 5.4(a) - (b)), η_g from E_{3+}, E_{4+}, ζ_4 from the moment of inertia variation (cf. Figure 5.5), and finally κ_2 from the overall energy scale of the spectrum. The parameters are either constant in a given isotope chain or change smoothly in accordance with the vibration-rotation shape transition, e.g., η_d decreases with increasing N as the nuclei considered become more rotational.

The representative observables chosen to describe the low-lying band structure are the band excitation energies E_β, E_γ, E_{3+}, E_{4+} (Table 5.2), the interband $E2$ m.e. for $2_{\beta,\gamma} \rightarrow 0_g$ transitions (Table 5.2), and the $E4$ m.e. for $4_{\gamma,3+,4+} \rightarrow 0_g$ transitions (Table 5.4). Note that the $E4$ m.e. are normalised with the ground transition, so that an effective $E4$ charge is not needed in Table 5.1. With a few exceptions to be discussed below, the general trends of the β and γ band systematics are well reproduced by the calculations. The sudden fluctuations seen in some of the band-head energies (Table 5.2) can be accommodated by a careful tuning of the parameters. Since our aim here is to delineate the systematic features of high-spin states, rather than to obtain refined fits to individual nuclei, we have not attempted such an improvement. Description of interband $E2$ transitions is one of the strong points of the IBM, and as can be seen from Table 5.2, they are very well reproduced using almost constant q values. The parameters in the $E4$ operator are determined from the conditions in eq. (2.16), hence the $E4$ m.e. ratios presented in Table 5.4 are parameter free predictions of the model. Again the overall agreement with the

Table 5.1: Parameters used in the *sdg*-IBM calculations. κ_2 is in keV and e_2 in eb.

Nucleus	N	κ_2	ζ_4	q	η_d	η_g	e_2
^{158}Dy	13	19.8	0.30	0.50	1.90	5.0	0.13
^{160}Dy	14	19.9	0.30	0.50	1.77	4.6	0.13
^{162}Dy	15	19.3	0.35	0.50	1.60	4.5	0.13
^{164}Er	14	22.0	0.40	0.50	1.50	5.0	0.14
^{166}Er	15	21.2	0.40	0.50	1.42	4.7	0.13
^{168}Er	16	23.1	0.40	0.50	1.22	4.6	0.13
^{168}Yb	14	19.7	0.35	0.50	1.68	5.0	0.14
^{170}Yb	15	20.6	0.35	0.50	1.63	4.7	0.13
^{172}Yb	16	20.5	0.25	0.60	1.78	5.0	0.13
^{174}Yb	17	22.2	0.25	0.60	1.66	4.1	0.12
^{176}Yb	16	20.1	0.35	0.60	1.83	5.3	0.12
^{170}Hf	13	19.1	0.10	0.50	2.04	4.9	0.14
^{172}Hf	14	19.5	0.10	0.50	1.99	4.5	0.13
^{174}Hf	15	20.7	0.10	0.50	1.91	4.1	0.13
^{176}Hf	16	22.0	0.10	0.50	1.80	3.5	0.13
^{178}Hf	15	21.8	0.10	0.50	1.83	4.1	0.13
^{228}Th	10	19.7	0.30	0.68	1.60	3.0	0.20
^{230}Th	11	15.5	0.40	0.68	1.59	4.4	0.20
^{232}Th	12	14.6	0.40	0.68	1.58	4.4	0.20
^{234}U	13	14.9	0.20	0.70	1.62	3.5	0.18
^{236}U	14	16.4	0.20	0.70	1.57	3.2	0.17
^{238}U	15	17.7	0.20	0.70	1.56	2.8	0.17

data is reasonable which gives confidence on the choice of the $E4$ operator. The quality of agreement obtained in Tables 5.2 - 5.4 indicates that the limited set of *sdg*-IBM parameters (Table 5.1) can describe the basic features of the low-lying bands in deformed nuclei.

In the study of high-spin states, we include the level energies for the ground and γ bands, and the yrast $E2$ transitions for each set of isotopes (Figures 5.6 - 5.17). We first comment on their general features. In all cases, the moment of inertia strongly deviates from the rigid rotor behaviour which would be represented by a horizontal line in the figures. Further, this deviation is not linear but curves up with increasing spin underscoring the importance of the cubic term in eq. (5.1).

Table 5.2: Comparison of the β, γ, and $K = 3^+, 4^+$ (single-phonon) band energies (in keV) with the *sdg*-IBM calculations in the and actinide regions. The data are from the most recent Nucl. Data Sheets for each nucleus.

	E_β		E_γ		E_{3+}		E_{4+}	
Nucleus	Cal.	Exp.	Cal.	Exp.	Cal.	Exp.	Cal.	Exp.
^{158}Dy	916	991	965	946	1461	-	1935	1895
^{160}Dy	1204	1275	998	966	1512	-	2085	-
^{162}Dy	1284	1205	1048	888	1617	-	2201	1536
^{164}Er	1233	1246	1145	860	1634	1702	2003	-
^{166}Er	1275	1460	1138	786	1704	-	2376	-
^{168}Er	1590	1217	1345	821	1892	1654	2483	2238
^{168}Yb	1085	1156	1028	984	1470	1452	1706	-
^{170}Yb	1218	1069	1138	1145	1501	-	1857	1408
^{172}Yb	1345	1043	1385	1466	1799	1663	2403	2073
^{174}Yb	1589	1487	1554	1634	1810	-	2545	-
^{176}Yb	1329	1779	1324	1261	1685	-	2407	-
^{170}Hf	868	880	985	961	1482	-	1528	-
^{172}Hf	982	871	1016	1075	1530	-	1604	-
^{174}Hf	1108	827	1137	1227	1547	1303	1669	-
^{176}Hf	1298	1150	1278	1341	1671	1578	1840	-
^{178}Hf	1231	1199	1202	1175	1710	1728	1809	1848
^{228}Th	791	832	846	969	1082	-	1458	-
^{230}Th	734	635	792	781	1004	-	1519	-
^{232}Th	769	730	813	785	1041	-	1574	-
^{234}U	825	809	871	927	1253	1496	1566	1723
^{236}U	986	919	1002	958	1325	-	1799	-
^{238}U	1080	993	1086	1060	1328	1059	1965	-

Note that because of the ample data available, these features are most clear in the ground bands and to a lesser extent in the γ bands. The yrast $E2$ m.e., on the other hand, follow closely the rigid rotor values with no sign of a boson cutoff effect. As emphasised in Section 2.2, these properties can be explained in the IBM by including the d-boson energy in the Hamiltonian. Below we comment on the specific features of each isotope chain.

1) $^{158-162}$Dy (Figures 5.6, 5.8(Left)): Among the deformed nuclei considered in this work, ^{158}Dy, together with ^{170}Hf, exhibit the largest changes in moment of in-

Table 5.3: A comparison of the interband $E2$ transitions (in eb) with the *sdg*-IBM calculations in the rare-earth and actinide regions. The data are from the most recent Nucl. Data Sheets for each nucleus.

	$\langle 2_\beta \|\| T(E2) \|\| 0_g \rangle$		$\langle 2_\gamma \|\| T(E2) \|\| 0_g \rangle$	
Nucleus	Cal.	Exp.	Cal.	Exp.
^{158}Dy	0.21	0.23 ± 0.02	0.41	0.39 ± 0.04
^{160}Dy	0.19	-	0.34	0.27 ± 0.04
^{162}Dy	0.17	-	0.35	0.35 ± 0.02
^{164}Er	0.17	-	0.34	0.37 ± 0.02
^{166}Er	0.16	-	0.41	0.39 ± 0.02
^{168}Er	0.15	<0.03	0.34	0.36 ± 0.01
^{168}Yb	0.20	0.22 ± 0.01	0.35	0.36 ± 0.04
^{170}Yb	0.19	0.17 ± 0.02	0.32	0.28 ± 0.03
^{172}Yb	0.16	0.09 ± 0.01	0.26	0.21 ± 0.03
^{174}Yb	0.14	-	0.24	0.22 ± 0.03
^{176}Yb	0.14	-	0.27	0.23 ± 0.03
^{170}Hf	0.23	-	0.36	-
^{172}Hf	0.19	-	0.31	-
^{174}Hf	0.20	-	0.33	0.37 ± 0.04
^{176}Hf	0.18	0.21 ± 0.02	0.34	0.35 ± 0.01
^{178}Hf	0.21	-	0.32	0.34 ± 0.02
^{228}Th	0.18	-	0.28	-
^{230}Th	0.20	0.21 ± 0.05	0.34	0.35 ± 0.06
^{232}Th	0.23	0.31 ± 0.07	0.38	0.36 ± 0.04
^{234}U	0.21	<0.24	0.32	0.35 ± 0.04
^{236}U	0.20	-	0.30	-
^{238}U	0.19	0.23 ± 0.03	0.31	0.36 ± 0.04

ertia. These nuclei have the lowest boson numbers among the rare-earth set and are clearly influenced by the vibration-rotation phase transition as indicated by the larger η_d values used. The ground band energies (Figure 5.6(Left)) are well described with relative errors of about 1-2%. The trend in γ band energies (Figure 5.6(Right)) is similarly reproduced (note the different scales in Figure 5.6(Left) - (Right)). The slight overprediction of energies here can be improved by fine tuning the hexadecapole interaction (cf. Figure 5.5(b)). The yrast $E2$ m.e. have been a sore point in applications of the sd-IBM to high-spin states due to the boson cutoff. For example,

Table 5.4: A comparison of the interband $E4$ transitions, normalised to inband ones, with the *sdg*-IBM calculations in the rare-earth and actinide regions. The data are from the most recent Nucl. Data Sheets for each nucleus.

	$\frac{\langle 4_\gamma \|T(E4)\|0_g\rangle}{\langle 4_g \|T(E4)\|0_g\rangle}$		$\frac{\langle 4_{3+} \|T(E4)\|0_g\rangle}{\langle 4_g \|T(E4)\|0_g\rangle}$		$\frac{\langle 4_{4+} \|T(E4)\|0_g\rangle}{\langle 4_g \|T(E4)\|0_g\rangle}$	
Nucleus	Cal.	Exp.	Cal.	Exp.	Cal.	Exp.
^{158}Dy	0.49	0.56 ± 0.44	1.14	-	0.32	-
^{160}Dy	0.50	0.63 ± 0.24	1.08	-	0.27	-
^{162}Dy	0.37	-	1.06	-	0.28	-
^{164}Er	0.44	-	1.05	-	0.23	-
^{166}Er	0.53	-	1.00	-	0.18	-
^{168}Er	0.46	1.32 ± 0.72	0.95	0.60 ± 0.33	0.15	0.25 ± 0.15
^{168}Yb	0.50	-	0.95	-	0.20	-
^{170}Yb	0.60	-	0.89	-	0.14	-
^{172}Yb	0.53	0.20 ± 0.19	0.82	0.69 ± 0.57	0.09	-
^{172}Yb	0.36	0.20 ± 0.19	0.78	0.69 ± 0.57	0.16	-
^{174}Yb	0.44	-	0.73	0.54 ± 0.29	0.11	-
^{176}Yb	0.37	-	0.81	-	0.17	-
^{170}Hf	0.44	-	1.17	-	0.43	-
^{172}Hf	0.45	-	1.12	-	0.38	-
^{174}Hf	0.50	-	1.04	-	0.28	-
^{176}Hf	0.44	-	1.01	-	0.28	-
^{178}Hf	0.43	-	1.08	-	0.34	-
^{228}Th	0.55	-	0.62	-	0.02	-
^{230}Th	0.44	-	0.71	-	0.07	-
^{232}Th	0.48	-	0.68	-	0.05	-
^{234}U	0.48	-	0.61	-	0.02	-
^{238}U	0.50	-	0.58	-	0.02	-

in ^{158}Dy, the sd-IBM would predict band termination at $L = 26$ which is not seen in the data (Figure 5.8(Left)). This problem has been resolved in the present *sdg*-IBM calculations which account for the yrast $E2$ data very well (Figure 5.8(Left)). A side remark for ^{162}Dy is that the band excitation energies in this nucleus do not follow the trend of $^{158-160}$Dy (Table 5.2), hence it requires individual attention for a better description.

2) $^{164-168}$Er (Figures 5.7, 5.8(Right)): The Er isotopes, and in particular ^{168}Er, are the exceptional cases mentioned above for which a consistent description of the data could not be obtained with our limited set of parameters. While the spin dependence of the ground and γ band moment of inertia (Figure 5.7) and the $E2$ m.e. (Figure 5.8(Right), Table 5.2) are well described, the band excitation energies are overpredicted (Table 5.2) and the $E4$ m.e. are rather poor (Table 5.4). The problem stems from the fact that, among all the deformed nuclei considered in this study, the Er isotopes have the lowest lying γ bands and the most rigid moment of inertia. As seen from Figure 5.4, these two quantities are correlated in the present parametrisation, so that a lower γ band obliges a softer moment of inertia (cf. Figure 5.4). Thus a proper description of the Er isotopes requires extension of the Hamiltonian (eq. (2.9)), and/or relaxation of the constraints on the quadrupole and hexadecapole parameters. For example, in a detailed study of ^{168}Er in the *sdg*-IBM [51], 14 parameters were employed. Here we will be content with exposing the exceptional nature of the Er isotopes and leave their detailed investigation for future work.

3) $^{168-176}$Yb (Figures 5.9 - 5.11): The Yb isotopes are uniformly well described and require little comment. In contrast to Er, the γ band energies in the Yb isotopes are higher in the spectra, which are well correlated with their relatively stiff moment of inertia (Figure 5.9). One point worthwhile to make is that the γ band moment of inertia is larger than that of the ground band; a fact which could not be explained without the hexadecapole interaction.

4) $^{170-178}$Hf (Figures 5.12 - 5.14): In the Hf isotopes, the γ band comes down but the moment of inertia is softer, and hence the correlation between the two quantities

is preserved (Figure 5.12). The staggering observed in the γ bands (Figure 5.13) requires inclusion of band mixing effects for a better description. Otherwise the data are well reproduced by the calculations.

5) $^{228-232}$Th (Figures 5.15, 5.17(Left)): Although boson numbers are relatively low in the actinide nuclei considered here, they exhibit characteristics of well deformed nuclei. The moments of inertia in actinides are typically twice as large as those in rare-earths so requiring smaller κ_2 values in analyses. The high-spin data are scarce in $^{228-230}$Th but in ^{232}Th, where data up to spin $L = 30$ are available, an excellent description is obtained. One interesting feature of the γ band moment of inertia in ^{232}Th is that it is larger and stiffer compared to the ground band. Both of these features require a large contribution from a hexadecapole interaction for their explanation.

6) $^{234-238}$U (Figures 5.16, 5.17(Right)): The most extensive high-spin data are available for the yrast bands in the U isotopes and that data are well described by the present calculations. The yrast $E2$ m.e. in the U isotopes (and ^{232}Th) were measured to check the boson cutoff predictions of the sd-IBM, i.e. $E2$ m.e. vanish at $L = 2N$. As seen in Figure 5.17(Right), the $E2$ data show no sign of falloff. This provides one of the strongest motivations for inclusion of the g bosons in the IBM. At the highest spins, the *sdg*-IBM calculations appear to underpredict the $E2$ measurements. That is not due to any boson cutoff effect but rather to deviation of the data from the rigid rotor values. That is, most models would have difficulty in explaining these $E2$ transition m.e. which are larger than the rigid rotor values (see, for example, [81]).

5.3 Applications to superdeformed nuclei

The analytic expressions derived for energies and $E2$ transitions will be useful in the study of high-spin states in both normal and superdeformed nuclei. Here, we present an application of the $1/N$ expansion formalism to superdeformation which is more topical and harder to be treated by numerical diagonalisation. In super IBM, as proposed by Otsuka and Honma [52–54], normal bosons are supplemented with

superdeformed bosons which correspond to the Cooper-pairs in the superdeformed potential. The number of superdeformed bosons, N_{super} is typically around 30-40, and because of large deformation, g boson effects are important. Thus, the super IBM offers a fertile ground for the application of the $1/N$ expansion. We use the energy formula given in eq. (4.17) to describe the superdeformed bands in the Hg isotopes. The dynamic moments of inertia, $\mathcal{J}^{(2)}$, which result from the quadrupole Hamiltonian are shown in Figure 5.18. The three quadrupole parameters q_{22}, q_{24}, q_{44} are scaled from their SU(3) values with a single factor q as in deformed nuclei. N_{super} is determined from microscopic calculations [52–54] and κ and q are fitted to the experimental data. A good description of experimental values of $\mathcal{J}^{(2)}$ (circles) is obtained. We note that the SU(3) limit corresponds to a rigid rotor and would give a flat line for $\mathcal{J}^{(2)}$. This happens because in the SU(3) limit, the mean fields x_l are constant (independent of L), and the structure does not change with rotation. In reality, one expects a gradual change in $\mathcal{J}^{(2)}$ due to the loss of pairing. The above study shows that this can be simulated by the breaking of the SU(3) symmetry which results in migration of the mean fields from s to d, and to g bosons with increasing spin. The q values obtained in the above fits indicate that this breaking is around 30%. It has been suggested that the identical band phenomenon may be due to an underlying symmetry [82, 83]. It would be of interest to pursue this suggestion by extending the present calculations to study other bands and also to predict the spectra properties of odd nuclei.

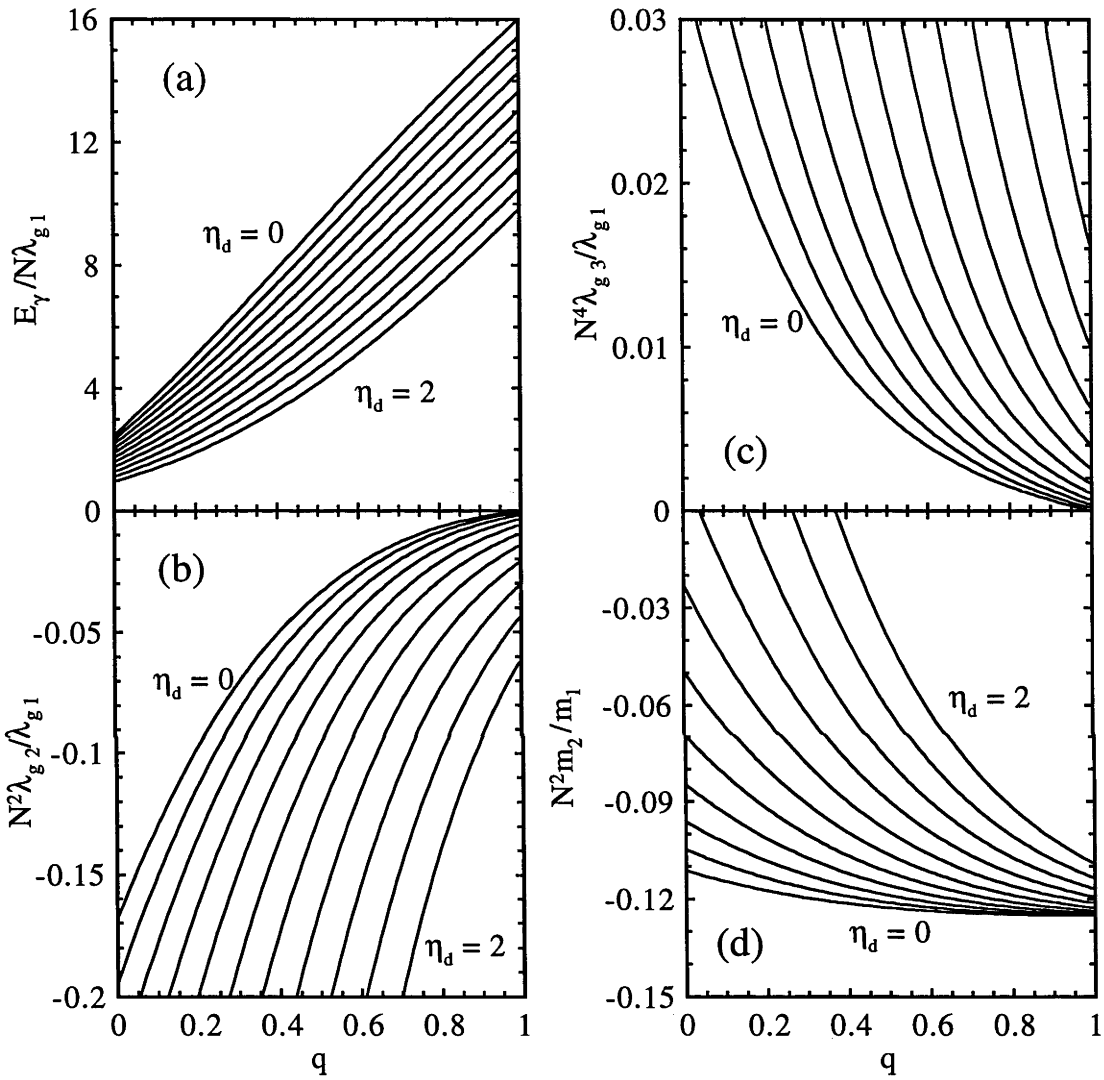

Figure 5.1: A sytematic study of moment of inertia (a), its spin dependence (b),(c), and the boson cutoff effect on $E2$ transitions (d) in the sd-IBM. The quadrupole parameter q is normalised to 1 in the SU(3) limit, and the d-boson energy parameter $\eta_d = \varepsilon_d/N\kappa$ is varied from 0-2 in 10 equal steps.

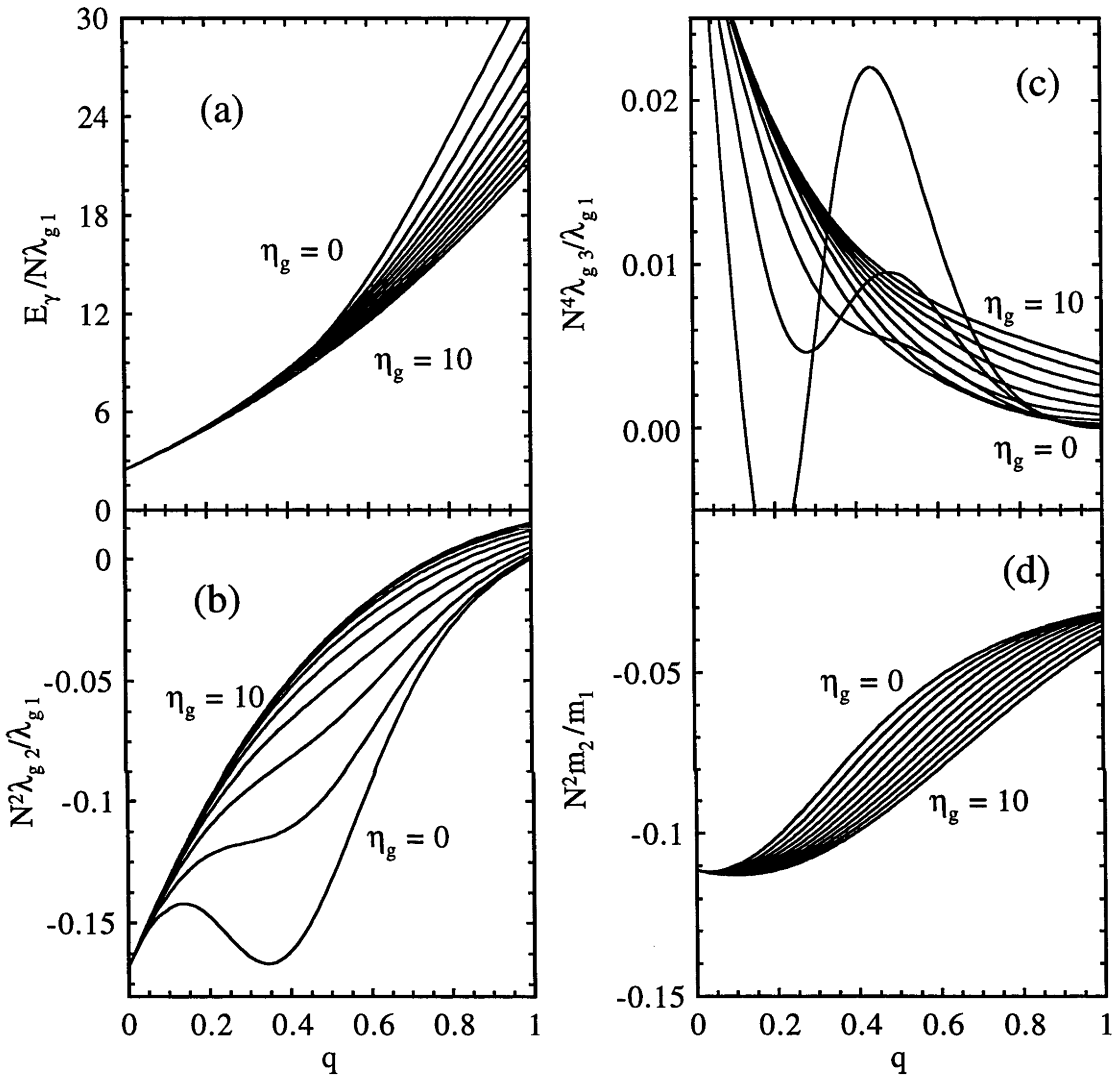

Figure 5.2: A sytematic study of the spin dependence of moment of inertia (a), its spin dependence (b),(c), and the boson cutoff effect on $E2$ transitions (d) in the *sdg*-IBM. The quadrupole parameters q_{22}, q_{24}, q_{44} are scaled from their SU(3) values with a single factor q, and the g-boson energy parameter $\eta_g = \varepsilon_g/N\kappa$ is varied from 0 - 10 in 20 equal steps.

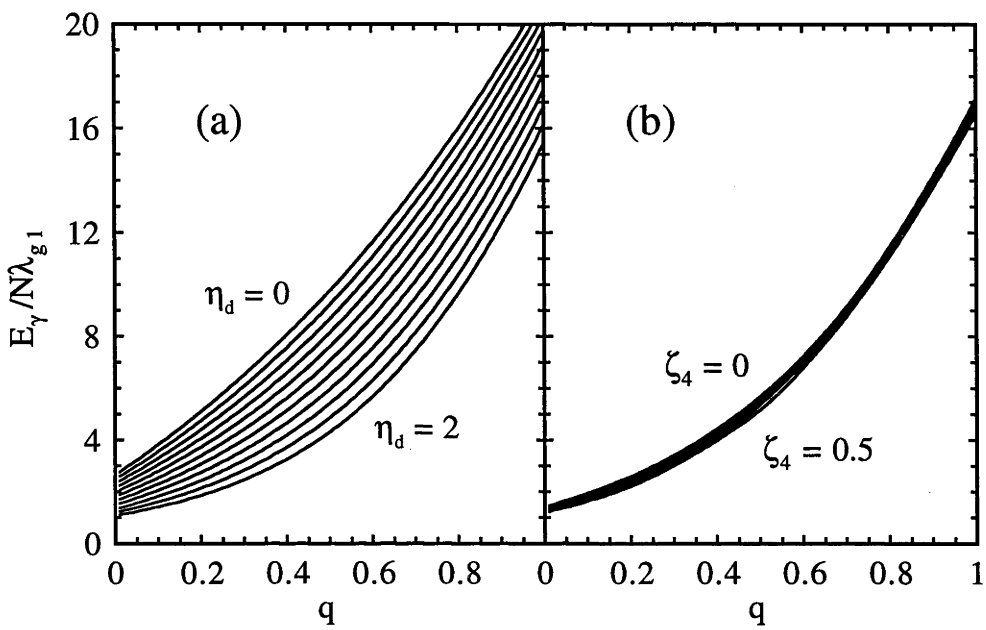

Figure 5.3: The effect of the d-boson energy (a) and the hexadecapole interaction (b) on the ratio $E_\gamma/N\lambda_{g1}$ which relates the energy scales of the γ and ground bands.

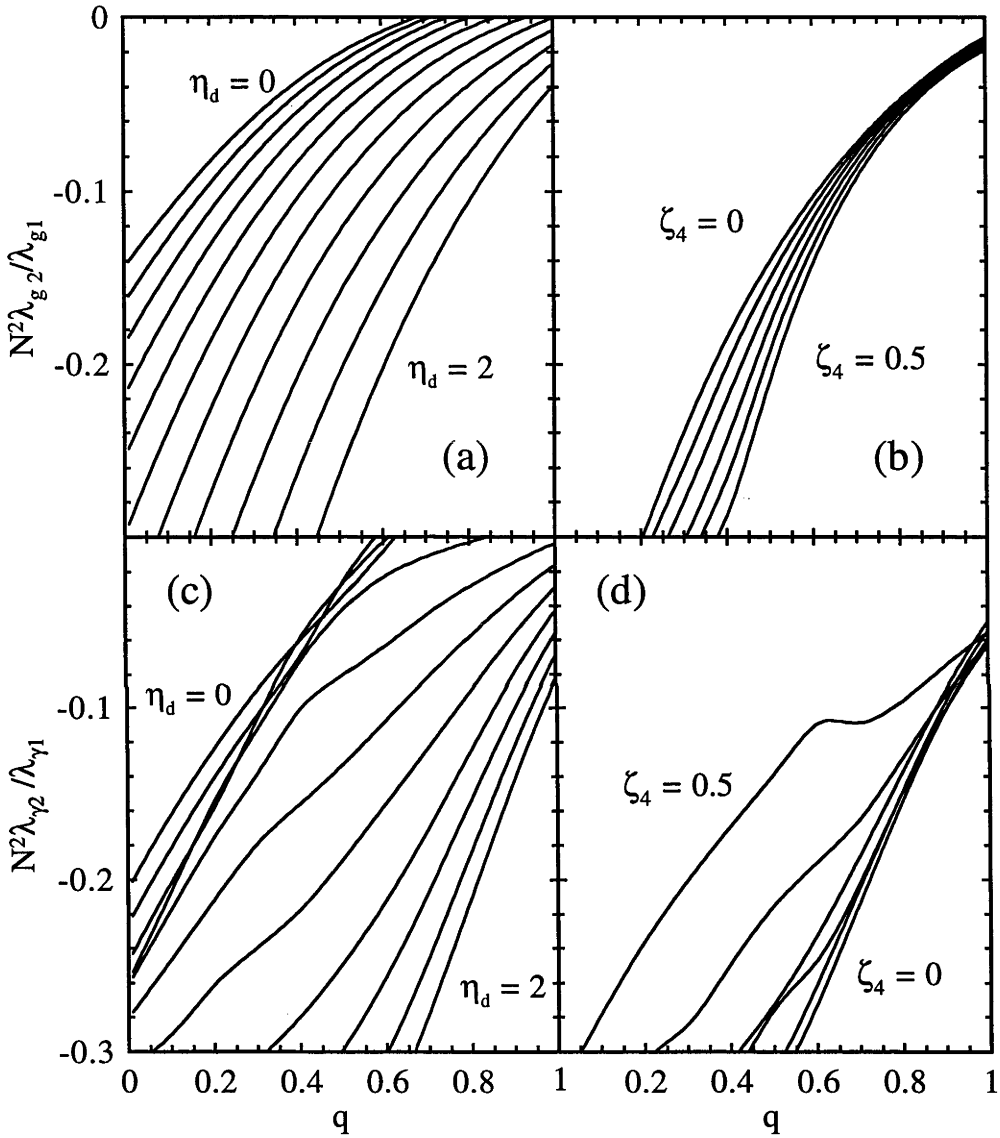

Figure 5.4: The effects of the d-boson energy and the hexadecapole interactions on the deviation of the moment of inertia from the rigid rotor behaviour in the ground band (a),(b) and γ-band (c),(d).

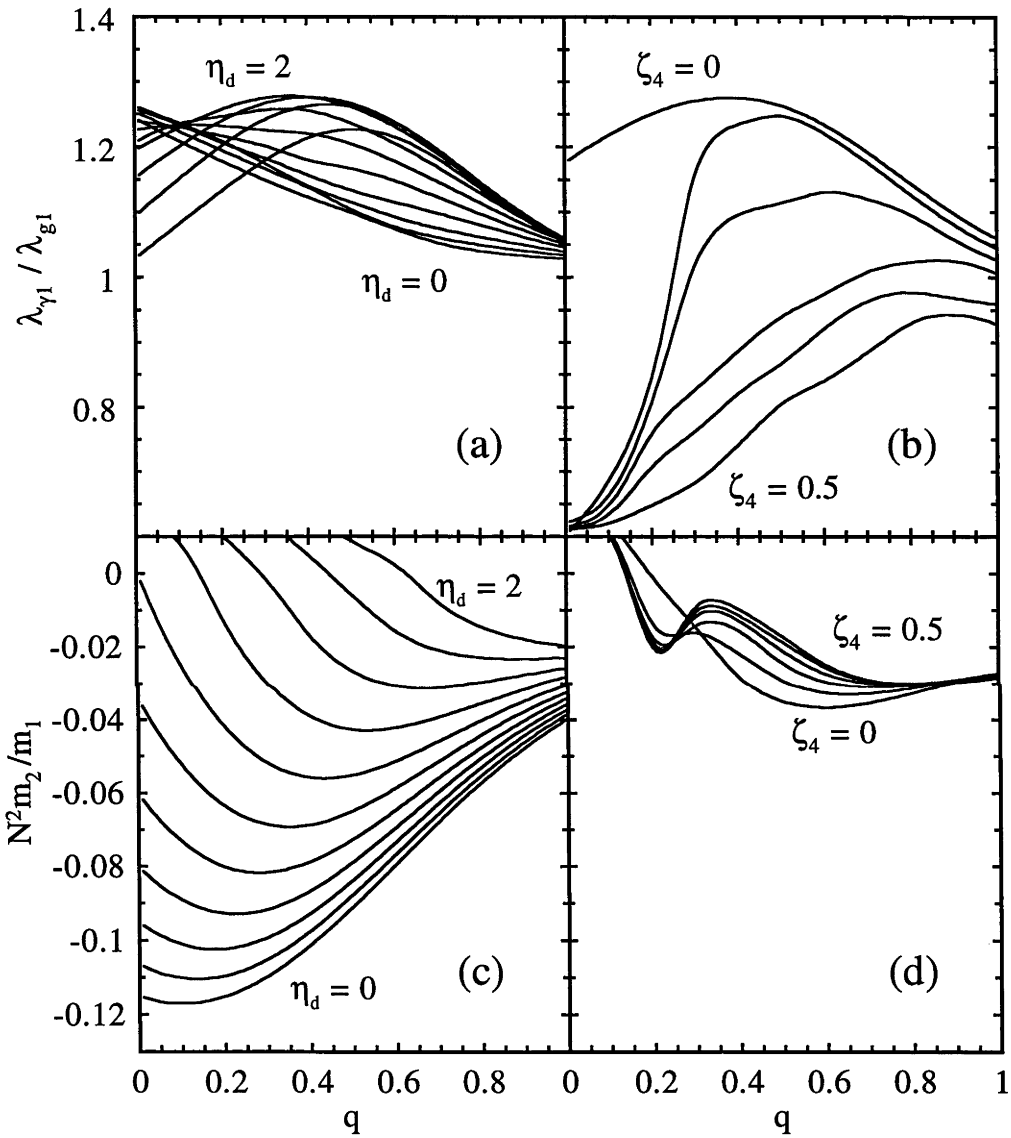

Figure 5.5: The effects of the d-boson energy and the hexadecapole interactions on the ratio $\lambda_{\gamma 1}/\lambda_{g1}$ (a),(b) and $N^2 m_2/m_1$ (c),(d). The quantity $N^2 m_2/m_1$ measures the boson cutoff effect.

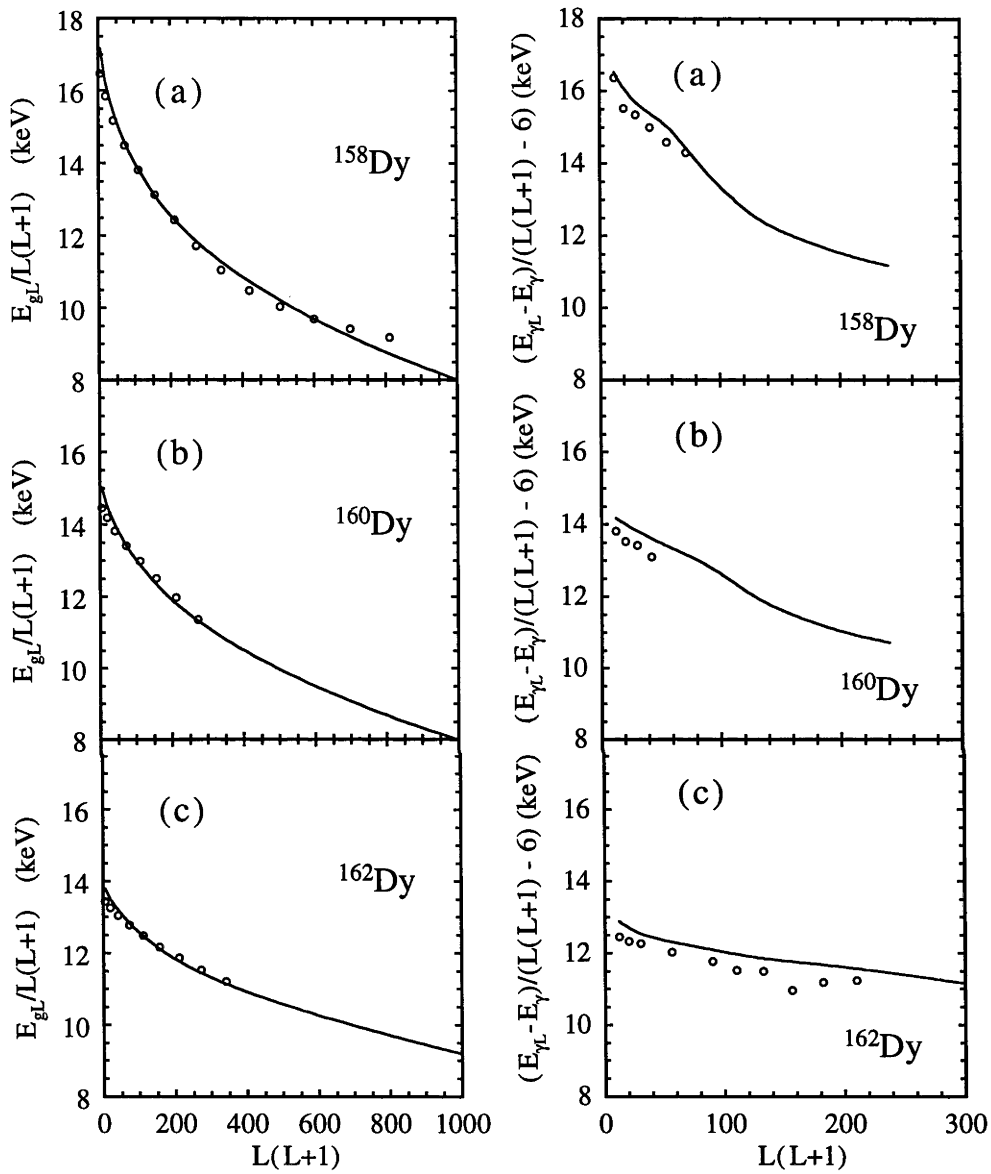

Figure 5.6: A comparison of the experimental (circles) and calculated (solid lines) energies of the ground band (left) and γ-band (right) in $^{156-160}$Dy. The scaled energies are in units of keV and the data are from Refs. [84–86].

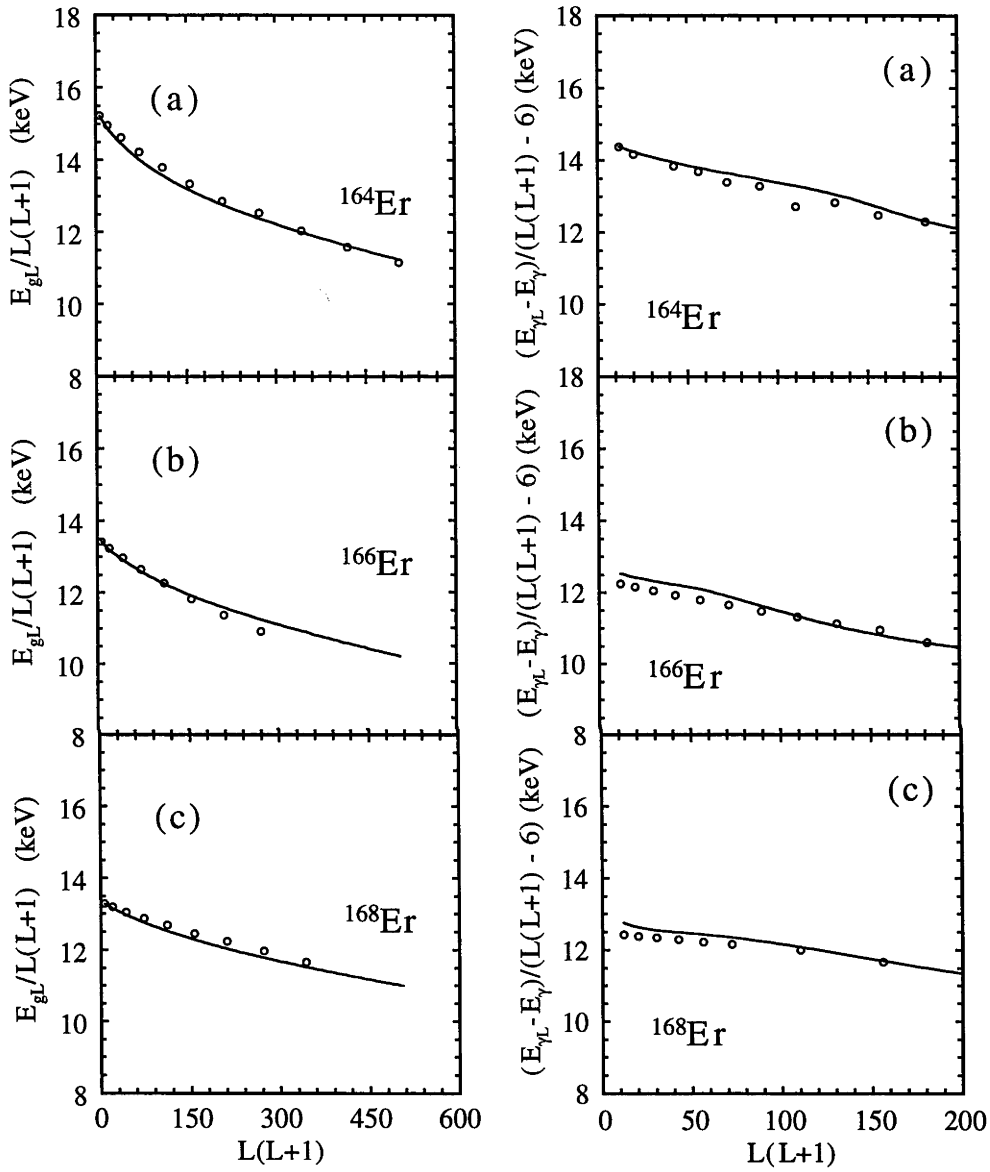

Figure 5.7: A comparison of the experimental (circles) and calculated (solid lines) energies of the ground band (left) and γ-band (right) in $^{164-168}$Er. The scaled energies are in units of keV and the data are from Refs. [87–89].

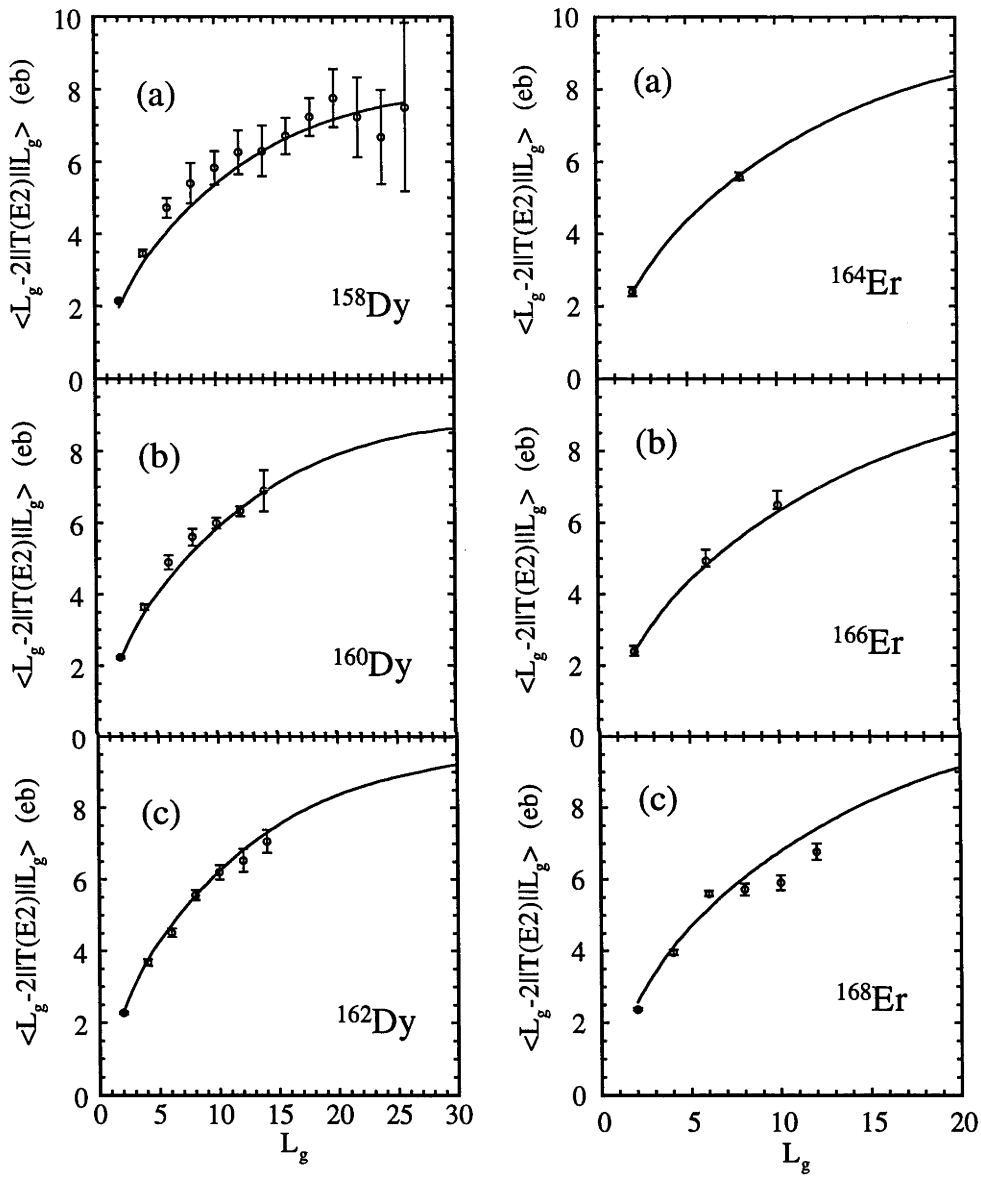

Figure 5.8: (Left) A comparison of the experimental (circles) and calculated (solid lines) yrast $E2$ transitions in $^{156-160}$Dy. The data are from Refs. [84–86]. (Right) Same as the left but in $^{164-168}$Er. The data are from Refs. [87–89].

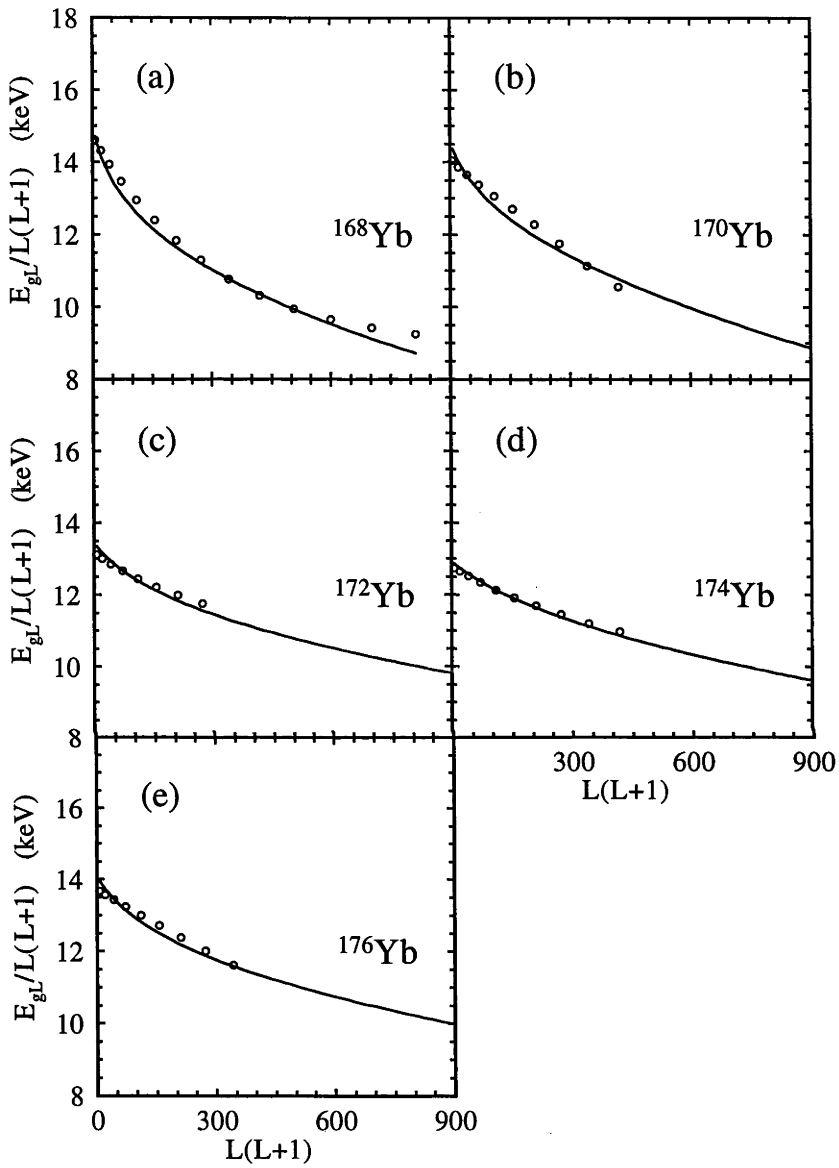

Figure 5.9: A comparison of the experimental (circles) and calculated (solid lines) energies of the ground band in $^{168-176}$Yb. The scaled energies are in units of keV and the data are from Refs. [89–93].

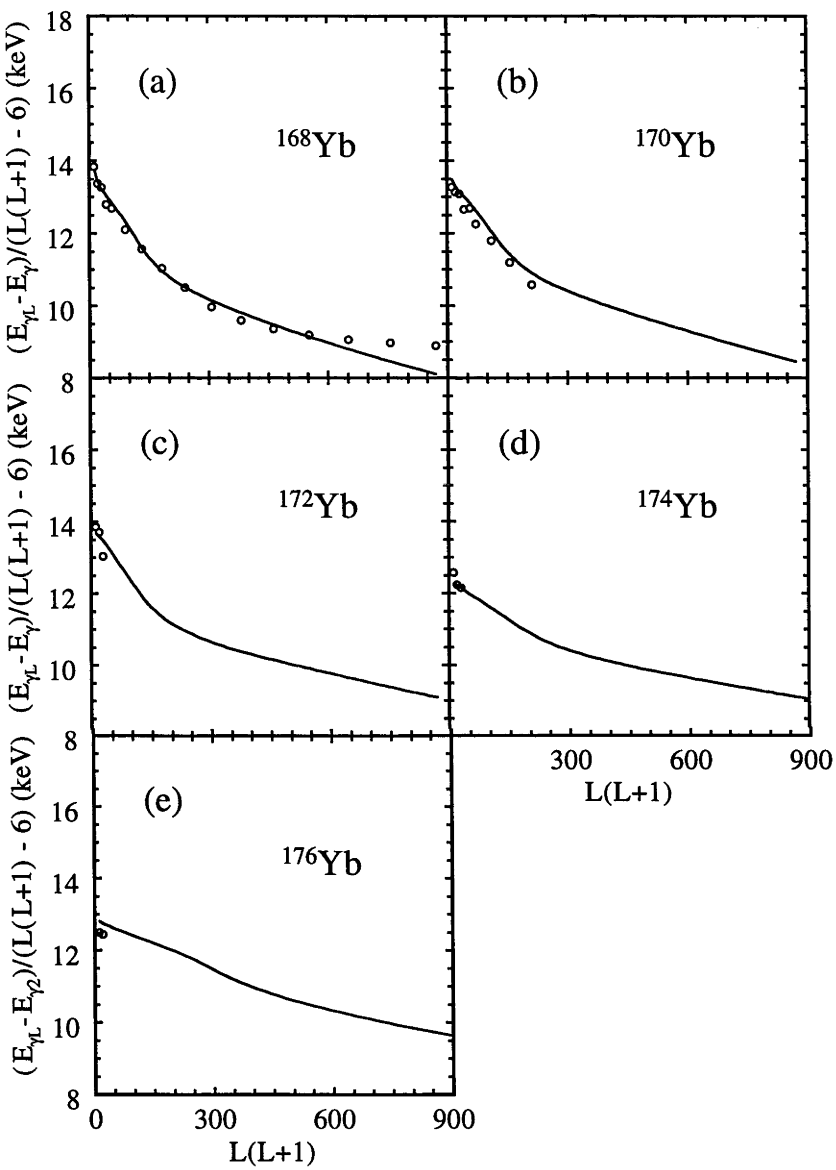

Figure 5.10: A comparison of the experimental (circles) and calculated (solid lines) energies of the γ-band in $^{168-176}$Yb. The scaled energies are in units of keV and the data are from Refs. [89–93].

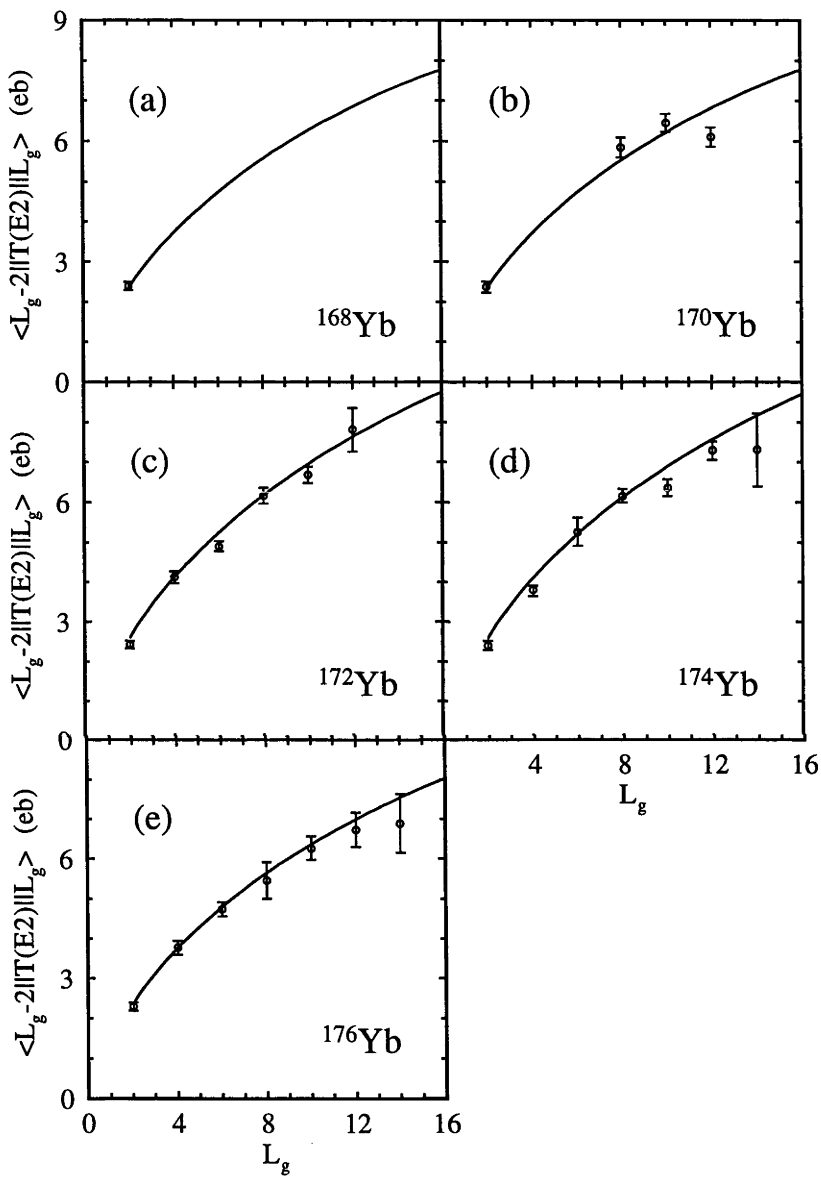

Figure 5.11: (Left) A comparison of the experimental (circles) and calculated (solid lines) yrast $E2$ transitions in $^{168-176}$Yb. The data are from Refs. [89–93].

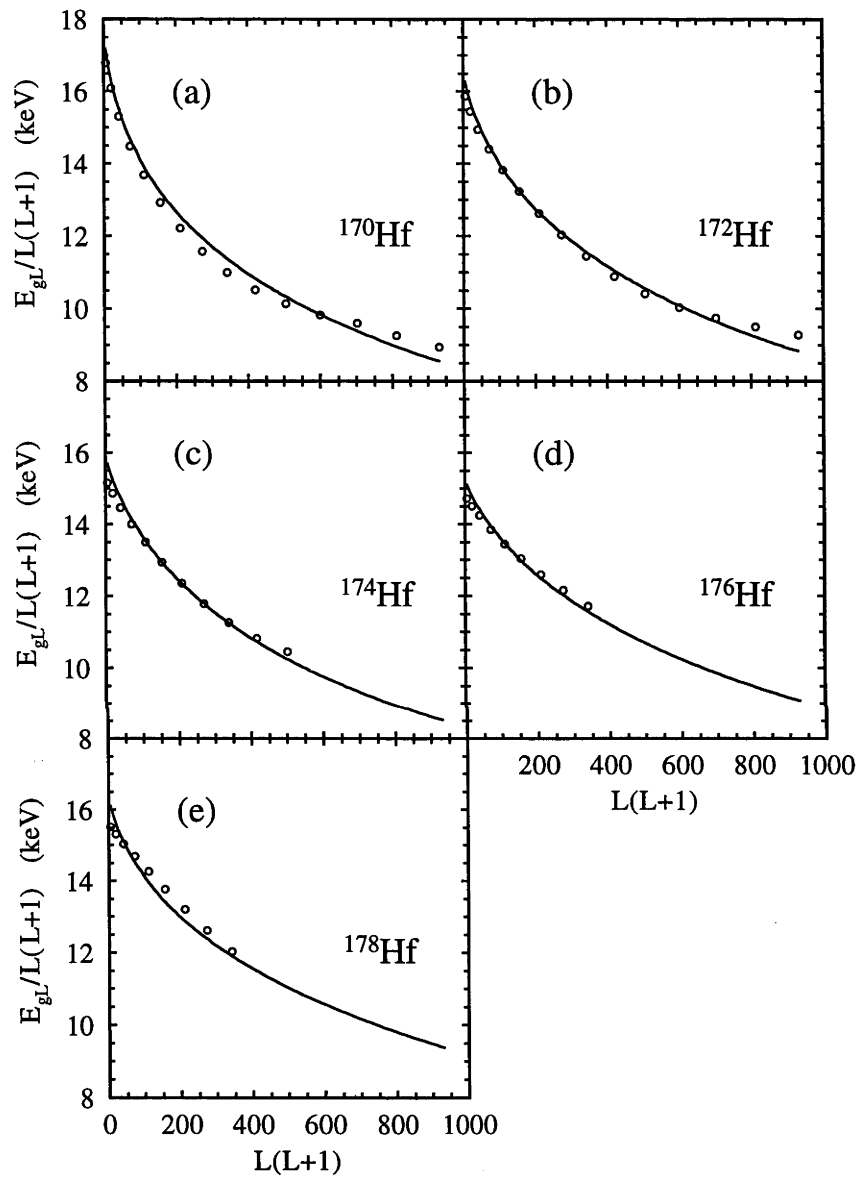

Figure 5.12: A comparison of the experimental (circles) and calculated (solid lines) energies of the ground band in $^{170-178}$Yb. The scaled energies are in units of keV and the data are from Refs. [90–94].

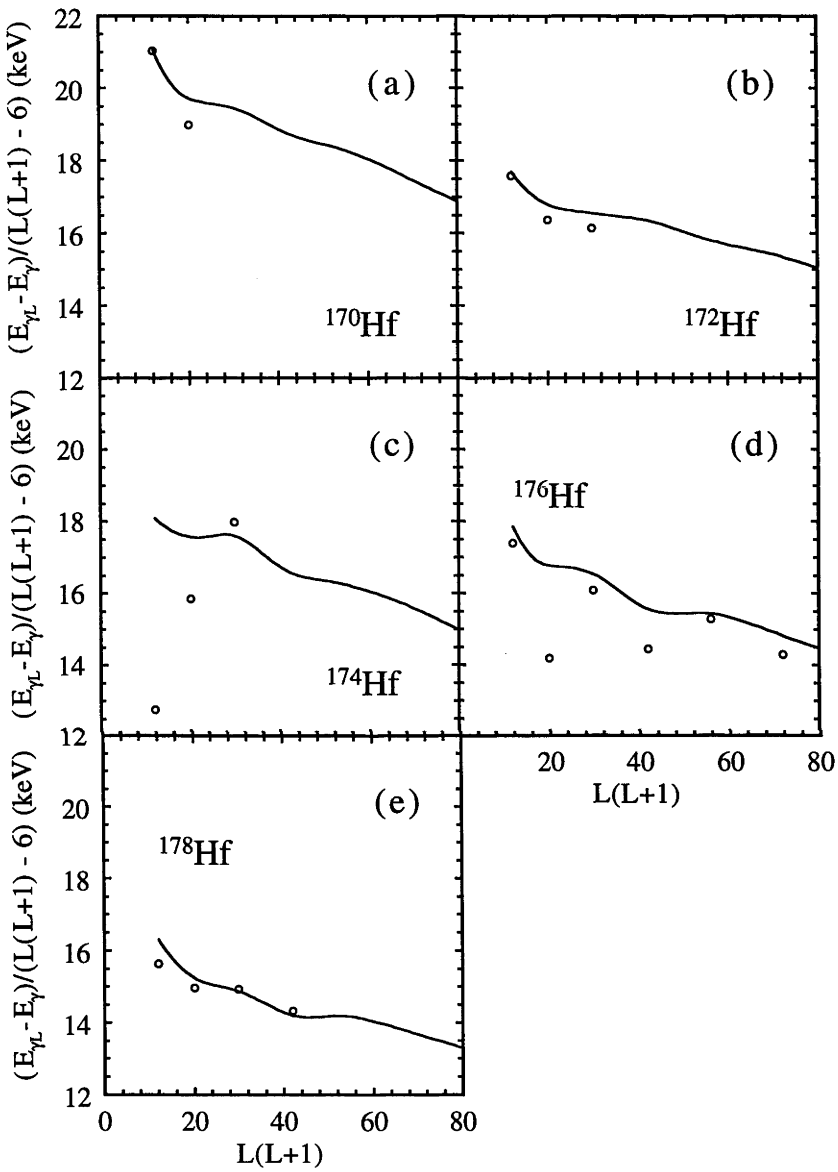

Figure 5.13: A comparison of the experimental (circles) and calculated (solid lines) energies of the γ-band in $^{170-178}$Yb. The scaled energies are in units of keV and the data are from Refs. [90–94].

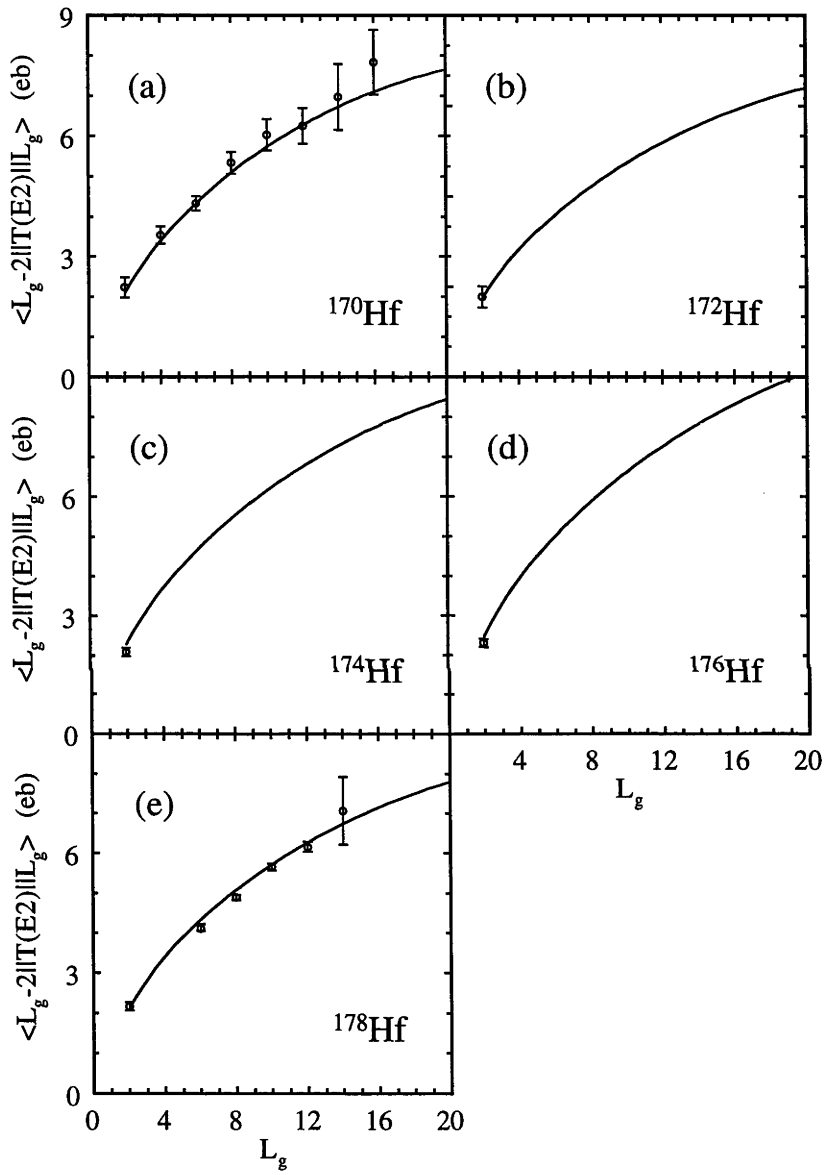

Figure 5.14: (Left) A comparison of the experimental (circles) and calculated (solid lines) yrast $E2$ transitions in $^{170-178}$Hf. The data are from Refs. [90–94].

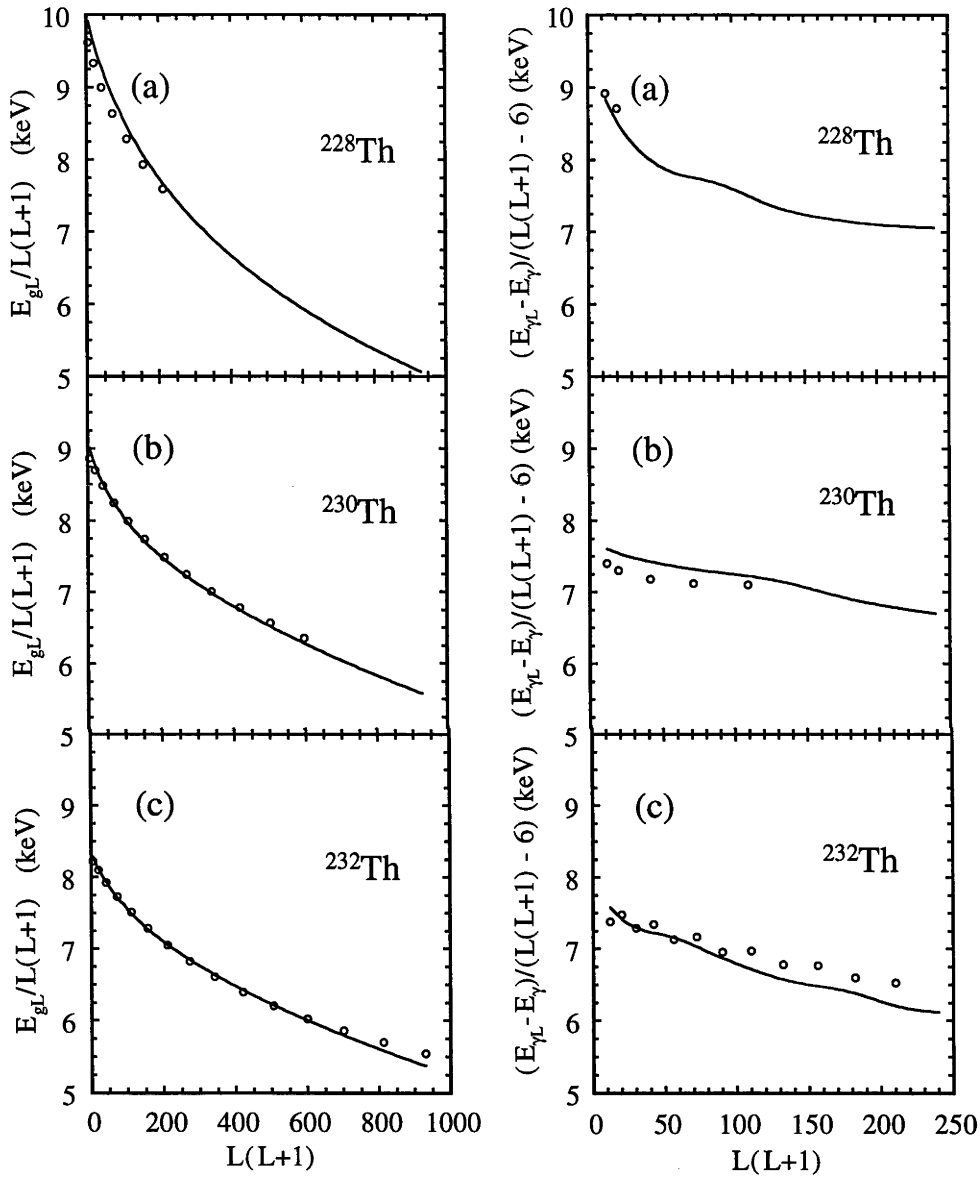

Figure 5.15: A comparison of the experimental (circles) and calculated (solid lines) energies of the ground band (left) and γ-band (right) in $^{228-232}$Th. The scaled energies are in units of keV and the data are from Refs. [95–97].

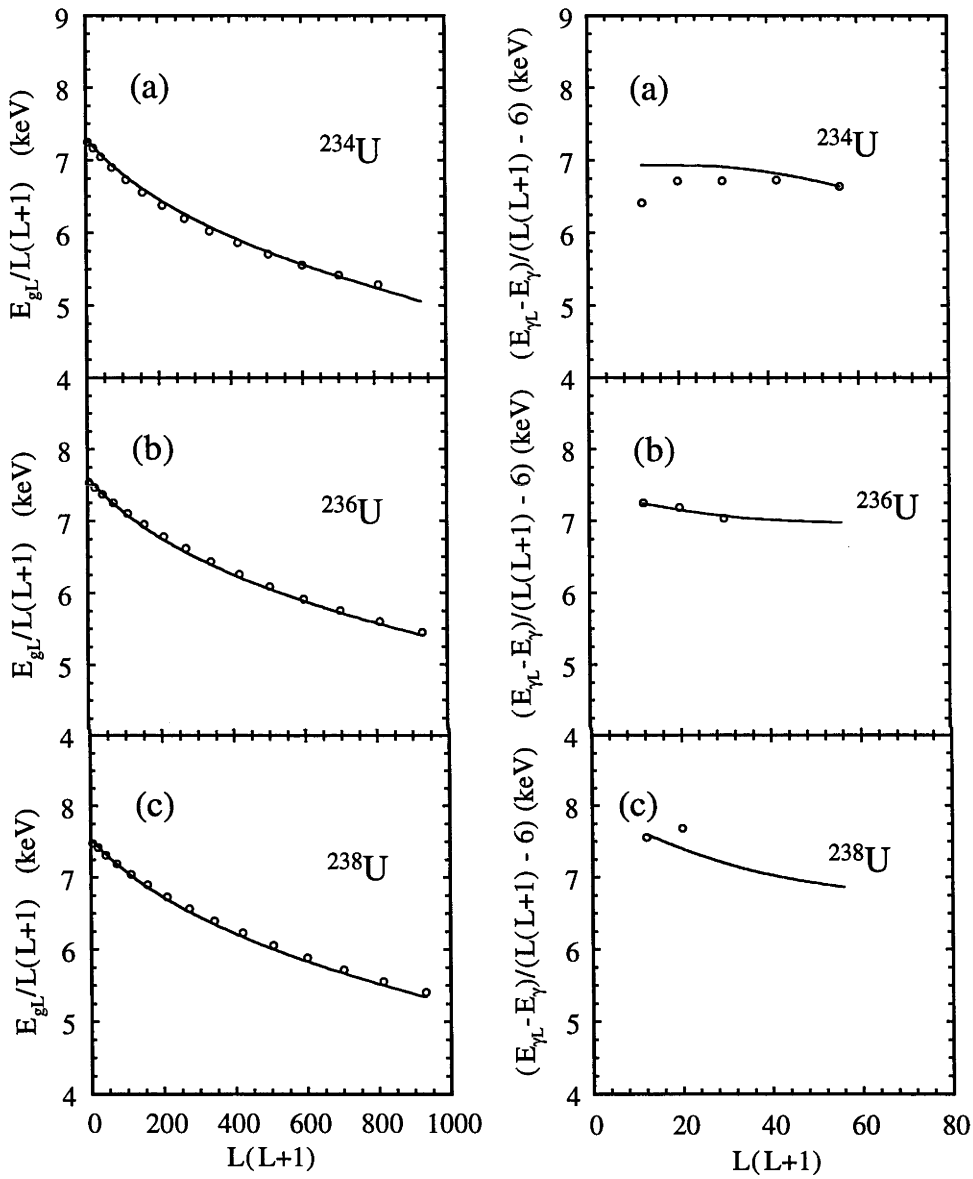

Figure 5.16: A comparison of the experimental (circles) and calculated (solid lines) energies of the ground band (left) and γ-band (right) in $^{234-238}$U. The scaled energies are in units of keV and the data are from Refs. [97–99].

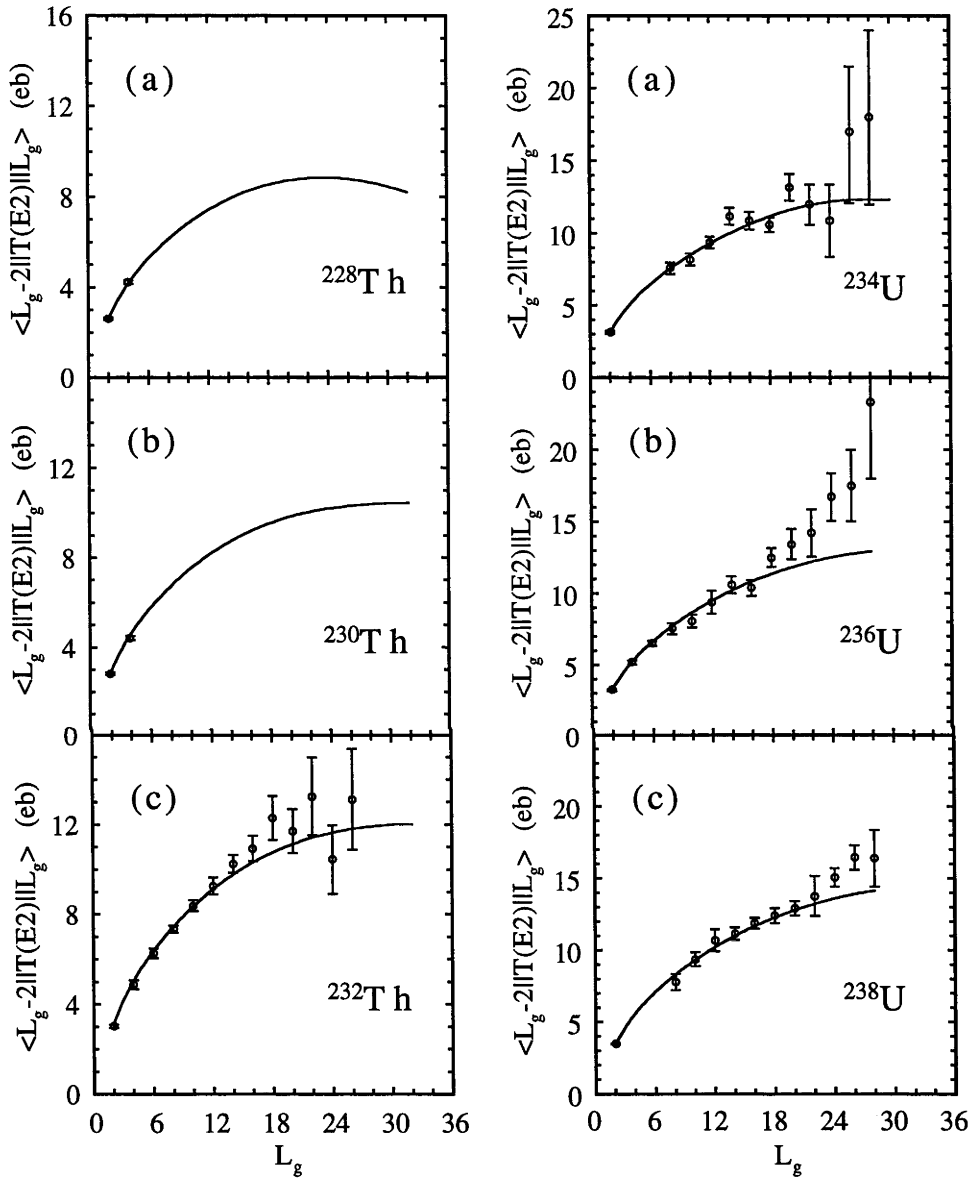

Figure 5.17: (Left) A comparison of the experimental (circles) and calculated (solid lines) yrast $E2$ transitions in $^{228-232}$Th. The data are from Refs. [84–86]. (Right) Same as the left but in $^{234-238}$U. The data are from Refs. [97–99].

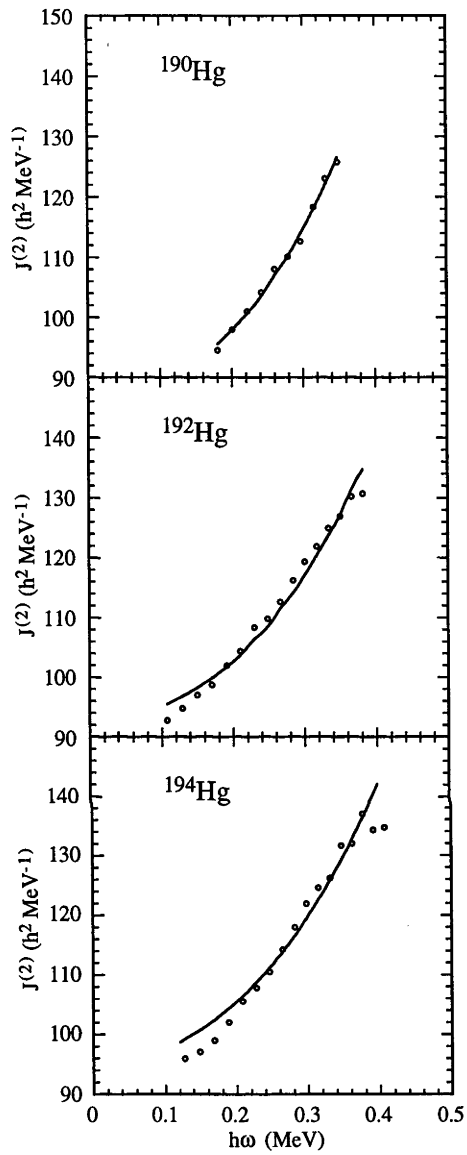

Figure 5.18: A comparison of the experimental dynamic moment of inertia in $^{190-194}$Hg (circles) with the super IBM calculations (solid lines). The data are from Ref. [100]. The parameters used in the fits are $N_{super} = 29, 30, 31$, $\kappa = -35, -34, -33$ keV, $q = 0.68, 0.72, 0.72$ for $^{190-192-194}$Hg, respectively.

CHAPTER 6

Triaxiality and anharmonicity

6.1 Overview

In the geometrical model, collective excitations of atomic nuclei have been interpreted as vibrational and rotational motions of a liquid drop. The vibrational degrees of freedom in both deformed and spherical nuclei are described by phonon excitations. In the spherical limit, the model exhibits harmonic vibrational motion with an excitation spectrum consisting of equally spaced degenerate phonon multiplets. Although exact harmonic phonon excitations have never been observed, there are numerous examples of nuclei exhibiting near-harmonic or anharmonic vibrational motion. In fact, multi-phonon vibrational excitations are known to be well established in near-spherical regions. In deformed regions, nuclei usually possess a well developed ground state rotational band as well as low lying single-phonon bands such as the β and γ, which can be interpreted as being built on collective quadrupole surface vibrational states. In addition to the single-phonon bands, one would anticipate the existence of collective two-phonon vibrations consisting of the type $\gamma\gamma$, $\beta\beta$ and $\beta\gamma$. However, the experimental knowledge of such states is scarce, and in some cases, there is ambiguity in and controversy over their assignments. A central question stems from the anharmonicity exhibited by most of the proposed candidates in which the $E_{\gamma\gamma}/E_{\gamma}$ ratio ranges from 1.5 to 2.5 [101,102]. The experimental signature offered for the $\gamma\gamma$-bands, the $\mathrm{B}(E2; 4^+_{\gamma\gamma} \rightarrow 2^+_{\gamma})/\mathrm{B}(E2; 2^+_{\gamma} \rightarrow 0^+_{g})$ ratios, can be explained by both the $\gamma\gamma$-phonon and the hexadecapole-phonon descriptions [32]. Thus, the $\mathrm{B}(E2)$ values alone do not provide a sensitive means of distinguishing

between the two interpretations. In regard to the $E4$ strength [66], single-nucleon-transfer reactions, β-decay studies and inelastic scattering experiments, Burke [32] argues that the $\gamma\gamma$-interpretation is actually in serious conflict with the data. He emphasises that the hexadecapole description can give an accurate account for the experimental results. As a result, there have been claims that the 4^+ bands are predominantly hexadecapole vibrations.

To address the above issue, one needs a model which can accommodate both the hexadecapole and quadrupole degrees of freedom on an equal footing. The *sd*-IBM certainly fails for this purpose as the hexadecapole degree of freedom is not included in the model space explicitly. Thus, there is an obvious need for the inclusion of g bosons to study this problem. Recently, there is a clue offered by the geometrical model calculations [42], suggesting that anharmonicity could result from a potential with static γ-deformation. It will be interesting to see if there is a similar linkage between triaxiality and anharmonicity within the framework of the *sdg*-IBM.

As seen from Chapter 5, the Hamiltonian with a q-scaled quadrupole interaction and a coherent hexadecapole interaction has been found very useful in the description of high-spin states in deformed nuclei. It is worth investigating how much triaxiality and anharmonicity can be generated by this choice of parametrisation. In the following sections, we will first present the energy surfaces for various multipole interactions, and then discuss the γ-degree of freedom in the *sdg*-IBM. Finally, by using the Hamiltonian prescribed in Section 2.2, the possibility of generating stable γ-deformation and large anharmonic effects is explored.

6.2 Energy surfaces

The energy surface of a boson system described by a general IBM Hamiltonian with one- and two- body interactions is given by

$$E(N, \mathbf{x}) = \langle N, \mathbf{x}|H|N, \mathbf{x}\rangle / \langle N, \mathbf{x}|N, \mathbf{x}\rangle, \tag{6.1}$$

By manipulating the boson algebra, the matrix element can be evaluated as [25]

$$E(N,\mathbf{x}) = \frac{N}{\mathcal{N}}\sum_l \varepsilon_l \beta_l^2 + \sum_k \kappa_k \Big(\frac{N(N-1)}{\mathcal{N}^2} \sum_\mu (-1)^\mu A(k,\mu) A(k,-\mu) + \frac{N}{\mathcal{N}} \sum_l c_{kl} \beta_l^2 \Big), \tag{6.2}$$

where β_l is the deformation parameter associated with the lth pole as $\beta_l^2 = \sum_m x_{lm}^2$, and $\mathcal{N}$ is the normalisation, $\mathcal{N} = \sum_l \beta_l^2$. The quadratic forms $A(k,\mu)$ correspond to the expectation value of the spherical tensor operator $T_\mu^{(k)}$ in the state $|N=1,\mathbf{x}\rangle$, and are given by

$$A(k,\mu) = \sum_{jmlm'} \langle jmlm'|k\mu\rangle t_{kjl} x_{jm} x_{lm'}. \tag{6.3}$$

It should be noted that, due to the symmetry in the intrinsic frame, m and m' take only even integer values. Finally, c_{kl} represents the effective one-body terms resulting from the contraction of two-body interactions, $c_{kl} = [(2k+1)/(2l+1)] \sum_j t_{kjl}^2$. Such terms can be incorporated into the single-boson energies, and hence the renormalised single boson energies can be written as $\varepsilon_l' = \varepsilon_l + \sum_k \kappa_k c_{kl}$. The functional dependence of the one-body terms makes it obvious that the resulting energy surface is axially symmetric. Hence, the one-body interactions do not exhibit any γ-dependence. Similarly, the two-body monopole interaction, which can be interpreted as the square of the one-body terms, have the same geometrical features, and thus they will be ignored in our study. In addition, due to the symmetry properties of Clebsch-Gordan coefficients, $A(k,\mu)$ vanishes for odd k and all the odd multipole interactions remain inert to shape asymmetry to leading order in the $1/N$ expansion. Of the remaining interactions, the quadrupole force dominates and determines the overall shape. Since there is no experimental evidence for multipole interactions higher than hexadecapole, they are also excluded from our study. To facilitate the evaluation of the expectation values of various multipole interactions, we give the explicit expressions for the quadratic forms given in eq. (6.2). We define $A(2,\mu) = Q_\mu$ and $A(4,\mu) = H_\mu$, such that

$$\begin{aligned} Q_0 \;=\; & 2x_{20} + \bar{q}_{22}(x_{20}^2 - 2x_{22}^2) + \bar{q}_{24}(2x_{20}x_{40} + 2\sqrt{\frac{5}{3}}x_{22}x_{42}) \\ & + \bar{q}_{44}(x_{40}^2 + \frac{4}{5}x_{42}^2 - \frac{14}{5}x_{44}^2), \end{aligned}$$

$$
\begin{aligned}
Q_2 &= 2x_{22} - 2\bar{q}_{22}x_{20}x_{22} + \bar{q}_{24}(\frac{1}{3}x_{22}x_{40} + \sqrt{\frac{5}{3}}x_{20}x_{42} + \frac{\sqrt{70}}{3}x_{22}x_{44}) \\
&\quad -\bar{q}_{44}(3\sqrt{\frac{3}{5}}x_{40}x_{42} + \frac{\sqrt{42}}{5}x_{42}x_{44}), \\
H_0 &= 2x_{40} + \bar{h}_{22}(x_{20}^2 + \frac{1}{3}x_{22}^2) + 2\bar{h}_{24}(x_{20}x_{40} - 3\sqrt{\frac{3}{5}}x_{22}x_{42}) \\
&\quad +\bar{h}_{44}(x_{40}^2 + \frac{14}{9}x_{44}^2 - \frac{11}{9}x_{42}^2), \\
H_2 &= 2x_{42} + \sqrt{\frac{5}{3}}\bar{h}_{22}x_{20}x_{22} - \bar{h}_{24}(3\sqrt{\frac{3}{5}}x_{22}x_{40} + \frac{\sqrt{42}}{5}x_{22}x_{44} - \frac{4}{5}x_{20}x_{42}) \\
&\quad +\bar{h}_{44}(\frac{\sqrt{70}}{3}x_{42}x_{44} - \frac{11}{9}x_{40}x_{42}), \\
H_4 &= 2x_{44} + \frac{1}{3}\sqrt{\frac{35}{2}}\bar{h}_{22}x_{22}^2 - \bar{h}_{24}(\frac{14}{5}x_{20}x_{44} + \frac{\sqrt{42}}{5}x_{22}x_{42}) \\
&\quad +\bar{h}_{44}(\frac{1}{3}\sqrt{\frac{35}{2}}x_{42}^2 + \frac{14}{9}x_{40}x_{44}).
\end{aligned} \tag{6.4}
$$

The energy surface can be simplified as

$$
E(N,\mathbf{x}) = \frac{N}{\mathcal{N}}\sum_l \varepsilon'_l\beta_l^2 + \frac{N(N-1)}{\mathcal{N}^2}\Big(\kappa_2(Q_0^2 + 2Q_2^2) + \kappa_4(H_0^2 + 2H_2^2 + 2H_4^2)\Big). \tag{6.5}
$$

To produce a general static asymmetric deformation, one has to find an energy surface whose absolute minimum has non-zero values of x_{22}, x_{24} or x_{44}. However, due to symmetry of shape, such non-zero mean-field solutions do not always guarantee a genuine triaxial shape. They may correspond to an equivalent representation of an axial nucleus rotated about the y-axis by $\frac{\pi}{2}$ ($z \rightarrow x$) or the x-axis by $\frac{-\pi}{2}$ ($z \rightarrow y$) in the body-fixed frame. Therefore, one has to derive conditions ensuring that the triaxial solutions do not result from rotations of axial shapes. To accomplish this, let us consider a general triaxial solution represented by the mean-fields $\{x_{lm}\}$. The corresponding equivalent representations can be obtained by effecting either the Eulerian rotations $R_y(\frac{\pi}{2}, \frac{\pi}{2}, 0)$ ($z \rightarrow x$) or $R_x(\pi, \frac{\pi}{2}, \frac{\pi}{2})$ ($z \rightarrow y$). By letting R_y act on the boson condensate, $\sum_{lm} b_{lm}^\dagger$, one has

$$
\begin{aligned}
\sum_{lm'} x_{lm'}b_{lm'}^\dagger &= R_y(\sum_{lm} x_{lm})R_y^{-1} \\
&= \sum_{lm} x_{lm}\sum_{m'} D^l_{m'm}(\frac{\pi}{2}, \frac{\pi}{2}, 0)b_{lm'}^\dagger \\
&= \sum_{lm'}\Big(\sum_m x_{lm}D^l_{m'm}(\frac{\pi}{2}, \frac{\pi}{2}, 0)\Big)b_{lm'}^\dagger.
\end{aligned} \tag{6.6}
$$

It can be noted that for even l and odd m', $d^l_{m'0}(\frac{\pi}{2}) = 0$ and $d^l_{m'm} + d^l_{m'-m}|_{\frac{\pi}{2}} = 0$, thus $x'_{lm'}$ vanishes when m' is odd. The disappearance of all the odd multipole mean-fields can be attributed to the reflection symmetry with respect to the $X-Y$, $Y-Z$ and $Z-X$ planes of the intrinsic system. Hence, one has the following mean-field transformation

$$\begin{aligned}
x'_{00} &= x_{00}, \\
x'_{20} &= \frac{-1}{2}x_{20} + \sqrt{\frac{3}{2}}x_{22}, \\
x'_{40} &= \frac{3}{8}x_{40} - \frac{1}{2}\sqrt{\frac{5}{2}}x_{42} + \frac{1}{4}\sqrt{\frac{35}{2}}x_{44}, \\
x'_{22} &= x'_{2-2} = \frac{-1}{2}(\sqrt{\frac{3}{2}}x_{20} + x_{22}), \\
x'_{42} &= x'_{4-2} = \frac{-1}{4}(-\sqrt{\frac{5}{2}}x_{40} + 2x_{42} + \sqrt{7}x_{44}), \\
x'_{44} &= x'_{4-4} = \frac{1}{8}(\sqrt{\frac{35}{2}}x_{40} + 2\sqrt{7}x_{42} + x_{44}).
\end{aligned} \tag{6.7}$$

The R_x rotation transforms with $D^l_{m'm}(\pi, \frac{\pi}{2}, \frac{\pi}{2})$, so it can be obtained from the above results by simply replacing x'_{l2} by $-x'_{l2}$, and x_{l2} by $-x_{l2}$. If the original intrinsic state is axial in shape, one has zero x_{lm} for all non-zero m. Therefore, the equivalent representations for the axial states are

$$\begin{aligned}
x'_{00} &= x_{00}, \\
x'_{20} &= \frac{-1}{2}x_{20}, \\
x'_{40} &= \frac{3}{8}x_{40}, \\
x'_{22} &= x'_{2-2} = \mp\sqrt{\frac{3}{8}}x_{20}, \\
x'_{42} &= x'_{4-2} = \pm\frac{1}{4}\sqrt{\frac{5}{2}}x_{40}, \\
x'_{44} &= x'_{4-4} = \frac{1}{8}\sqrt{\frac{35}{2}}x_{40},
\end{aligned} \tag{6.8}$$

where the upper sign and lower sign correspond to R_y and R_x rotations respectively. On the other hand, if the intrinsic state is axially symmetric but with x or y as symmetry axes, the inverse rotations R_y^{-1} or R_z^{-1} should lead to vanishing x_{lm} for

non-zero m. Thus, given a general set of mean-fields x_{lm}, the conditions for an axial solution are

$$x_{22} = \mp\sqrt{\frac{3}{2}}x_{20}, \quad x_{42} = \mp\frac{\sqrt{10}}{3}x_{40}, \quad x_{44} = \frac{1}{3}\sqrt{\frac{25}{2}}x_{40}. \tag{6.9}$$

By applying the inverse transformations, the axial mean-fields with z as the symmetry axis are

$$x'_{20} = -2x_{20}, \qquad x'_{40} = \frac{8}{3}x_{40}. \tag{6.10}$$

The conditions given by eq. (6.9) are very useful in searching for static triaxiality as they provide a convenient way of eliminating all the unwanted axial solutions generated during the minimisation process.

6.3 The γ-degree of freedom

In the *sdg*-IBM, the energy surface of a triaxial nucleus in general is represented by a set of five mutually-independent mean-fields, x_{lm}. Instead of working on such a five dimensional space, one would like to choose a subspace which is easier to handle. By exploiting the rich group structure of U(15), one can derive the seven dynamical symmetry limits [103] which correspond to different geometrical shapes. In the present study, instead of exploring the diverse geometric properties of the dynamical group, U(15), we search for subspace which possesses the features which are common to both the *sd*- and *sdg*-models. This particular approach will be useful in enabling one to extend the the properties of *sd* system to the *sdg* system and so help us to select an appropriate set of parameters for general *sdg*-IBM calculations. Therefore, similar to the procedure used with the *sd*-model, we parametrise the energy surface in the *sdg*-IBM in terms of the quadrupole and hexadecapole deformation parameters β_2 and β_4 and of the asymmetry angle γ. The manifestation of the γ-degree of freedom is of particular importance as it is a meaningful measure of triaxiality in the intrinsic frame.

The scheme for generating the γ-degree of freedom in the *sdg*-IBM adopted in this study stems from the generalisation of the procedure used in the *sd*-case [104].

In the *sd*-model, the asymmetry angle γ is just a simple a parameter of the unitary operator $\exp[-i\gamma X_5]$, where X_5 is a generator of the O(5) group. Following along the same lines, the γ-degree of freedom of a system consisting of arbitrary bosons $(s, d, g, \ldots)$, can be manifested by a finite $O(5)\oplus O(9)\oplus\cdots$ rotation carried out by the generalised unitary operator $\exp[i\gamma\hat{X}]$. The operator, $\hat{X}$ is a linear combination of generators of the corresponding orthogonal groups $O(2j+1)$ $(j = 2, 4, \ldots)$, namely

$$\hat{X} = i\sum_j \sum_{\mu\neq\lambda,-\lambda} C^j_{\mu\lambda} b^\dagger_{j\mu} b_{j\lambda}, \tag{6.11}$$

where $C^j_{\mu\lambda}$ is antisymmetric in μ and λ. To ensure that the unitary transformation preserves the reflection symmetry about the three body-fixed axes, $C^j_{\mu\lambda}$ must satisfy

$$C^j_{\mu\lambda} = \begin{cases} -C^j_{\lambda\mu} & \text{if both } \mu \text{ and } \lambda \text{ are even} \\ 0 & \text{otherwise.} \end{cases} \tag{6.12}$$

In the *sdg*-IBM, $\hat{X}$ can be written as $X_5 + X_9$ where

$$X_5 = iC^2_{02}[d^\dagger_0(d_2 + d_{-2}) - (d^\dagger_2 + d^\dagger_{-2})d_0],$$

and

$$\begin{aligned} X_9 = i\Big\{ & C^4_{02}[g^\dagger_0(g_2 + g_{-2}) - (g^\dagger_2 + g^\dagger_{-2})g_0] \\ & + C^4_{04}[g^\dagger_0(g_4 + g_{-4}) - (g^\dagger_4 + g^\dagger_{-4})g_0] \\ & + C^4_{24}[(g^\dagger_2 + g^\dagger_{-2})(g_4 + g_{-4}) - (g^\dagger_4 + g^\dagger_{-4})(g_2 + g_{-2})]\Big\}. \end{aligned} \tag{6.13}$$

Since the transformation is unitary, the norm of the intrinsic states should be conserved, hence the coefficient C^2_{02} can be uniquely determined, up to an arbitrary phase angle, by imposing the normalisation condition of the general d-boson intrinsic state. However, in case of the g-boson states, there are three coefficients which cannot be fixed by the unitary properties alone, thus different parametrisations are possible for the X_9 operator. Here we fix $C^4_{\mu\lambda}$ by requiring that a general γ-rotation, $e^{i\gamma\hat{X}}$ should leave the γ-unstable energy surface invariant. In this case, the operators become

$$X_5 = \frac{-i}{\sqrt{2}}[d^\dagger_0(d_{-2} + d_2) - (d^\dagger_{-2} + d^\dagger_2)d_0],$$

and

$$X_9 = -i[\sqrt{\frac{5}{6}} g^\dagger_0(g_2 + g_{-2}) + \sqrt{\frac{7}{12}}(g^\dagger_2 + g^\dagger_{-2})(g_4 + g_{-4}) + h.c.]. \tag{6.14}$$

To derive the triaxial state resulting from the special $O(5) \oplus O(9)$ transformation, we have to apply the BCH formula which is given as

$$e^{-iA}Be^{iA} = B + i[B,A] + \frac{i^2}{2!}[[B,A],A] + \frac{i^3}{3!}[[[B,A],A],A] + \cdots . \tag{6.15}$$

By evaluating all the nested boson commutation relations, we obtain

$$\begin{aligned}
&[s^\dagger, \hat{X}] = 0 \\
&[d_0^\dagger, \hat{X}] = \frac{-i}{\sqrt{2}}(d_2^\dagger + d_{-2}^\dagger) \\
&[[d_0^\dagger, \hat{X}], \hat{X}] = d_0^\dagger \\
&[[[d_0^\dagger, \hat{X}], \hat{X}], \hat{X}] = \frac{-i}{\sqrt{2}}(d_2^\dagger + d_{-2}^\dagger) \\
&\qquad \vdots \qquad\qquad \vdots \\
&[g_0^\dagger, \hat{X}] = i\sqrt{\frac{5}{6}}(g_2^\dagger + g_{-2}^\dagger) \\
&[[g_0^\dagger, \hat{X}], \hat{X}] = \frac{5}{3}g_0^\dagger - \sqrt{\frac{70}{6}}(g_4^\dagger + g_{-4}^\dagger) \\
&[[[g_0^\dagger, \hat{X}], \hat{X}], \hat{X}] = 2i\sqrt{\frac{10}{3}}(g_2^\dagger + g_{-2}^\dagger) \\
&[[[[g_0^\dagger, \hat{X}], \hat{X}], \hat{X}], \hat{X}] = \frac{20}{3}g_0^\dagger - 2\sqrt{\frac{70}{3}}(g_4^\dagger + g_{-4}^\dagger) \\
&[[[[[g_0^\dagger, \hat{X}], \hat{X}], \hat{X}], \hat{X}], \hat{X}] = 8i\sqrt{\frac{10}{3}}(g_2^\dagger + g_{-2}^\dagger) \\
&[[[[[[g_0^\dagger, \hat{X}], \hat{X}], \hat{X}], \hat{X}], \hat{X}], \hat{X}] = \frac{80}{3}g_0^\dagger - 8\sqrt{\frac{70}{3}}(g_4^\dagger + g_{-4}^\dagger) \\
&\qquad \vdots \qquad\qquad \vdots
\end{aligned} \tag{6.16}$$

The above manipulations can be performed efficiently by Mathematica [75]. According to the BCH formula, we have the following infinite series

$$\begin{aligned}
e^{-i\gamma\hat{X}} s^\dagger e^{i\gamma\hat{X}} &= s^\dagger, \\
e^{-i\gamma\hat{X}} d_0^\dagger e^{i\gamma\hat{X}} &= (1 - \frac{\gamma^2}{2!} + \frac{\gamma^4}{4!} + \cdots)d_0^\dagger \\
&\quad + \frac{1}{\sqrt{2}}(\gamma - \frac{\gamma^3}{3!} + \frac{\gamma^5}{5!} + \cdots)(d_2^\dagger + d_{-2}^\dagger)
\end{aligned}$$

and

$$
\begin{aligned}
e^{-i\gamma\hat{X}} g_0^\dagger e^{i\gamma\hat{X}} &= [\frac{7}{12} + \frac{5}{12}(1 - \frac{4\gamma^2}{2!} + \frac{16\gamma^4}{4!} + \cdots)]g_0^\dagger \\
&+\sqrt{\frac{5}{24}}(2\gamma - \frac{8\gamma^3}{3!} + \frac{32\gamma^5}{5!} + \cdots)(g_2^\dagger + g_{-2}^\dagger) \\
&+\frac{\sqrt{35}}{12\sqrt{2}}[1 - (1 - \frac{4\gamma^2}{2!} + \frac{16\gamma^4}{4!} + \cdots)](g_4^\dagger + g_{-4}^\dagger). \qquad (6.17)
\end{aligned}
$$

Hence the rotated axial boson operators in the product space can be expressed as

$$
\begin{aligned}
e^{-\gamma\hat{X}} d_0^\dagger e^{i\gamma\hat{X}} &= \cos\gamma d_0^\dagger + \frac{1}{\sqrt{2}}\sin\gamma(d_{-2}^\dagger + d_2^\dagger), \\
e^{-\gamma\hat{X}} g_0^\dagger e^{i\gamma\hat{X}} &= (\frac{7}{12} + \frac{5}{12}\cos 2\gamma)g_0^\dagger + \frac{\sqrt{5}}{\sqrt{24}}\sin 2\gamma(g_2^\dagger + g_{-2}^\dagger) + \\
&\frac{\sqrt{35}}{12\sqrt{2}}(1 - \cos 2\gamma)(g_4^\dagger + g_{-4}^\dagger). \qquad (6.18)
\end{aligned}
$$

As a result, the axial state is tranformed as

$$
\begin{aligned}
&[s^\dagger + \beta_2 d_0^\dagger + \beta_4 g_0^\dagger]|0\rangle \overset{O5\oplus O(9)}{\longrightarrow} \\
&\Big\{s^\dagger + \beta_2[\cos\gamma d_0^\dagger + \frac{1}{\sqrt{2}}\sin\gamma(d_{-2}^\dagger + d_2^\dagger)] + \\
&\beta_4[(\frac{7}{12} + \frac{5}{12}\cos 2\gamma g_0^\dagger + \sqrt{\frac{5}{24}}\sin 2\gamma(g_2^\dagger + g_{-2}^\dagger) + \\
&\frac{\sqrt{35}}{6\sqrt{2}}\sin^2\gamma(g_4^\dagger + g_{-4}^\dagger)]\Big\}|0\rangle. \qquad (6.19)
\end{aligned}
$$

It is straightforward to check that the norms of the above intrinsic states remain intact and thus the unitary condition is preserved. The mean-fields x_{lm} can finally be written as

$$
\begin{aligned}
&x_{00} = 1, \quad x_{20} = \beta_2\cos\gamma, \quad x_{40} = \frac{\beta_4}{12}(7 + 5\cos 2\gamma), \quad x_{22} = \frac{\beta_2}{\sqrt{2}}\sin\gamma, \\
&x_{42} = \sqrt{\frac{5}{24}}\beta_4\sin 2\gamma, \quad x_{44} = \sqrt{\frac{35}{72}}\beta_4\sin^2\gamma. \qquad (6.20)
\end{aligned}
$$

By substituting the mean-fields into eqs. (6.2) and (6.5), the expectation values of the quadrupole-quadrupole and hexadecapole-hexadecapole interactions are

$$
\begin{aligned}
\langle Q\cdot Q\rangle &= \frac{N(N-1)}{(1+\beta_2^2+\beta_4^2)}\Big[\beta_2^2(4 + \beta_2^2\bar{q}_{22}^2) + \frac{1}{3}\beta_2^2\beta_4(12\beta_4\bar{q}_{24}^2 + 7\beta_4\bar{q}_{22}\bar{q}_{44} \\
&+24\bar{q}_{24}) + \frac{25}{18}\beta_4^4\bar{q}_{44}^2 + 4\beta_2(1 + \beta_4\bar{q}_{24})(\beta_2^2\bar{q}_{22} + \beta_4^2\bar{q}_{44})\cos 3\gamma \\
&-\frac{1}{18}\beta_4^2\bar{q}_{44}(6\beta_2^2\bar{q}_{22} + 7\beta_4^2\bar{q}_{44})\cos 6\gamma\Big], \qquad (6.21)
\end{aligned}
$$

and

$$\begin{aligned}\langle H\cdot H\rangle &= \frac{N(N-1)}{(1+\beta_2^2+\beta_4^2)}\Big[\beta_2^4\bar{h}_{22}^2+\beta_2^2\beta_4(4\bar{h}_{22}+\frac{17}{6}\beta_4\bar{h}_{24}^2+\frac{112}{81}\beta_4\bar{h}_{22}\bar{h}_{44})\\ &+\beta_4^2(4+\frac{224}{81}\beta_4\bar{h}_{44}+\frac{1837}{2187}\beta_4^2\bar{h}_{44}^2)+4\beta_2\beta_4\bar{h}_{24}(2\beta_4+\beta_2^2\bar{h}_{22}\\ &+\beta_2^2\bar{h}_{44})\cos 3\gamma+\frac{1}{4374}\beta_4^2(5103\beta_2^2\bar{h}_{24}^2+5400\beta_4\bar{h}_{44}\\ &+2700\beta_2^2\bar{h}_{22}\bar{h}_{44}+700\beta_4^2\bar{h}_{44}^2)\cos 6\gamma\Big]. \qquad (6.22)\end{aligned}$$

From eqs. (6.21) and (6.22), it is obvious that the energy surface can be written generally as

$$E(\beta_2,\beta_4,\gamma)=a_0+a_1\cos 3\gamma+a_2\cos 6\gamma, \qquad (6.23)$$

where a_0, a_1 and a_2 are functions of $q_{jl}, h_{jl}, \varepsilon_l, \kappa_l$ and β_l.

In the following study of triaxiality, the parametrisations P(1) and P(2) defined in Section 2.2 are employed. To search for the non-axial minimum, γ is varied from 0° to 60° and the energy surface, $E(\beta_2,\beta_4,\gamma)$ is minimised at each particular γ-angle, i.e. the study will be confined on a two dimensional surface spanned by β_2 and β_4. In particular, the solution obtained at $\gamma = 0°$, corresponds to the axial minimum. In Figure 6.1, the energy profiles of various Hamiltonian are depicted. It should be noted that each point on the curve may correspond to different β_2 and β_4 values. It is shown in Figure 6.1(a) - (b) that a single quadrupole interaction with parametrisations P(1) and P(2), is incapable of generating a stable triaxial shape. In Figure 6.1(c), with the P(1) parametrisation given in Section 2.2, a global non-axial minimum is developed at $q \leq 0.3$. These minima are characterised by having a large β_4 value. For example, at $q = 0.3$, the energy and mean fields correspond to the non-axial minimum are: $E_0 = E_{\min}/N(N-1)\kappa_2 = -14.2$, $x_{00} = 0.18$, $x_{20} = 0.03$, $x_{40} = 0.92$, $x_{22} = 0.01$, $x_{42} = -0.33$, and $x_{44} = -0.10$. They can be compared with the solutions, $E_0 = -16.1$, $x_{00} = 0.15$, $x_{20} = 0.00$, $x_{40} = 0.19$, $x_{22} = 0.00$, $x_{42} = -0.60$, and $x_{44} = -0.34$, obtained from the minimisation of a general five dimensional surface using the simplex method. The above results indicate that the asymmetric shape is caused by the excitation of the non-axial g-bosons, $g_{\pm 2}$ and $g_{\pm 4}$. In short, the ground state is represented by a condensate

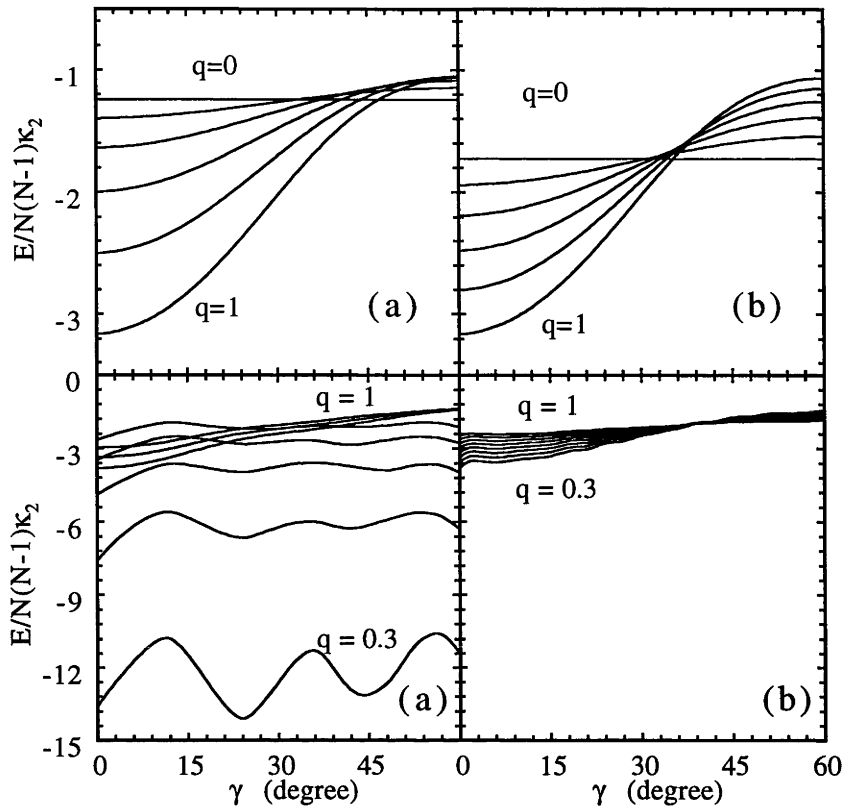

Figure 6.1: The energy profile generated by the quadrupole interaction with the parametrisation given by (a) P(1), (q, q, q) and (b) P(2), $(q, 1, q)$, defined in Section 2.2. The q-value is varied from 0 - 1 in 5 steps. The parameters are $N = 14$, $\zeta_4 = 0$, $\eta_d = 0$ and $\eta_g = 0$. The energy have been scaled down by the factor $N(N-1)\kappa_2$. In (c) and (d), the same quantities are presented as in (a) and (b) respectively but with the addition of a coherent hexadecapole interaction where $\zeta_4 = 0.4$ and $q =$ varies from 0.3 - 1 in 7 steps.

of the s and g bosons. As the hexadecapole deformation generally is regarded as a small perturbation to the overall nuclear shape, the above results therefore are not useful in realistic descriptions of nuclei. On the other hand, the minimisation carried out in the O(5) subspace, does not give accurate results. It provides only a qualitative guidance to the search for triaxiality. In Figure 6.1(d), there is no sign of triaxiality and the result is similar to that in Figure 6.1(b). In Figure 6.2(a), the axial-triaxial phase transition induced by the hexadecapole interaction is shown. In the above discussion, because of the lack of γ-dependence in the one-body terms,

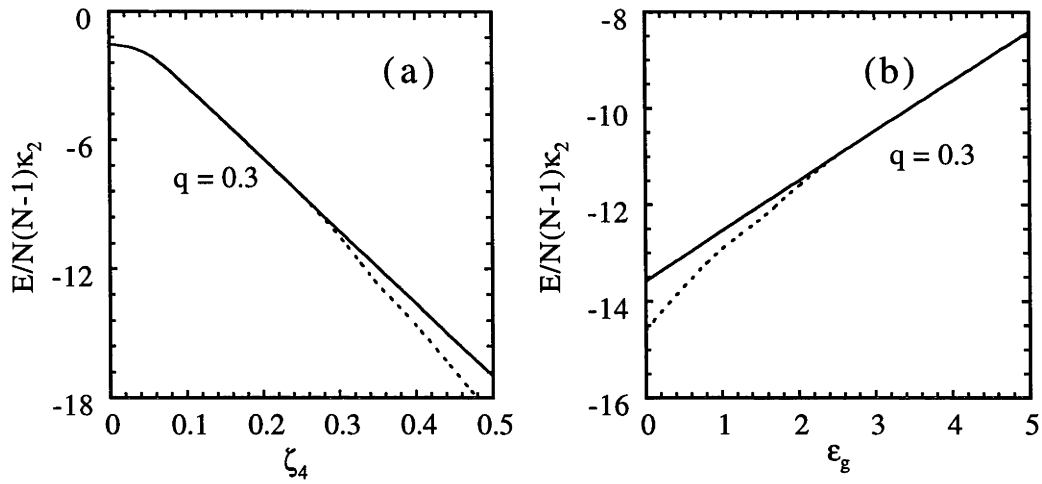

Figure 6.2: (a) Axial-triaxial phase transition induced by the coherent hexadecapole interaction. The parameters are the same as those defined in Figure 6.1(c) but with $q = 0.3$ and ζ_4 varying from 0 - 0.5. The solid line shows the axial minimum while the dotted line represents the triaxial minimum. (b) Axial-triaxial phase transition induced by the g-boson energy. The parameters are the same as those defined in (a) with $\zeta_4 = 0.4$ and η_g varying from 0 - 5.

they have been excluded so far. In most applications of the sdg-IBM to deformed and transitional nuclei (excluding superdeformed nuclei) [45,61,62,66–68], the g bosons are weakly coupled, it is therefore desirable to include the effect of g-boson energy on shape transition. It is shown in Figure 6.2(b) that η_g triggers the phase transition from triaxial to axial shapes, counteracting the effect of the hexadecapole interaction. It is interesting to note that, though the one-body terms have no γ-dependence, they do significantly alter the profile of the energy surface and specifically the relative depths of the minima. Also, it is easy to understand the influence of the g-boson energy on shape asymmetry. A large η_g will suppress the excitation of the g bosons, especially $g_{\pm 2}$ and $g_{\pm 4}$, so that axial symmetry prevails.

6.4 Anharmonic effects

Before presenting the results of the *sdg*-IBM, it is worth discussing the capability of the *sd*-model to describe the anharmonicity in double-phonon bands which lie within its model space. This question is ignored in most of the literature and will provide a useful reference point for the *sdg*-IBM calculations. In Table 6.1,

Table 6.1: Band energy and $E2$ transition systematics of γ- and $\gamma\gamma$-bands for a quadrupole Hamiltonian in the *sd*-IBM. The parameters are $N = 12$, $\kappa_1 = 0$, $\kappa_2 = -20$keV, and χ is varied with $\chi_{SU(3)} = -\sqrt{7}/2$. The $E2$ matrix elements should be multiplied by e_2 for comparison with experiment.

$\chi/\chi_{su(3)}$	1.0	0.875	0.75	0.5	0.25	0.00
$E_{\gamma\gamma}/E_{\gamma}$	1.87	1.88	1.88	1.89	1.91	2.80
$E2(2_g^+ \rightarrow 0_g^+)$	18.0	17.3	16.6	15.3	14.1	13.8
$E2(2_\gamma^+ \rightarrow 0_g^+)$	0.00	0.50	0.99	1.97	3.04	0.29
$E2(2_\gamma^+ \rightarrow 2_g^+)$	0.00	0.64	1.28	2.69	4.82	16.31
$E2(4_{\gamma\gamma}^+ \rightarrow 2_g^+)$	0.00	0.00	0.00	0.01	0.25	0.00
$E2(4_{\gamma\gamma}^+ \rightarrow 2_\gamma^+)$	0.00	1.12	2.21	4.34	5.98	0.16

we present the consistent-Q formalism calculations with the Hamiltonian given in eq. (2.6). The calculations are performed along the SU(3)-O(6) leg of the Casten triangle as the χ parameter is varied from $-\sqrt{7}/2$ to 0 with $\eta_d = 0$. The first row shows the energy ratio of the $\gamma\gamma$- to γ-bands, and the rest are various interband reduced $E2$ matrix elements among the ground, γ- and $\gamma\gamma$-bands. Leaving aside the dynamical symmetry limits, all the ratios remain remarkably constant. In particular, one has ratios $E_{\gamma\gamma}/E_{\gamma} \approx 1.9$ and $E2(4_\gamma^+ \rightarrow 2_\gamma^+)/(E2(2_\gamma^+ \rightarrow 0_g^+) \approx 2.2$. These are very close to the geometrical model values of 2 and 2.25, respectively. In fact, in the large N limit, the agreement would be exact. Thus the double-phonon bands in the *sd*-IBM are very close to the harmonic limit of the geometrical model, even after allowing for variations in the χ parameter. In other words, the standard *sd*-model is not flexible enough to describe either the anharmonicity in band energies or the variations in interband $E2$ transitions from the Alaga rules. To investigate whether large anharmonic effects are manifest in the *sdg*-IBM description of deformed nuclei,

Table 6.2: Effect of the hexadecapole interaction on γ, $\gamma\gamma$ and $K^\pi = 4_h^+$ band properties in the *sdg*-IBM. The prescription for the quadrupole and hexadecapole interactions is given by P(1) in Section 2.2 with $q = 0.5$. The other parameters are $N = 12$, $\kappa_2 = 20$keV, $\eta_d = 1.5$, $\eta_g = 4.5$.

ζ_4	-0.4	-0.2	0.0	0.2	0.4
$E_{\gamma\gamma}/E_\gamma$	1.97	1.98	1.99	2.01	2.02
E_{4h}/E_γ	2.51	2.26	1.91	1.63	1.43
$E2(2_g^+ \to 0_g^+)$	12.2	12.6	12.4	12.3	12.2
$E2(2_\gamma^+ \to 0_g^+)$	2.25	2.22	2.20	2.17	2.15
$E2(2_\gamma^+ \to 2_g^+)$	4.32	4.56	4.85	5.12	5.38
$E2(4_{\gamma\gamma}^+ \to 2_g^+)$	0.02	0.03	0.04	0.06	0.07
$E2(4_{\gamma\gamma}^+ \to 2_\gamma^+)$	4.21	4.05	3.88	3.48	3.02
$E2(4_h^+ \to 2_g^+)$	0.50	0.48	0.45	0.44	0.42
$E2(4_h^+ \to 2_\gamma^+)$	0.09	0.26	0.62	1.81	3.31

we have carried out numerical studies using the *super*-SDGBOSON code [56]. In particular, we are interested in the effect of the interplay between quadrupole and hexadecapole interactions. In Tables 6.2 and 6.3, various energy ratios and $E2$ transitions for both the $\gamma\gamma$ and the hexadecapole vibrational 4^+ states are depicted. To study the effect of the hexadecapole force on the spectra, the relative coupling strength, ζ_4 is varied from -0.4 to 0.4. In Tables 6.2 and 6.3, the γ- and $\gamma\gamma$-bands show almost no dependence on κ_4. In fact, the energy and $E2$ ratios are almost identical to the *sd*-calculations. The 4_h^+ state, on the other hand, is seen to be sensitive to variations in κ_4 as would be anticipated. Particularly in Table 6.2, the E_{4h}/E_γ ratio ranges from 1.4 to 2.5 and the $E2(4_h^+ \to 2_\gamma^+)$ strength is comparable with that of $E2(4_{\gamma\gamma}^+ \to 2_\gamma^+)$ at $\zeta_4 = 0.4$.

Mean-field approach

The mean-field and $1/N$ expansion techniques are economical tools for large scale of systematic study of the double-phonon vibrational bands. The axial intrinsic state prescribed for the $\gamma\gamma$-band in Section 4.5 is a good approximation since no stable triaxial shape is found for the Hamiltonian with a weak coupling of g bosons

Table 6.3: Same as Table 6.2. The prescription for the quadrupole and hexadecapole interactions is given by P(2) in Section 2.2. The other parameters are $N = 12$, $\kappa_2 = 20$keV, $\eta_d = 0$, $\eta_g = 4$.

ζ_4	-0.4	-0.2	0.0	0.2	0.4
$E_{\gamma\gamma}/E_\gamma$	1.88	1.89	1.90	1.91	1.92
E_{4h}/E_γ	2.32	2.26	2.19	2.10	1.98
$E2(2_g^+ \to 0_g^+)$	16.6	16.8	17.0	17.2	17.3
$E2(2_\gamma^+ \to 0_g^+)$	2.24	2.24	2.24	2.24	2.25
$E2(2_\gamma^+ \to 2_g^+)$	2.89	2.92	2.94	2.98	3.02
$E2(4_{\gamma\gamma}^+ \to 2_g^+)$	0.01	0.01	0.01	0.02	0.08
$E2(4_{\gamma\gamma}^+ \to 2_\gamma^+)$	5.14	5.11	5.07	5.04	4.98
$E2(4_h^+ \to 2_g^+)$	2.14	2.51	2.41	1.96	1.26
$E2(4_h^+ \to 2_\gamma^+)$	0.68	0.32	0.45	0.66	0.89

(i.e. large η_g) as discussed above. To improve the accuracy, one should include the orthogonality and mixing terms. However, when compared with the results of exact calculations, the above mean-field expressions give results with deviations of less than 4%; an accuracy which justifies the use of the meanfield approach to the systematic studies of anharmonic effects. In Figure 6.3, it is shown that within the chosen parametrisations for the quadrupole and hexadecapole interactions, one has the $E_{\gamma\gamma}/E_\gamma$ ratio ranging from 1.9 to 2.2, which is consistent with the numerical diagonalisation results. It is thus quite clear that neither η_d nor ζ_4 is capable of generating large anharmonic effects.

To understand the lack of anharmonicity within the chosen parametrisations, it will be useful to look at the analytic expressions derived from the $1/N$ expansion. Since we are concerned only with the bandhead energies, it suffices to examine the first layer $1/N$ results. According to the formulae given in Section 4.5 and Appendix E, we can obtain the excitation energies for both the single- and double-phonon bands by subtracting away the ground state energy. We then have

$$E_{\gamma\gamma,L} = 2N^2 \sum_l \Big\{ \frac{1}{aN} \Big(\kappa_l (4aU_l'' - 2aU_l) + \varepsilon_l (-ax_l^2 + ax_{l2}^2)/N \Big)$$

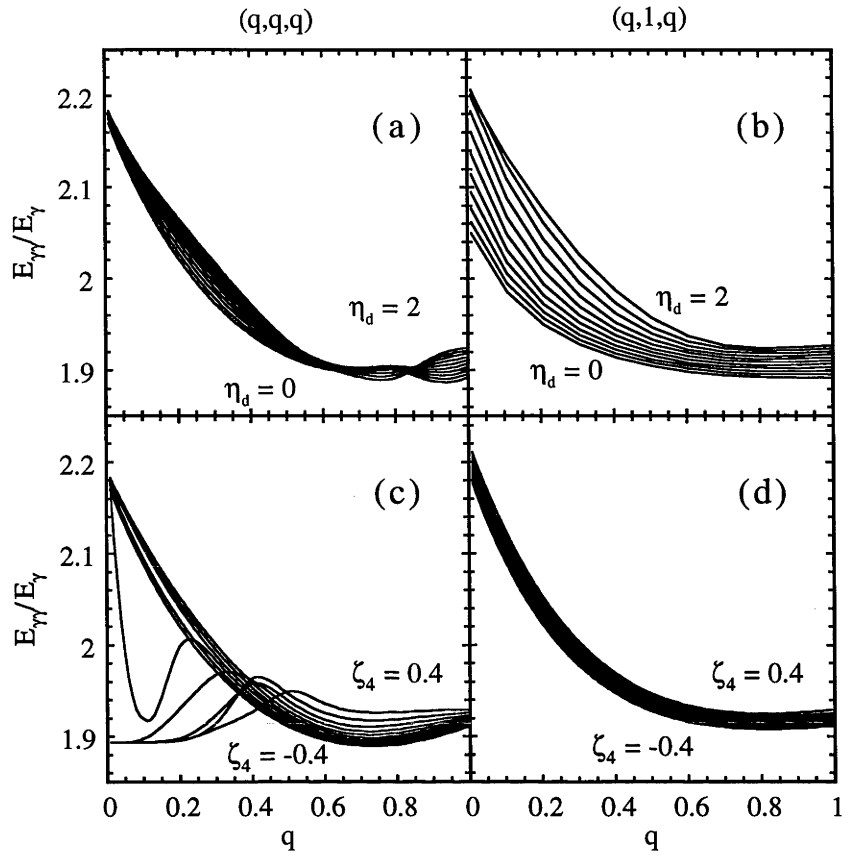

Figure 6.3: Systematic study of anharmonicity generated by quadrupole + hexadecapole interactions. Parametrisation P(1) and P(2) are used in (a),(c) and (b),(d), respectively. In (a), (b), η_d is varied from $0-2$ in 10 equal steps with $\eta_g = 4.5$. In (c), (d), η_d and η_g are fixed at 1.5 and 4.5, respectively, while ζ_4 is varied from -0.4 to 0.4 in 10 equal steps.

$$
\begin{aligned}
& + \frac{\bar{L}}{(aN)^2}\Big(\kappa_l(-2aU_l + U_{l1}) + \varepsilon_l(\bar{l}-a)/N\Big)\Big\}, \\
E_{\gamma,L} \;=\; & N^2 \sum_l \Big\{ \frac{1}{aN}\Big(\kappa_l(4aU_l'' - 2aU_l) + \varepsilon_l(-ax_l^2 + ax_{l2}^2)/N\Big) \\
& + \frac{\bar{L}}{(aN)^2}\Big(\kappa_l(-2aU_l + U_{l1}) + \varepsilon_l(\bar{l}-a)/N\Big)\Big\}. \qquad (6.24)
\end{aligned}
$$

Once again, it can be seen clearly that the ground band and all the vibrational bands (including the single- and double-phonon ones) have the same leading order results. If the L-dependent terms are ignored (i.e. putting the moment-of-inertia to zero) in the above analytic expressions, one finds that the ratio of double-phonon and single-phonon excitation energies is exactly two. In other words, the harmonicity is preserved at the first layer of the expansion which is in line with the numerical

diagonalisation and mean-field results.

In regard to the above investigation, it can be concluded that the parametrisations used in Chapter 5, which have been found useful for the description of deformed nuclei, can neither generate stable triaxial shape for the ground band nor large anharmonic effects for the $\gamma\gamma$-band. In fact, the large g-boson energy suppresses the excitation of the non-axial g-bosons and restores the axial symmetry of the system.

CHAPTER 7

Conclusion

In this investigation, the recent developments in numerical diagonalisation and the analytic $1/N$ expansion method have been presented. The effects of various truncation schemes on the computation of physical quantities have been discussed in Chapter 3. The devised schemes such as the coupling of one g boson to the sd-core ($n_g \leq 1$), are usually geared towards reproducing the low-lying spectrum and cannot be expected to give reliable results for high-spin states. In regard to the low-lying states, our results indicate that, with the truncation of the sdg space to a maximum of $n_{g\,\mathrm{max}}$ g bosons ($n_{g\,\mathrm{max}} \approx N/3$), level energies and transition rates converge to better than 1 %, which is sufficient for purposes of spectroscopy. However, due to the large model space involved in the sdg-IBM, diagonalisation is only possible for $N \leq 14$. In addition, numerical diagonalisation is time consuming and expensive, and therefore not an effective tool for carrying out extensive studies of the effects of a multitude of parameters in the sdg-IBM.

The angular momentum projected mean field theory, which leads to a $1/N$ expansion for physical quantities [26], presumably offers the only viable alternative for a realistic description of high-spin states in the sdg-IBM. An obstacle to realising this goal, namely the evaluations of matrix elements up to order $\bar{L}^3/N^6$ 09 are necessary for an accurate representation of high-spin states, has been overcome through the use of computer algebra and details of the results for the ground and γ-bands have been illustrated in Chapter 4.

By employing the $1/N$ formulae, a systematic description of high-spin states for both deformed and superdeformed nuclei within the framework of the sdg-IBM has

been presented in Chapter 5. Systematic studies of the model parameters using the $1/N$ expansion formulae have indicated that some of the long standing problems associated with the description of moment of inertia and $E2$ transitions in the IBM can be resolved by including the d-boson energy in the Hamiltonian. The perceived problems with the sd-IBM in its description of spin dependent quantities are not due to a lack of higher spin bosons but rather due to the energy surface not being soft enough. Inclusion of the d-boson energy, together with the extension to the sdg space, can successfully resolve these problems. The g bosons are necessary for extending the model space but otherwise they play a marginal role in the dynamics of the ground band and cannot resolve the problems mentioned above. The hexadecapole interaction has a minor effect on the ground band but could play a decisive role on γ and other excited band properties. This feature of the hexadecapole interaction does not appear to be well appreciated in the literature. For example, the recently observed staggering effect in some superdeformed bands has been attributed to the hexadecapole degrees of freedom. If this is true, then it would have profound effects on the neighbouring non-yrast bands. The application of the sdg-IBM Hamiltonian consisting of single-boson energies, and quadrupole and hexadecapole interactions (with constrained parameters) resulted in a mostly uniform and successful description of both the low-lying band structures and high-spin states across the rare-earth and actinide regions. In the past, many experimental results for high-spin states were compared with the sd-IBM calculations with negative connotations. Presumably, this was due to the lack of sdg-IBM calculations, the extensive sdg-IBM results presented in this work should help remedying this situation. The limited parametrisation used here, does not work as well in the case of the Er isotopes which appear to have rather exceptional properties. To describe the Er isotopes, one needs to carry out a more detailed study without imposing the constraints used in Chapter 5. It should be noted that ^{168}Er, which has been used as a benchmark case in tests of phenomenological models, is far from being a typical deformed nuclei. The study of triaxiality suggests that the asymmetric shapes, generated by the quadrupole interaction ($q \leq 0.3$) and the coherent hexade-

capole interaction with $\varepsilon_g = 0$, are dominated by a large hexadecapole deformation. Therefore, they are not useful in realistic analyses of data. In addition, using large g-boson energies can suppress the excitation of g bosons, especially $g_{\pm 2}, g_{\pm 4}$. Thus, with a weak coupling of the g bosons to the sd-core, the system will remain axial in shape. It is because of this fact, the parametrisation used in Chapter 5, which leads to successful descriptions of the high-spin states and $E2$ properties in deformed nuclei, does not generate triaxiality. In regard to the study of anharmonic effects in vibrational bands, the results indicate that within the (q, q, q) and $(q, 1, q)$ parametrisations defined in Chapter 2, the $E_{\gamma\gamma}/E_{\gamma}$ ratio ranges only from 1.9 to 2.2. This range is not large enough to describe the anharmonicity claimed to be observed in some proposed $\gamma\gamma$-bands. It is therefore worth stressing that one should be cautious in band assignments, as the hexadecapole 4_h^+ band could be misinterpreted as the $\gamma\gamma$-band. In fact, the $\gamma\gamma$-phonon description is not the only explanation for the B($E2$) values. Our calculations show that, with a suitable choice of Hamiltonian, the $E2(4_h^+ \rightarrow 2_{\gamma}^+)$ strength can be comparable to that of $E2(4_{\gamma\gamma}^+ \rightarrow 2_{\gamma}^+)$. In order to avoid confusion, it is therefore desirable to pin down the hexadecapole features by looking at the $E4$ transitions, as well as (e, e') and (p, p') experiments in the rare-earth region.

APPENDIX A

Representations of basis states

32-bit representation

In the sdg-IBM, each boson is free to occupy one of the 15 quantum states (s, d, and g). In the bit-pattern representation, 1 denotes the partition while 0 denotes the boson, therefore we have 14 partitions separating the bosons into 15 cells. If we arrange the 15 cells in the order

$$[g_{-4}][g_{-3}][g_{-2}][g_{-1}][g_0][g_1][g_2][g_3][g_4][d_{-2}][d_{-1}][d_0][d_1][d_2][s],$$

states such as $(s^\dagger)^{12}|0\rangle$ and $(d_0^\dagger)^6(s^\dagger)^6|0\rangle$ can be represented as

$$11111111111111\overbrace{000000000000}^{s}, \qquad 11111111111\overbrace{000000}^{d_0}111\overbrace{000000}^{s},$$

respectively.

64-bit representation

In this 64-bit representation, an N boson system with occupation numbers $n_1, n_2, n_3, \cdots, n_i, n_{i+1}, \cdots n_{15}$ can be specified by an integer I_p given by $\sum_i n_i \times 16^i$, where p denotes the ordering of the basis states. Therefore, a list of integers arranged in descending or ascending numerical order is created. For example, the corresponding bit-patterns for the states $(s^\dagger)^{12}|0\rangle$ and $(d_0^\dagger)^6(s^\dagger)^6|0\rangle$ are

$$\overbrace{0000}^{d_{-2}}\ \overbrace{0000}^{d_{-1}}\ \overbrace{0000}^{d_0}\ \overbrace{0000}^{d_1}\ \overbrace{0000}^{d_2}\ \overbrace{1100}^{s},$$
$$\overbrace{0000}^{d_{-2}}\ \overbrace{0000}^{d_{-1}}\ \overbrace{0110}^{d_0}\ \overbrace{0000}^{d_1}\ \overbrace{0000}^{d_2}\ \overbrace{0110}^{s}.$$

(since the first 40 bits are zero, for simplicity, we only show the pattern of the last 24 bits). In this new scheme, N must be less than 16 otherwise the one-to-one mapping between I and the basis states will be destroyed. This restriction seems to make such a scheme less attractive. However, in spite of this, the *sdg*-IBM calculations cannot be performed with N going beyond 16 in most of the modern computers due to limitation in memory capacity. On the other hand, under this new scheme, the manipulations between matrix operators and basis states can be done in a simple bitwise manner. In the *sdg*-IBM, the Hamiltonian usually consists of one- and two-body operators containing terms of the form $b_i^\dagger b_j$ and $b_i^\dagger b_j^\dagger b_k b_l$ where $i, j, k, l = 1, 2, \cdots, 15$. All $b_i^\dagger$, or b_i are denoted by integers $M_i (= 1 \times 16^i)$. These operations can be performed conveniently in this 64-bit representation without resorting to any packing or unpacking procedure. For example, let a typical basis be ϕ_p, then

$$b_i^\dagger \phi_p = I_p + M_i, \qquad b_j \phi_p = I_p - M_j. \tag{A.1}$$

However, in carrying out the annihilation by b_j, it is necessary to check that the occupation number n_j is non-zero. To retrieve this information, we first define a new integer m_i such that $m_i = 16^{i+1} - M_i$. By evaluating the logical sum (AND) of I_p and m_i, we are able to extract the number $n_i \times 16^i$, thus the occupancy of the $i-$th quantum state is known.

APPENDIX B

Boson calculus

B.1 General evaluation of matrix elements

The boson algebra is based on the fundamental boson commutation relations given by

$$[f(b), b^\dagger] = b^\dagger \frac{\partial f(b)}{\partial b}, \qquad [b, f(b^\dagger)] = \frac{\partial f(b^\dagger)}{\partial b^\dagger} b. \tag{B.1}$$

Without the loss of generality, we consider a general intrinsic states $b_K^{\dagger N_K}|0\rangle$. The matrix elements of a general two-body multipole force is given by

$$\langle 0| \prod_{K=0}^{p} b_K^{N_K} T^{(k)} \cdot T^{(k)} \prod_{K'=0}^{p} b_{K'R}^{\dagger N'_{K'}} |0\rangle =$$
$$\langle 0| \sum_{n_0=0}^{N'_0} \sum_{n_1=0}^{N'_1} \cdots \sum_{n_p=0}^{N'_p} \frac{N'_0! N'_1! \cdots N'_p!}{n_0! n_1! \cdots n_p! (N'_0 - n_0)! (N'_1 - n_1)! \cdots (N'_p - n_p)!} \times$$
$$\frac{\partial^{N_0} \partial^{N_1} \cdots \partial^{N_p}}{\partial b_0^{\dagger N_0} \partial b_1^{\dagger N_1} \cdots \partial b_p^{\dagger N_p}} \frac{\partial^{n_0} \partial^{n_1} \cdots \partial^{n_p}}{\partial b_{0R}^{n'_0} \partial b_{1R}^{n'_1} \cdots \partial b_{pR}^{n'_p}} \left(b_{0R}^{\dagger N'_0 - n_0} b_{1R}^{\dagger N'_1 - n_1} \cdots b_{pR}^{\dagger N'_p - n_p} T^{(k)} \cdot T^{(k)} \right) |0\rangle, \tag{B.2}$$

where T_k is multipole tensor defined in Chapter 2, $b_{KR}^\dagger$ is given by

$$b_{KR}^\dagger = e^{-i\beta J_y} b_K^\dagger e^{i\beta J_y} = \sum_{lm} x_{lK} d_{mK}^l b_{lm}^\dagger, \tag{B.3}$$

and p is the highest boson spin in the model. The normalisation $\mathcal{N}(\phi_K, L)$ can be derived in a similar fashion and therefore it is not shown here.

B.2 Boson calculus for the full γ band

To simplify the discussion, it is convenient to define

$$Y_{mm'} = \frac{\partial b^\dagger_{m'R}}{\partial b^\dagger_m} = \sum_l x_{lm} x_{lm'} d^l_{mm'}, \tag{B.4}$$

where $Y_{00} = Z$. In the following, the direct, exchange and orthogonality terms of the matrix elements of the full γ band are given.

$$\begin{aligned}
&\langle 0|b^{N-1} b_2 e^{-i\beta J_y} T^k \cdot T^k (b^\dagger)^{N-1} b_2^\dagger|0\rangle = \\
&\quad (N-1)! Z^{N-4} \langle 0| \Big\{ \Big[(N-1) Z^2 \frac{\partial}{\partial b_R} \frac{\partial}{\partial b_{2R}} \frac{\partial}{\partial b^\dagger} \frac{\partial}{\partial b_2^\dagger} + \frac{(N-1)(N-2)}{4} Z \\
&\quad \times \Big(2Y_{02} \frac{\partial}{\partial b_R} \frac{\partial}{\partial b_{2R}} (\frac{\partial}{\partial b^\dagger})^2 + 2Y_{20} (\frac{\partial}{\partial b_R})^2 \frac{\partial}{\partial b^\dagger} \frac{\partial}{\partial b_2^\dagger} + Y_{22} (\frac{\partial}{\partial b_R})^2 (\frac{\partial}{\partial b^\dagger})^2 \Big) + \\
&\quad \frac{(N-1)(N-2)(N-3)}{4} Y_{02} Y_{20} (\frac{\partial}{\partial b_R})^2 (\frac{\partial}{\partial b^\dagger})^2 \Big] + \\
&\quad \Big[Z^3 \frac{\partial}{\partial b_{2R}} \frac{\partial}{\partial b_2^\dagger} + (N-1) Z^2 \Big(2Y_{02} \frac{\partial}{\partial b_{2R}} \frac{\partial}{\partial b^\dagger} + Y_{22} \frac{\partial}{\partial b_R} \frac{\partial}{\partial b^\dagger} \Big) + \\
&\quad (N-1)(N-2) Z Y_{02} Y_{20} \frac{\partial}{\partial b_R} \frac{\partial}{\partial b^\dagger} \Big] \Big\} T^k \cdot T^k |0\rangle,
\end{aligned} \tag{B.5}$$

$$\begin{aligned}
&\langle 0|b^{N-2} b_1^2 e^{-i\beta J_y} T^k \cdot T^k (b^\dagger)^{N-2} (b_1^\dagger)^2|0\rangle = \\
&\quad (N-2)! Z^{N-6} \langle 0| \Big\{ \Big[Z^4 (\frac{\partial}{\partial b_{1R}})^2 (\frac{\partial}{\partial b_1^\dagger})^2 + \\
&\quad \frac{(N-2)(N-3)(N-4)(N-5)}{4} Y_{01}^2 Y_{10}^2 (\frac{\partial}{\partial b_R})^2 (\frac{\partial}{\partial b^\dagger})^2 + \\
&\quad 4(N-2) Z^3 \Big(Y_{01} (\frac{\partial}{\partial b_{1R}})^2 \frac{\partial}{\partial b^\dagger} \frac{\partial}{\partial b_1^\dagger} + Y_{11} \frac{\partial}{\partial b_R} \frac{\partial}{\partial b_{1R}} \frac{\partial}{\partial b^\dagger} \frac{\partial}{\partial b_1^\dagger} \Big) + \\
&\quad (N-2)(N-3)(N-4) Z \Big(2Y_{01}^2 Y_{10} \frac{\partial}{\partial b_R} \frac{\partial}{\partial b_{1R}} (\frac{\partial}{\partial b^\dagger})^2 + \\
&\quad Y_{01} Y_{10} Y_{11} (\frac{\partial}{\partial b_R})^2 (\frac{\partial}{\partial b^\dagger})^2 \Big) + \frac{(N-2)(N-3)}{2} Z^2 \Big(2Y_{01}^2 (\frac{\partial}{\partial b_{1R}})^2 (\frac{\partial}{\partial b^\dagger})^2 \\
&\quad 8Y_{01} Y_{11} \frac{\partial}{\partial b_R} \frac{\partial}{\partial b_{1R}} (\frac{\partial}{\partial b^\dagger})^2 + 8Y_{01} Y_{10} \frac{\partial}{\partial b_R} \frac{\partial}{\partial b_{1R}} \frac{\partial}{\partial b^\dagger} \frac{\partial}{\partial b_1^\dagger} + \\
&\quad Y_{11}^2 (\frac{\partial}{\partial b_R})^2 (\frac{\partial}{\partial b^\dagger})^2 \Big) \Big] + \\
&\quad \Big[(N-2)(N-3)(N-4) Z Y_{01}^2 Y_{10}^2 \frac{\partial}{\partial b_R} \frac{\partial}{\partial b^\dagger} + 4Y_{1,1} \frac{\partial}{\partial b_{1R}} \frac{\partial}{\partial b_1^\dagger} +
\end{aligned}$$

$$4(N-2)(N-3)Z^2\Big(Y_{01}^2Y_{10}\frac{\partial}{\partial b_{1R}}\frac{\partial}{\partial b^\dagger}+Y_{01}Y_{10}Y_{11}\frac{\partial}{\partial b_R}\frac{\partial}{\partial b^\dagger}\Big)+$$
$$2(N-2)\Big(2Y_{01}Y_{10}\frac{\partial}{\partial b_{1R}}\frac{\partial}{\partial b_1^\dagger}+4Y_{01}Y_{11}\frac{\partial}{\partial b_{1R}}\frac{\partial}{\partial b^\dagger}+Y_{11}^2\frac{\partial}{\partial b_R}\frac{\partial}{\partial b^\dagger}\Big)$$
$$\Big]\Big\}T^k\cdot T^k|0\rangle, \tag{B.6}$$

$$\langle 0|b^{N-1}b_2e^{-i\beta J_y}T^k\cdot T^k(b^\dagger)^{N-2}(b_1^\dagger)^2|0\rangle =$$
$$(N-1)!Z^{N-5}\langle 0|\Big\{\Big[Z^3(\frac{\partial}{\partial b_{1R}})^2\frac{\partial}{\partial b^\dagger}\frac{\partial}{\partial b_2^\dagger}+\frac{(N-2)(N-3)(n-4)}{4}$$
$$Y_{02}Y_{10}^2(\frac{\partial}{\partial b_R})^2(\frac{\partial}{\partial b^\dagger})^2+(N-2)Z^2\Big(\frac{Y_{02}}{2}(\frac{\partial}{\partial b_{1R}})^2(\frac{\partial}{\partial b^\dagger})^2+$$
$$2Y_{10}\frac{\partial}{\partial b_R}\frac{\partial}{\partial b_R}\frac{\partial}{\partial b^\dagger}\frac{\partial}{\partial b_2^\dagger}+Y_{12}\frac{\partial}{\partial b_R}\frac{\partial}{\partial b_{1R}}(\frac{\partial}{\partial b^\dagger})^2\Big)+\frac{(N-2)(N-3)Z}{2}\times$$
$$\Big(2Y_{02}Y_{10}\frac{\partial}{\partial b_R}\frac{\partial}{\partial b_{1R}}(\frac{\partial}{\partial b^\dagger})^2+$$
$$Y_{10}^2(\frac{\partial}{\partial b_R})^2\frac{\partial}{\partial b^\dagger}\frac{\partial}{\partial b_2^\dagger}+Y_{10}Y_{12}(\frac{\partial}{\partial b_R})^2(\frac{\partial}{\partial b^\dagger})^2\Big)\Big]+$$
$$\Big[2(N-2)(N-3)ZY_{01}^2Y_{20}\frac{\partial}{\partial b_R}\frac{\partial}{\partial b^\dagger}+(N-2)Z^2\Big(Y_{01}^2\frac{\partial}{\partial b_{2R}}\frac{\partial}{\partial b^\dagger}+$$
$$2Y_{01}Y_{20}\frac{\partial}{\partial b_R}\frac{\partial}{\partial b_1^\dagger}+Y_{01}Y_{21}\frac{\partial}{\partial b_R}\frac{\partial}{\partial b^\dagger}\Big)+2Z^3\Big(Y_{01}\frac{\partial}{\partial b_{2R}}\frac{\partial}{\partial b_1^\dagger}+$$
$$Y_{21}\frac{\partial}{\partial b_R}\frac{\partial}{\partial b_1^\dagger}\Big)\Big]\Big\}T^k\cdot T^k|0\rangle. \tag{B.7}$$

B.3 Derivatives of two-body scalar operators

By manipulating the boson algebra, one gets

$$\langle 0|\frac{\partial}{\partial b_K^\dagger}\frac{\partial}{\partial b_{K''}^\dagger}\frac{\partial}{\partial b_{K'R}}\frac{\partial}{\partial b_{K'''R}}T^{(k)}\cdot T^{(k)}|0\rangle$$
$$=\sum_{jlj'l'Mmm'}(-1)^{M-m-m'}t_{kjl}t_{kj'l'}\langle jmlM-m|kM\rangle\langle j'm'l'-M-m'|k-M\rangle$$
$$\times\Big\{x_{l'K'''}x_{lK'}d^{l'}_{m'+M,K'''}d^{l}_{m-M,K'}(x_{jK}\delta_{mK}x_{j'K''}\delta_{m'K''}+x_{jK'}\delta_{mK'}x_{j'K}\delta_{m'K})+$$
$$x_{lK'''}x_{l'K'}d^{l}_{m-M,K'''}d^{l'}_{m'+M,K'}(x_{jK}\delta_{mK}x_{j'K''}\delta_{m'K''}+x_{jK''}\delta_{mK''}x_{j'K}\delta_{m'K})\Big\}, \tag{B.8}$$

where t_{kjl} are the structural constants defined in Chapter 4. Due to the Kronecker delta functions, those m and m' within the summation sign vanish. Since the Hamil-

tonian is invariant under rotation, its matrix elements therefore should be independent of M, the magnetic quantum number of the spherical tensor $T^{(k)}$. The M independence of the above expression rests implicitly on the summation over M. The manifestation of rotational invariance will be more apparent if one further reduces the expression by using identities in six-j symbols [105]. In this case, the expression can be readily reduced to

$$\begin{aligned}
\mathcal{H}^{KK''}_{K'K'''}(k) = (2k+1)\sum_{jlj'l'J} t_{kjl}t_{kj'l'}d^{J}_{K+K'',K'+K'''}\left\{\begin{array}{ccc} j & j' & J \\ l' & l & k \end{array}\right\} \times \Big(\\
\langle jKj'K''|JK+K''\rangle\langle l'K'''lK'|JK'+K'''\rangle x_{jK}x_{j'K''}x_{l'K'''}x_{lK'} \quad + \\
\langle jK''j'K|JK+K''\rangle\langle l'K'''lK'|JK'+K'''\rangle x_{jK'}x_{j'K}x_{l'K'''}x_{lK''} \quad + \\
\langle jKj'K''|JK+K''\rangle\langle l'K'lK'''|JK'+K'''\rangle x_{jK}x_{j'K''}x_{l'K'}x_{lK'''} \quad + \\
\langle jK''j'K|JK+K''\rangle\langle l'K'lK'''|JK'+K'''\rangle x_{jK''}x_{j'K}x_{l'K'}x_{lK'''}\Big). \qquad \text{(B.9)}
\end{aligned}$$

By playing the same trick, one can obtain the expressions for the effective one-body part as

$$\begin{aligned}
&\langle 0|\frac{\partial}{\partial b^{\dagger}_{K}}\frac{\partial}{\partial b_{K'R}}T^{(k)}\cdot T^{(k)}|0\rangle \\
&= \sum_{jlj'l'Mmm'}(-1)^{M-m-m'}t_{kjl}t_{kj'l'}\langle jmlM-m|kM\rangle\langle j'm'l'-M-m'|k-M\rangle \\
&\quad \times \; x_{l'K'}x_{jK}d^{l'}_{m'+M,K'}\delta_{mK}\delta_{m-Mm'} \\
&= \sum_{jll'}\frac{2k+1}{\sqrt{(2j+1)(2l+1)}}t_{kjl}t_{kll'}x_{lK'}x_{jK}d^{l}_{KK'} \\
&\quad \sum_{M}\times\langle lK-MkM|jK\rangle\langle lK-MkM|l'K\rangle \\
&= \sum_{l}\Big(\sum_{l'}\frac{2k+1}{2l'+1}t^{2}_{kl'l'}\Big)x_{lK}x_{lK'}d^{l}_{KK'}, \qquad \text{(B.10)}
\end{aligned}$$

where the term $\sum_{l'}(2k+1)/(2l'+1)t^{2}_{kl'l'}$ can be regarded as the effective one-body energy denoted by $\varepsilon_{eff,l}$.

APPENDIX C

Coefficients of the ground band normalisation

$$a_{10} = 1 + a - a_1/2a$$

$$a_{21} = 4 + 6\,a - 3\,a_1/a$$

$$a_{32} = 10 + 18\,a - 9\,a_1/a$$

$$a_{43} = 20 + 40\,a - 20\,a_1/a$$

$$a_{54} = 35 + 75\,a - 75\,a_1/2\,a$$

$$a_{65} = 56 + 126\,a - 63\,a_1/a$$

$$a_{76} = 84 + 196\,a - 98\,a_1/a$$

$$a_{87} = 120 + 288\,a - 144\,a_1/a$$

$$a_{20} = 2 + 6\,a + 2\,a^2 - 3\,a_1 - 10\,a_1/3\,a + 3\,{a_1}^2/(2\,a^2) - a_2/3\,a$$

$$a_{31} = 18 + 72\,a + 42\,a^2 - 54\,a_1 - 40\,a_1/a + 45\,{a_1}^2/2\,a^2 - 4\,a_2/a$$

$$a_{42} = 88 + 400\,a + 300\,a^2 - 360\,a_1 - 220\,a_1/a + 135\,{a_1}^2/a^2 - 20\,a_2/a$$

$$a_{53} = 308 + 1500\,a + 1300\,a^2 - 1500\,a_1 - 2450\,a_1/3\,a + 525\,{a_1}^2/a^2 - 200\,a_2/3\,a$$

$$a_{64} = 868 + 4410\,a + 4200\,a^2 - (4725 + 2380/a)\,a_1 + 1575\,a_1^2/a^2 - 175\,a_2/a$$

$$a_{75} = 2100 + 10976\,a + 11172\,a^2 - (12348 + 5880/a)\,a_1 + 3969\,{a_1}^2/a^2 - 392a_2/a$$

$$a_{86} = 868 + 4410\,a + 4200\,a^2 - (4725 + 2380/a)\,a_1 + 1575\,{a_1}^2/a^2 - 175\,a_2/a$$

$$a_{30} = 6 + 36\,a + 42\,a^2 + 6\,a^3 + (55/2\,a^2 + 27/a)\,{a_1}^2 - 45\,{a_1}^3/4\,a^3 -$$
$$(6 + 5/a)\,a_2 + a_1\,(-60 - 22/a - 21\,a + 5\,a_2/a^2) - a_3/4\,a$$

$$
\begin{aligned}
a_{41} &= 96 + 720\,a + 1200\,a^2 + 360\,a^3 + (660/a^2 + 900/a)\,{a_1}^2 - 315\,{a_1}^3/a^3 - \\
&\quad (160 + 100/a)\,a_2 - a_1\,(1600 + 440/a - 900\,a + 120\,a_2/a^2) - 5\,a_3/a \\
a_{52} &= 796 + 6600\,a + 13000\,a^2 + 5400\,a^3 + (6300/a^2 + 10125/a)\,{a_1}^2 - \\
&\quad 3150\,{a_1}^3/a^3 - (1500 + 2450/3\,a)\,a_2 - a_1\,(16500 + 11900/3\,a - 11700\,a + \\
&\quad 1050\,a_2/a^2) - 75\,a_3/2\,a \\
a_{63} &= 4464 + 38808\,a + 84000\,a^2 + 42000\,a^3 + (37100/a^2 + 66150/a)\,{a_1}^2 - \\
&\quad 18900\,{a_1}^3/a^3 - (8400 + 4200/a)\,a_2 + a_1\,(-102900 - 22904/a - \\
&\quad 84000\,a + 5600\,a_2/a^2) - 175\,a_3/a \\
a_{74} &= 19108 + 170128\,a + 391020\,a^2 + 220500\,a^3 + (160965/a^2 + \\
&\quad 308700/a)\,{a_1}^2 - 165375\,{a_1}^3/2\,a^3 - (34300 + 16170/a)\,a_2 - a_1\,(466480 + \\
&\quad 98784/a - 418950\,a + 22050\,a_2/a^2) - 1225\,a_3/2\,a \\
a_{85} &= 67072 + 604800\,a + 1448832\,a^2 + 889056\,a^3 + (564480/a^2 + \\
&\quad 1143072/a)\,{a_1}^2 - 291060\,{a_1}^3/a^3 - (112896 + 50960/a)\,a_2 - \\
&\quad a_1\,(1693440 + 346304/a - 1629936\,a + 70560\,a_2/a^2) - 1764\,a_3/a
\end{aligned}
\tag{C.1}
$$

APPENDIX D

Numerical evaluation of the reduced normalisation integral

In the SU(3) limit, the reduced normalisation integral becomes

$$F(N,I) = \int_0^1 dx P_I(x) x^{pN} = \frac{(pN)!}{(pN-I)!!(pN+I+1)!!}, \tag{D.1}$$

where $I \leq pN$ and I must be even. By making use of the above result, one can evaluate the general $F(N,I)$, namely,

$$\begin{aligned} & F(N,I) \\ & = \int_0^{\frac{\pi}{2}} d\beta \sin\beta P_I(\beta)[z(\beta)]^N \\ & = \int_0^1 dx P_I(x)[a_0 + a_2 x^2 + a_4 x^4]^N \\ & = \sum_{m=0}^{N} \sum_{n=0}^{N-m} \frac{N! a_0^{N-n-m} a_2^n a_4^m (2n+4m)!}{m!n!(N-m-n)!(2n+4m-I)!!(2n+4m+I+1)!!}, \end{aligned} \tag{D.2}$$

where

$$a_0 = x_{00}^2 - \frac{1}{2}x_{20}^2 + \frac{3}{8}x_{04}^2, \quad a_2 = \frac{3}{2}x_{20}^2 - \frac{15}{4}x_{40}^2, \quad a_4 = \frac{35}{8}x_{40}^2. \tag{D.3}$$

Notice that $2n + 4m \geq I$ and I must be even.

APPENDIX E

$1/N$ expansion formulae for the γ band

E.1 The orthogonality coefficient

The $1/N$ expansion of ξ_γ up to the second layer is given by

$$
\begin{aligned}
\xi_\gamma = \frac{-b_2}{2b_1^2}\Big\{ & 1 + \frac{1}{aN}\Big(3b_{11}/b_1 - b_{21}/b_2 - 3a\Big) \\
& + \frac{1}{(aN)^2}\Big(6a - 3a_1/a - 15b_{11}/2 - 3b_{11}/2a + 3a_1b_{11}/a^2 + \\
& \quad 9b_{11}^2/4a + (b_{11}/2 + 6b_{11}^2 - b_{12})/ab_1^2 + 6b_{21} + \\
& \quad b_{21}/a - 2a_1b_{21}/a^2 - 3b_{11}b_{21}/2a + (-15b_{11} - 5b_{11}/2a + \\
& \quad 6a_1b_{11}/a^2 + 9b_{11}^2 - b_{12}/a - 3b_{11}b_{21}/a)/b_1 + b_{22}/2a\Big) \\
& + \frac{\bar{L}}{(aN)^2}\Big[a - b_{11}/2 - b_{11}/b_1 + b_{21}/3 + \\
& \quad \frac{1}{aN}\Big(-2a - 8a^2 + 4a_1 + 2b_{11} + 7ab_{11} - 3a_1b_{11}/a - \\
& \qquad 3b_{11}^2/2 + (-b_{11}/3 - 4b_{11}^2 + 2b_{12}/3)/b_1^2 - 4b_{21}/3 - \\
& \qquad 16ab_{21}/3 + 2a_1b_{21}/2 + b_{11}b_{21} + (11b_{11}/3 + 14ab_{11} - \\
& \qquad 6a_1b_{11}/a - 6b_{11}^2 + 2b_{12}/3 + 2b_{11}b_{21})/b_1 - b_{22}/3\Big)\Big] \\
& + \frac{\bar{L}^2}{2(aN)^4}\Big[a + 4a^2 - 3a_1/2 - 3b_{11}/4 - 3ab_{11} + a_1b_{11}/a + b_{11}^2/2 + \\
& \quad (b_{11}/6 + 3b_{11}^2 - b_{12}/3)/2b_1^2 + b_{21}/2 + 2ab_{21} - \\
& \quad 2a_1b_{21}/3a - b_{11}b_{21}/3 + (-17b_{11}/24 - 3ab_{11} + a_1b_{11}/a + \\
& \quad b_{11}^2 - b_{12}/12 - b_{11}b_{21}/3)/2b_1 + b_{22}/12\Big]\Big\},
\end{aligned}
\tag{E.1}
$$

where

$$b_{2n} = \sum_l \bar{l}^n \sqrt{\bar{l}(\bar{l}-2)} x_l x_{l2}, \qquad b_{1n} = \sum_l \bar{l}^n \sqrt{\bar{l}} x_l x_{l1}. \tag{E.2}$$

The subscript n is suppressed when it is zero. The SU(3) limit offers a good check to this expression. When we substitute $(x_0, x_2, x_4) = (\sqrt{1/5}, \sqrt{4/7}, \sqrt{8/35})$; $(x_{22}, x_{42}) = (\sqrt{1/7}, \sqrt{6/7})$; and $(x_{21}, x_{41}) = (\sqrt{3/7}, \sqrt{4/7})$ into eq.(E.1), all the $\bar{L}$ and N dependent terms vanish. We get ξ_γ equal to $-\sqrt{6}/4$ which is the same as the value given in the SU(3) prescription. When SU(3) symmetry is broken, it is apparent from the $1/N$ expansion expression that ξ_γ has spin-dependence.

E.2 Third layer $1/N$ formulas for the γ band

The $1/N$ expansion of the one-body matrix elements for the γ band (with ζ_γ) is given by

$$\begin{aligned}
\langle \hat{n}_l \rangle_{\gamma,L} = N x_l^2 \Big\{ & 1 + \frac{1}{aN}\Big(-\bar{l} + a x_{l2}^2/x_l^2 \Big) \\
& + \frac{1}{(aN)^2}\Big(((7-a')(a-\bar{l}) + (a_1 + b_2^2)(1/2 - \bar{l}/a) + \bar{l}^2/2) + b_2 x_{l2}/x_l \\
& \quad + (aa' - b_2^2/2 - a\bar{l}) x_{l2}^2/x_l^2 \Big) \\
& + \frac{1}{(aN)^3}\Big((a^2(-7+a') + a_1(41/3 - 2a')(1 - 3\bar{l}/2a) - a_2(1/3 + \bar{l}/2a) \\
& \quad + b_2^2(5+a')(1-3\bar{l}/2a) + a(25 - 6a' - a'^2 + a_1' - a_1/2 - b_2^2/2) \\
& \quad - b_2 b_{21}(2 + 3\bar{l}/a) + (5a_1^2/4 + 5a_1 b_2^2/2 - b_2^4/4)(1/a - 2\bar{l}/a^2 \\
& \quad + (-25 + a(7-a') + 6a' + a'^2 - a_1' + a_1 + b_2^2)\bar{l} + (41/6 - a/2 - a' \\
& \quad + 5(a_1 + b_2^2)\bar{l}^2/4a - \bar{l}^3/6 + ((-ab_2 + (5+a')b_2 + (5a_1 b_2 - b_2^3)/2a \\
& \quad - b_{21}) - b_2\bar{l}) x_{l2}/x_l + ((-a^2 a' + a' a_1 - (5/2 + a')b_2^2 + a(3a' + a'^2 \\
& \quad - a_1'/2 + b_2^2/2) + b_2^4 - 5a_1 b_2^2)/4a + b_2 b_{21}) + (a^2 - a(3+a') - a_1 \\
& \quad + b_2^2/2)\bar{l} + a\bar{l}/2 \Big) \\
& + \frac{\bar{L}}{(aN)^2}\Big[\bar{l} - a + \frac{1}{aN}\Big(a^2 + a(-6+2a') - 2(a_1 + b_2^2) + (6 - a - 2a' \\
& \quad + 3(a_1 + b_2^2)/a)\bar{l} - \bar{l}^2 \Big) \\
& + \frac{1}{(aN)^2}\Big((-a^3 + 8a^2(4-a') + 9(a' - 7/2)a_1 + 3a_2/2 + 3(5 - 3a')b_2^2/2
\end{aligned}$$

$$
\begin{aligned}
&+a(9-6a'+3a'^2-3aa_1+7a_1+7b_2^2)+(3b_2^4/2-15a_1^2/2-15a_1b_2^2)/a\\
&+9b_2b_{21})+(-9+a^2+6a'-3a'^2+8a(a'-4)+3a_1'-21a_1/2-21b_2^2/2\\
&+(25a_1^2+25a_1b_2^2-5b_2^4/2)a^2+(6(7-2a')a_1-2a_2+(6a'-10)b_2^2\\
&-12b_2b_{21}))\bar{l}/a+(-21/2+7a/2+3a'-5(a_1+b_2^2)/2)\bar{l}^2+\bar{l}^3/2\\
&+((7ab_2+(5-3a')b_2+(-10a_1b_2+2b_2^3)/a+3b_{21})+3b_2\bar{l})x_{l2}/x_l\\
&+((4a^2a'-3a'a_1(3a'-5/2)b_2^2+a(2a'-2a'^2+a_1'-7b_2^2/2)\\
&+(5a_1b_2^2-b_2^4)/a-3b_2b_{21})+(-4a^2+a(-2+2a')\\
&+3a_1-3b_2^2/2)\bar{l}+a\bar{l}^2)x_{l2}^2/x_l^2\Big)\Big]\\
&+\frac{\bar{L}^2}{2(aN)^4}\Big[(-1-1/2a+3(a_1+b_2^2)/4a^2)+(1/2a^2+1/a-(a_1+b_2^2)/a^3)\bar{l}\\
&+\bar{l}^2/4a^2+b_2x_{l2}/(2a^2x_l)-b_2^2x_{l2}^2/x_l^2\\
&+\frac{1}{aN}\Big((4+(6a'-15)/a+(-18+10a'-2a'^2+a_1'-21a_1/2-21b_2^2/2)/a^2\\
&+(13a_1^2/2+13a_1b_2^2-5b_2^4/2)(a-3\bar{l}/2)/a^5+((8-4a')a_1-a_2+(5a'\\
&-18)b_2^2-6b_2b_{21})(a-4\bar{l}/5)/a^4+((15-6a')/a^2-4/a+(18-10a'\\
&+2a'^2-a_1'+14a_1+14b_2^2)/a^3)\bar{l}+(-7/2a^2+(2-a')/a^3+13(a_1\\
&+b_2)/4a^4)\bar{l}^2-\bar{l}^3/4a^3+((-7b_2/a^2+(13a_1b_2-5b_2^3)/2a^4+(5a'/2\\
&-9)b_2-3b_{21}/2)/a^3)-3b_2\bar{l}/2a^3)x_{l2}/x_l+((-2a'/a+(-5a'+a'^2\\
&-a_1'/4+7b_2^2/2)a^2+(-13a_1b_2^2+5b_2^4/4)/a^4+(a'a_1+(9/2-5a'/2)b_2^2\\
&+3b_2b_{21}/2)/a^3)+(2/a+(5/2-a')/a^2+(-a_1+5b_2^2/4)/a^3)\bar{l}\\
&+\bar{l}^2/4a^2)x_{l2}^2/x_l^2\Big)\Big]\\
&+\frac{\bar{L}^3}{3(aN)^6}\Big[(-2(1+1/a)+2(1/a^2+1/a)\bar{l}+(a_1^2/4+a_1b_2^2/2-5b_2^4/4)(-5a\\
&+7\bar{l})/a^5+(5a_1/3+a_2/6+(6-3a'/2)b_2^2+b_2b_{21})(5a/6-\bar{l})/a^4\\
&+(a_1+b_2^2)(3a^2-15a\bar{l}/4-\bar{l}^2)/a^4-1/3a^2+\bar{l}/3a^3+(5/18a^3\\
&+3/4a^2)\bar{l}^2+\bar{l}^3/26a^3+((3b_2/2a^2+b_2^3-a_1b_2)/a^4+((2-a'/2)b_2\\
&+b_{21}/6)/a^3+b_2/6a^3)x_{l2}/x_l+(-3b_2^2/4a^2+(a_1b_2^2-b_2^4)/2a^4\\
&+((-6+3a')b_2^2-b_2b_{21})/6a^3-b_2^2/4a^3)x_{l2}^2/x_l^2\Big]\Big\},
\end{aligned}
\tag{E.3}
$$

where

$$a'_n = \sum_l \bar{l}^{n+1} x_{l2}^2. \tag{E.4}$$

For matrix elements of two-body multipole interactions without the orthogonality term (i.e. $\zeta_\gamma = 0$), we have

$$\begin{aligned}
\langle T^{(k)} \cdot T^{(k)} \rangle_{\gamma,L} \;=\; & N^2\Big\{U_k + \frac{1}{aN}\Big(4aU''_k - aU_k - U_{k1} + aC_k\Big) \\
& + \frac{1}{(aN)^2}\Big((7a(2-a') + a_1 + b_2^2)U_k + (a' - (a_1+b_2^2)/a - 7)U_{k1} + U_{k2}/2 \\
& \quad + 2b_2 U'_k + 2(2aa' - b_2^2)U''_k - 4aU''_{k1} - aC_{k1} + a^2 C_k\Big) \\
& + \frac{1}{(aN)^3}\Big((2a^2(a'-7) + (82/3 - 4a')a_1 - 2a_2/3 + (10+2a')b_2^2 \\
& \quad + a(50 - 12a' - 2a'^2 + 2a'_1 - a_1 - b_2^2) + (5a_1^2 + 10a_1 b_2^2 - b_2^4)/2a \\
& \quad - 4b_2 b_{21})U_k + (-25 + a(a'-7) + 6a' + a'^2 - a'_1 - a_1/2 - b_2^2/2 \\
& \quad + (b_2^4 - 5a_1^2 - 10a_1 b_2^2)/2a^2 + ((6a'-41)a_1 + a_2 - (15+3a')b_2^2 \\
& \quad + 6b_2 b_{21})/2a)U_{k1} + (41/6 - a' + 5(a_1+b_2^2)/4a)U_{k2} - U_{k3}/6 \\
& \quad + ((10+2a')b_2 + (5a_1 b_2 - b_2^3)/a - 2b_{21})U'_k - 2b_2 U'_{k1} + (4(7-a')a^2 \\
& \quad + 4a'a_1 - (10+4a')b_2^2 + a(12a' + 4a'^2 - 2a'_1 + 2a_1 + 2b_2^2) + (b_2^4 \\
& \quad - 5a_1 b_2^2)/a + 4b_2 b_{21})U''_k + (2b_2^2 - 4a(a'+3) - 4a_1)U''_{k1} + 2aU''_{k2} \\
& \quad + a(7-a')(aC_k - C_{k1}) + (a_1 + b_2^2)(aC_k/2 - C_{k1}) + aC_{k2}/2 \\
& \quad + (a^2 a' - ab_2^2/2)C''_k - a^2 C''_{k1} + ab_2 C'_k\Big) \\
& + \frac{\bar{L}}{(aN)^2}\Big[-2aU_k + U_{k1} \\
& \quad + \frac{1}{aN}\Big(2(a^2 + 2a(a'-3) - 2a_1 - 2b_2^2)U_k + (6 + a - 2a' + 3(a_1+b_2^2)/a)U_{k1} \\
& \quad\quad - U_{k2} - 4b_2 U'_k + 4(b_2^2 - a^2 - aa')U''_k + 4aU''_{k1} + aC_{k1} - a^2 C_k\Big) \\
& \quad + \frac{1}{(aN)^2}\Big((-2a^3 + 4(11-3a')a^2 + 9(2a'-7)a_1 + 3a_2 + 3(5-3a')b_2^2 \\
& \quad\quad + a(6(3 - 2a' + a'^2 - a'_1) + 11(a_1+b_2^2)) + 3(b_2^4 - 5a_1^2 - 10a_1 b_2^2)/a \\
& \quad\quad + 18b_2 b_{21})U_k + (6a' - 9 - a^2 - 2a'^2 + 2a'_1 - a_1 - b_2^2 + 25(a_1^2 + 2a_1 b_2^2 \\
& \quad\quad - b_2^4/5)/2a^2 + (6(7-2a')a_1 - 2a_2 + (6a'-10)b_2^2 - 12b_2 b_{21})/a)U_{k1} \\
& \quad\quad + (-21/2 + a + 3a' - 5(a_1+b_2^2)/a)U_{k2} + U_{k3}/2 + (4ab_2 + (10-6a')/b_2
\end{aligned}$$

$$
\begin{aligned}
&+4(b_2^3-5a_1b_2)/2+6b_{21})U_k'+6b_2U_{k1}'+(4a^3+12a^2(a'-2)-12a'a_1\\
&+(12a'-10)b_2^2+4a(4a'-4a'^2+a_1'-2a_1-3b_2^2)+4(5a_1b_2^2-b_2^4)/a\\
&-12b_2b_{21})U_k'+4(2a(a'-1)-a^2+3a_1-3b_2^2/2)U_{k1}''-4aU_{k2}''\\
&+(a^2+2a(a'-3))(aC_k-C_{k1})+(a_1+b_2^2)(3C_{k1}-2aC_k)-aC_{k2}\\
&+\left(a(b_2^2-aa')C_k''+a(C_{k1}''-2b_2C_k'\right)\Big]\\
+\frac{\bar{L}^2}{2(aN)^4}&\Big[(-2a-2a^2+3a_1+3b_2^2)U_k+(1-2(a_1+b_2^2)/a)U_{k1}\\
&+U_{k2}/2+2b_2U_k'-2b_2^2U_k'')\\
&+\frac{1}{aN}\Big((10a^3+(16a'-38)a^2+16(2-a')a_1-4a_2+4(5a'-18)b_2^2\\
&+a(40a'-72-8a'^2+4a_1'-31(a_1+b_2^2))+(26a_1^2+52a_1b_2^2-10b_2^4)/a\\
&-24b_2b_{21})U_k+(36+2a^2+a(10-4a')-20a'+4a'^2-2a_1'\\
&+21(a_1+b_2^2)/2+(15b_2^4-39a_1(a_1+2b_2^2)/2a^2+(10(a'-2)a_1+5a_2/2\\
&+5(9-5a'/2)b_2^2+15b_2b_{21})/a)U_{k1}+(4-7a/2-2a'+13(a_1+b_2^2)/2a)U_{k2}\\
&-U_{k3}/2+((10a'-36)b_2-14ab_2+(26a_1b_2-10b_2^3)/a-6b_{21})U_k'\\
&-6b_2U_{k1}'+(8a'a_1-8a^3-4a^2(2a'+1)+4(9-5a')b_2^2+2a(4a'^2\\
&-10a'-a_1'+3a_1+10b_2^2)+(10b_2^4-26a_1b_2^2)/a+12b_2b_{21})U_k''+(8a^2+\\
&4a(5-2a')-8a_1+10b_2^2)U_{k1}''+2aU_{k2}''\\
&+a(1+2a)(C_{k1}-aC_k)+(a_1+b_2^2)(3C_k/2-2C_{k1})+\\
&aC_{k2}/2ab_2(C_k'-b_2C_k''/2)\Big)\Big]\\
+\frac{\bar{L}^3}{3(aN)^6}&\Big[(-9a^2-6a^3+25a_1/3+5a_2/6+(30-15a'/2)b_2^2+a(-2+27a_1/2\\
&+27b_2^2/2)-15(a_1^2+2a_1b_2^2-b_2^4)/2a+5b_2b_{21})U_k+(1+3a-6a_1-6b_2^2\\
&+21(a_1^2+2a_1b_2^2-b_2^4)/4a^2+(-5a_1-a_2/2+(-18+9a'/2)b_2^2\\
&-3b_2b_{21})/a)U_{k1}+(5/6+3a/2-3(a_1+b_2^2)/(2a))U_{k2}+U_{k3}/12+(6ab_2\\
&+(12-3a')b_2+6(b_2^3-a_1b_2)/a+b_{21})U_k'+b_2U_{k1}'+6((a'-2)b_2^2\\
&+(a_1b_2^2-b_2^4)/a-ab_2^2-b_2b_{21}/3)U_k''-3b_2^2U_{k1}''\Big]\Big\},
\end{aligned}
\tag{E.5}
$$

where t_{kjl} is defined in eq. (4.8), and

$$\begin{aligned} C'_{kn} &= (2k+1)\sum_{jl} \bar{l}^n \sqrt{\bar{l}(\bar{l}-2)}(t_{kjl})^2 x_l x_{l2}/(2l+1), \\ C''_{kn} &= (2k+1)\sum_{jl} \bar{l}^n (t_{kjl}x_{l2})^2/(2l+1), \end{aligned} \tag{E.6}$$

and

$$\begin{aligned} U'_{kn} &= (2k+1)\sum_{jlj'l'I} \bar{I}^n \sqrt{\bar{I}(\bar{I}-2)}\langle j0j'0|I0\rangle\langle l'0l2|I2\rangle \\ &\quad \times \left\{ \begin{array}{ccc} j & j' & I \\ l' & l & k \end{array} \right\} t_{kjl}t_{kj'l'}x_j x_l x_{j'} x_{l'2}, \\ U''_{kn} &= \frac{(2k+1)}{2}\sum_{jlj'l'I} \bar{I}^n \langle j2j'0|I2\rangle(\langle l'0l2|I2\rangle x_{l'}x_{l2} + \langle l'2l0|I2\rangle x_{l'2}x_l) \\ &\quad \times \left\{ \begin{array}{ccc} j & j' & I \\ l' & l & k \end{array} \right\} t_{kjl}t_{kj'l'}x_{j2}x_{j'}. \end{aligned} \tag{E.7}$$

By manipulating the sum over *six-j* symbols [105], we have

$$\begin{aligned} U'_2 &= A(12A' + (A'_{02} + 3A'_{20} - 14A'_{01} - 18A'_{10})/4) + (6A_1 + A_{11} \\ &\quad -A_2)(5A'_{01} + A'_{10} - (A'_{02} + A'_{20})/2 + A'_{11} - 12A')/24 \\ U'_{21} &= A'(-90A + 51A_1 + 2A_{11} - 5A_2) + (33A - 19A_1 - (29A_{11} - 59A_2)/24) \\ &\quad -A'_{01}(3A + 13A_2/48) + A'_{10}(42A - 43A_1/2 + (37A_2 - 31A_{11})/24) \\ &\quad +A'_{11}(-5A + A_1 + (5A_{11} + A_2)/24) + A(3A'_{12} + 3A'_{30} - 2A'_{21})/4 \\ &\quad -(9A + 25A_2/48)A'_{20} + (A_3 - A_{12})(A'/4 + (A'_{20} - 2A'_{11} - 2A'_{10} \\ &\quad +A'_{02} - 10A'_{01}) + (A^2 - A_{11} - 6A_1)(A'_{12} - 2A'_{21} + A'_{30})/16 \\ &\quad +(12A_1 + A_{11})(7A'_{02} + 19A'_{20}), \\ U''_2 &= ((A'_{02} - 2A'_{10} - 2(12A' - 5A'_{01}))^2 + (A'_{20} - 2A'_{11})^2)/192 + (2A'_{11} - A'_{20}) \\ &\quad \times(10A'_{01} + 2A'_{10} - A'_{02} - 24A')/96 + A(12A'' - 7A''_1 + A''_2/2) \\ U''_{21} &= (A'_{12} + A'_{21} - A'_{03} - A'_{30})(2(5A'_{01} + A'_{11} + A'_{10}) - A'_{20} - A'_{02} - 24A')/192 \\ &\quad +A'_{01}((29A_{02} + 23A'_{20})/48 - (3A'_{01} + A_{10})/4 + A'_{11}/6) + A'_{10}(12A'_{10} \\ &\quad +7A'_{02} - 8A'_{11} + 13A'_{20}) + -A'_{20}(A'_{20} + 2A'_{11})/96 + A'_{02}(6A'_{11} - 5A'_{02} \\ &\quad -8A'_{20}/12) + A'(9A' - 3(A'_{01} + A'_{10})/2 - A'_{11} - A'_{20}) - A(36A'' + 33A''_1 \\ &\quad -7A''_{11}/2 + A''_{12}/4 + A_1(12A'' - 7A''_1 + A''_2/2) - A(5A''_2 + A''_3/4), \end{aligned} \tag{E.8}$$

where

$$
\begin{aligned}
A'_{mn} &= \sum_{jl} \frac{\bar{j}^m \bar{l}^n}{\sqrt{\bar{j}(\bar{j}-2)}} \langle j0l0|40\rangle t_{2jl} x_{j2} x_l, \\
A''_{mn} &= \sum_{jl} \frac{\bar{j}^m \bar{l}^n}{\sqrt{\bar{j}(\bar{j}-2)}\sqrt{\bar{l}(\bar{l}-2)}} \langle j0l0|40\rangle t_{2jl} x_{j2} x_{l2}, \\
B'_{mn} &= \sum_{jl} \frac{\bar{j}^m \bar{l}^n}{\sqrt{\bar{j}(\bar{j}-2)}} \langle j0l0|40\rangle t_{2jl} x_{j2} x_l, \\
B''_{mn} &= \sum_{jl} \frac{\bar{j}^m \bar{l}^n}{\sqrt{\bar{j}(\bar{j}-2)}\sqrt{\bar{l}(\bar{l}-2)}} \langle j0l0|40\rangle t_{2jl} x_{j2} x_{l2}.
\end{aligned}
\tag{E.9}
$$

APPENDIX F

Contributions of various terms in $1/N$ expansion

			zeroth	1st	2nd	3rd
ξ_γ^0	$F(N-1,I)$	x_{j2}^2	1	$\frac{I^2}{N^2}$	$\frac{I^4}{N^4}$	$\frac{I^6}{N^6}$
	$F(N-2,I)$	$R_2(l'20,l02;j)$	$\times$	$\frac{I^3}{N^3}$	$\frac{I^5}{N^5}$	$\frac{I^7}{N^7}$
ξ_γ	$F(N-2,I)$	$R_2(l'21,l01;j)$	$\times$	$\frac{I^2}{N^2}$	$\frac{I^4}{N^4}$	$\frac{I^6}{N^6}$
	$F(N-3,I)$	$R_3(k10,k'10,l20;l',j)$	$\times$	$\frac{I^3}{N^3}$	$\frac{I^5}{N^5}$	$\frac{I^7}{N^7}$
ξ_γ^2	$F(N-2,I)$	$R_2(l'11,l11;j)$	$\times$	$\frac{I}{N}$	$\frac{I^3}{N^3}$	$\frac{I^5}{N^5}$
	$F(N-3,I)$	$R_3(k10,k'01,l11;l',j)$	$\times$	$\frac{I^2}{N^2}$	$\frac{I^4}{N^4}$	$\frac{I^6}{N^6}$
	$F(N-4,I)$	$R_3(k10,k'10,l01,l'01;k'',l'',j)$	$\times$	$\frac{I^3}{N^3}$	$\frac{I^5}{N^5}$	$\frac{I^7}{N^7}$

Table F.1: The contributions of various terms to different layers in the $1/N$ expansion of the normalisation of the γ-band.

			zeroth	1st	2nd	3rd
ξ^0_γ	$F(N-1,I)$	x^2_{l2}	$\times$	$\times$	$\frac{I^3}{N^3}$	$\frac{I^5}{N^5}$
	$F(N-2,I)$	$R_2(l'22,l00;j)$	$\times$	$\frac{I}{N}$	$\frac{I^3}{N^3}$	$\frac{I^5}{N^5}$
		$R_2(l'20,l02;j)$	$\times$	$\times$	$\times$	$\frac{I^5}{N^5}$
	$F(N-3,I)$	$R_3(k20,k'02,l00;l',j)$	$\times$	$\times$	$\frac{I^4}{N^4}$	$\frac{I^6}{N^6}$
ξ_γ	$F(N-2,I)$	$R_2(l'21,l01;j)$	$\times$	$\times$	$\times$	$\frac{I^4}{N^4}$
		$R_2(l'01,l21;j)$	$\times$	$\times$	$\times$	$\frac{I^4}{N^4}$
	$F(N-3,I)$	$R_3(k20,k'01,l00;l',j)$	$\times$	$\times$	$\frac{I^3}{N^3}$	$\frac{I^5}{N^5}$
		$R_3(k20,k'01,l01;l',j)$	$\times$	$\times$	$\times$	$\frac{I^5}{N^5}$
		$R_3(k10,k'10,l02;l',j)$	$\times$	$\times$	$\times$	$\frac{I^5}{N^5}$
	$F(N-4,I)$	$R_4(k10,k'10,l'02,l00;k'',l'',j)$	$\times$	$\times$	$\frac{I^4}{N^4}$	$\frac{I^6}{N^6}$
ξ^2_γ	$F(N-2,I)$	$R_2(l'11,l11;j)$	$\times$	$\times$	$\times$	$\frac{I^3}{N^3}$
	$F(N-3,I)$	$R_3(k11,k'11,l00;l',j)$	$\times$	$\times$	$\frac{I^2}{N^2}$	$\frac{I^4}{N^4}$
		$R_3(k11,k'10,l01;l',j)$	$\times$	$\times$	$\times$	$\frac{I^4}{N^4}$
		$R_3(k10,k'01,l11;l',j)$	$\times$	$\times$	$\times$	$\frac{I^4}{N^4}$
	$F(N-4,I)$	$R_4(k11,k'10,l'01,l00;k'',l'',j)$	$\times$	$\times$	$\frac{I^3}{N^3}$	$\frac{I^5}{N^5}$
		$R_4(k10,k'10,l'01,l01;k'',l'',j)$	$\times$	$\times$	$\times$	$\frac{I^5}{N^5}$
	$F(N-5,I)$	$R_5(k10,k'10,l'01,j'01,l00;k'',l'',j'',j)$	$\times$	$\times$	$\frac{I^4}{N^4}$	$\frac{I^6}{N^6}$

Table F.2: The contributions of various terms to different layers in the $1/N$ expansion of the one-body matrix elements of the γ-band.

			zeroth	1st	2nd	3rd
ξ^0_γ	$F(N-2,I)$	-	$\times$	$\frac{I}{N}$	$\frac{I^3}{N^3}$	$\frac{I^5}{N^5}$
	$F(N-3,I)$	x^2_{i2}	1	$\frac{I^2}{N^2}$	$\frac{I^4}{N^4}$	$\frac{I^6}{N^6}$
		$x_{i2}x_i$	$\times$	$\times$	$\frac{I^4}{N^4}$	$\frac{I^6}{N^6}$
	$F(N-4,I)$	$R_2(k20,k'02;i)$	$\times$	$\frac{I^3}{N^3}$	$\frac{I^5}{N^5}$	$\frac{I^7}{N^7}$
ξ_γ	$F(N-2,I)$	-	$\times$	$\times$	$\frac{I^2}{N^2}$	$\frac{I^4}{N^4}$
	$F(N-3,I)$	$x_{i2}x_{i1}$	$\times$	$\times$	$\frac{I^3}{N^3}$	$\frac{I^5}{N^5}$
		$x_{i2}x_i$	$\times$	$\times$	$\times$	$\frac{I^5}{N^5}$
		$x_{i1}x_i$	$\times$	$\times$	$\frac{I^3}{N^3}$	$\frac{I^5}{N^5}$
	$F(N-4,I)$	$R_2(k21,k'01;i)$	$\times$	$\frac{I^2}{N^2}$	$\frac{I^4}{N^4}$	$\frac{I^6}{N^6}$
		$R_2(k20,k'01;i)$	$\times$	$\times$	$\frac{I^4}{N^4}$	$\frac{I^6}{N^6}$
		$R_2(k10,k'10;i)$	$\times$	$\times$	$\frac{I^4}{N^4}$	$\frac{I^6}{N^6}$
	$F(N-5,I)$	$R_3(k10,k'10,i'02;k'',i)$	$\times$	$\frac{I^3}{N^3}$	$\frac{I^5}{N^5}$	$\frac{I^7}{N^7}$
ξ^2_γ	$F(N-2,I)$	-	$\times$	$\times$	$\times$	$\frac{I^3}{N^3}$
	$F(N-3,I)$	x^2_{i1}	$\times$	$\times$	$\times$	$\frac{I^4}{N^4}$
		$x_{i1}x_i$	$\times$	$\times$	$\times$	$\frac{I^4}{N^4}$
	$F(N-4,I)$	$R_2(k11,k'11;i)$	$\times$	$\frac{I}{N}$	$\frac{I^3}{N^3}$	$\frac{I^5}{N^5}$
		$R_2(k11,k'10;i)$	$\times$	$\times$	$\frac{I^3}{N^3}$	$\frac{I^5}{N^5}$
		$R_2(k10,k'01;i)$	$\times$	$\times$	$\frac{I^3}{N^3}$	$\frac{I^5}{N^5}$
		$R_2(k10,k'10;i)$	$\times$	$\times$	$\times$	$\frac{I^5}{N^5}$
	$F(N-5,I)$	$R_3(k11,k'10,i'01;k'',i)$	$\times$	$\frac{I^2}{N^2}$	$\frac{I^4}{N^4}$	$\frac{I^6}{N^6}$
		$R_3(k10,k'10,i'01;k'',i)$	$\times$	$\times$	$\frac{I^4}{N^4}$	$\frac{I^6}{N^6}$
	$F(N-6,I)$	$R_4(k10,k'10,i'01,i''01;k'',l'',i)$	$\times$	$\frac{I^3}{N^3}$	$\frac{I^5}{N^5}$	$\frac{I^7}{N^7}$

Table F.3: The contributions of various terms to different layers in the $1/N$ expansion of the two-body matrix elements of the γ-band.

	zeroth	1st	2nd
$F(N-2,I)$	1	$\frac{I^2}{N^2}$	$\frac{I^4}{N^4}$
$F(N-3,I)$	$\times$	$\frac{I^3}{N^3}$	$\frac{I^5}{N^5}$
$F(N-4,I)$	$\times$	$\times$	$\frac{I^6}{N^6}$

Table F.4: The contributions of various terms to different layers in the $1/N$ expansion of the normalisation of the $\gamma\gamma$-band.

		zeroth	1st	2nd	3rd
$F(N-2,I)$	$R_2(l'22,l22;j)$	$\times$	$\times$	$\frac{I^2}{N^2}$	$\frac{I^4}{N^4}$
$F(N-3,I)$	$R_3(k22,k'22,l00;l',j)$	$\times$	$\frac{I}{N}$	$\frac{I^3}{N^3}$	$\frac{I^5}{N^5}$
	$R_3(k22,k'20,l02;l',j)$	$\times$	$\times$	$\times$	$\frac{I^5}{N^5}$
	$R_3(k20,k'02,l22;l',j)$	$\times$	$\times$	$\times$	$\frac{I^5}{N^5}$
$F(N-4,I)$	$R_4(k22,k'20,l'02,l00;k'',l'',j)$	$\times$	$\times$	$\frac{I^4}{N^4}$	$\frac{I^6}{N^6}$
	$R_4(k20,k'20,l'02,l02;k'',l'',j)$	$\times$	$\times$	$\times$	$\times$
$F(N-5,I)$	$R_5(k20,k'20,l'02,j'02,l00;k'',l'',j'',j)$	$\times$	$\times$	$\times$	$\times$

Table F.5: The contributions of various terms to different layers in the $1/N$ expansion of the one-body matrix elements of the $\gamma\gamma$-band.

		zeroth	1st	2nd	3rd
$F(N-2,I)$	-	$\times$	$\times$	$\frac{I^2}{N^2}$	$\frac{I^4}{N^4}$
$F(N-3,I)$	x_{i2}^2	$\times$	$\frac{I}{N}$	$\frac{I^3}{N^3}$	$\frac{I^5}{N^5}$
	$x_{i2}x_i$	$\times$	$\times$	$\times$	$\frac{I^5}{N^5}$
$F(N-4,I)$	$R_2(k22,k'22;i)$	1	$\frac{I^2}{N^2}$	$\frac{I^4}{N^4}$	$\frac{I^6}{N^6}$
	$R_2(k22,k'20;i)$	$\times$	$\times$	$\frac{I^4}{N^4}$	$\frac{I^6}{N^6}$
	$R_2(k20,k'02;i)$	$\times$	$\times$	$\frac{I^4}{N^4}$	$\frac{I^6}{N^6}$
	$R_2(k20,k'20;i)$	$\times$	$\times$	$\times$	$\times$
$F(N-5,I)$	$R_3(k22,k'20,i'02;k'',i)$	$\times$	$\frac{I^3}{N^3}$	$\frac{I^5}{N^5}$	$\frac{I^7}{N^7}$
	$R_3(k20,k'20,i'02;k'',i)$	$\times$	$\times$	$\times$	$\frac{I^7}{N^7}$
$F(N-6,I)$	$R_4(k20,k'20,i'02,i''02;k'',l'',i)$	$\times$	$\times$	$\frac{I^6}{N^6}$	$\frac{I^8}{N^8}$

Table F.6: The contributions of various terms to different layers in the $1/N$ expansion of the two-body matrix elements of the $\gamma\gamma$-band.

Bibliography

[1] F. Iachello and A. Arima, The interacting boson model (Cambridge University Press, Cambridge, 1987).

[2] O. Haxel, J. H. Jensen and H.E. Suess, Phys. Rev. 75 (1949) 1766.

[3] M.G. Mayer, Phys. Rev. 75 (1949) 1969.

[4] A. Bohr and B.M. Mottelson, Nuclear Structure, Vol. 2 (Benjamin, Reading, 1975).

[5] J.P. Elliott, Proc. R. Soc. London Ser A, 245 (1958) 128.

[6] J.P. Elliott, Proc. R. Soc. London Ser A, 245 (1958) 562.

[7] J.P. Elliott and M. Harvey, Proc. R. Soc. London Ser A, 272 (1963) 557.

[8] R.D. Ratna Raju, J.P. Draayer and K.T. Hecht, Nucl. Phys. A202 (1973) 1973.

[9] J.P. Draayer, K.J. Weeks and K.T. Hecht, Nucl. Phys. A381 (1982) 1.

[10] J.P. Draayer and K.J. Weeks, Phys. Rev. Lett., 51 (1983) 1422.

[11] J.P. Draayer and K.J. Weeks, Ann. Phys. 156 (1984) 41.

[12] J.P. Draayer and G. Rosensteel, Nucl. Phys. A439 (1985) 61.

[13] D. Bonatsos and A. Klein, Phys. Rev. C31 (1985) 992.

[14] F. Iachello and A. Arima, Phys. Lett. B53 (1974) 309.

[15] H. Feshbach and F. Iachello, Ann. Phys. 84 (1974) 211.

[16] R.F. Casten and D.D. Warner, Rev. Mod. Phys. 66 (1988) p.389.

[17] D. Warner and R. Casten, Phys. Rev. Lett. 48 (1982) 1385.

[18] R.L. Hatch and S. Levit, Phys. Rev. C25 (1982) 614.

[19] J.N. Ginocchio and M.W. Kirson, Phys. Rev. Lett., 44 (1980) 1744.

[20] J.N. Ginocchio and M.W. Kirson, Nucl. Phys. A350 (1980) 31.

[21] A.E.L. Dieperink, O. Scholten and F. Iachello, Phys. Rev. Lett., 44 (1980) 1747.

[22] N. Yoshinaga, Nucl. Phys. A456 (1986) 21-47.

[23] H.C. Wu and A.E.L. Dieperink, Phys. Rev. C34 (1986) 703.

[24] A. Leviatan, Ann. Phys. 179 (1987) 201.

[25] S. Kuyucak and I. Morrison, Phys. Lett. B255 (1990) 305.

[26] S. Kuyucak and I. Morrison, Ann. Phys. (N.Y.) 181 (1988) 7, ibid, 195 (1989) 126.

[27] P. Ring and P. Schuck, The nuclear many-body problem, (Springer-verlag, 1980).

[28] T. Otsuka, A. Arima and F. Iachello, Nucl. Phys. A390 (1978) 1.

[29] F. Iachello and I. Talmi, Rev. Mod. Phys. 59 (1987) 339.

[30] N. Yoshinaga, A. Arima and T. Otsuka, Phys. Lett. B 143 (1984) 5.

[31] V.O. Nesterenko *et al.*, Sov. J. Nucl. Phys. 44 (1986) 938.

[32] D.G. Burke, Phys. Rev. Lett. 73 1994 14 1899.

[33] V.G. Soloviev and N. Yu. Shirikova, Z. Phys. A334 (1989) 149

[34] V.G. Soloviev, A.V. Sushkov and N.Yu. Shirikova, Nucl. Phys. A568 (1994) 244.

[35] P.T. Deason *et al.*, Phys. Rev. C23 (1981) 1414.

[36] W.T.A. Borghols *et al.* Phys. Lett. B152 (1985) 330.

[37] W. Boeglin *et al.* Nucl. Phys. A477 (1988) 399.

[38] F. Todd Baker *et al.*, Nucl. Phys. A501 (1989) 546.

[39] A. Sethi *et al.* Nucl. Phys. A518 (1990) 536.

[40] A. Sethi *et al.* Phys. Rev. C44 (1991) 700.

[41] S. Kuyucak, V.S. Lac, I. Morrison and B.R. Barrett, Phys. Lett. B263 (1991) 347.

[42] A. Bohr and B.R. Mottelson, Physica Scripta 25 (1982) 28.

[43] N. Yoshida, H. Sagawa, T. Otsuka and A. Arima, Phys. Lett. B 256 (1991) 129.

[44] P. Van Isacker and J.Q. Chen, Phys. Rev. C24 (1980) 684.

[45] K. Heyde, P. van Isacker, M. Waroquier and J. Moreau, Phys. Rev. C29 (1984) 1420.

[46] R.F. Casten *et al.*, Nucl. Phys. A439 (1985) 289.

[47] Y.D. Devi and V.K.B. Kota, Pramana-J. Phys. 39 (1992) 413.

[48] T. Otsuka, A. Arima and N. Yoshinaga, Phys. Rev. Lett. 48 (1982) 387.

[49] J. Dobaczewski and J. Sskalski, Phys. Rev. C38 (1988) 580.

[50] J. Dobaczewski and J. Sskalski, Phys. Rev. C40 (1989) 1025.

[51] N. Yoshinaga, Y. Akiyama and A. Arima, Phys. Rev. C38 (1988) 419.

[52] T. Otsuka and M. Honma, Phys. Lett. B268 (1992) 305.

[53] M. Honma, Superdeformation in the Hg-Pb region and an extension of IBM, Ph.D. thesis, University of Tokyo, 1993.

[54] M. Honma and T. Otsuka, Proc. int. conf. on perspectives for the interacting boson model (Padova, June 1994), (World Scientific, Singapore, 1994) p. 343.

[55] S. Kuyucak, T. Otsuka and M. Honma, Phys. Rev. C53 (1996) in press.

[56] S.C. Li, *super*-SDGBOSON for the supercomputer (ANU, 1993).

[57] H.C. Wu, Phys. Lett. B110 (1982) 1.

[58] H.C. Wu and X.Q. Zhou, Nucl. Phys. A417 (1984) 67.

[59] S. Pittel, *et al.*, Phys. Lett. B144 (1984)145.

[60] S. Kuyucak and S.C. Li, Phys. Lett. B349 (1995) 253.

[61] S. Kuyucak and S.C. Li, Phys. Lett. B354 (1995) 189.

[62] S.C. Li and S. Kuyucak, Nucl. Phys. A (1996) in press.

[63] S. Kuyucak, I. Morrision and T. Sebe, Phys. Rev. C43 (1991) 1187.

[64] H.C. Wu *et al.*, Phys. Rev. C38 (1988) 1638.

[65] I. Morrison, Computer code SDGBOSON (University of Melbourne, 1986).

[66] V.S. Lac and S. Kuyucak, Nucl. Phys. A539 (1992) 418.

[67] P. van Isacker, K. Heyde, M. Waroquier and G. Wenes, Phys. Lett. B104 (1981) 5.

[68] P. van Isacker, K. Heyde, M. Waroquier and G. Wenes, Nucl. Phys. A380 (1982) 323.

[69] K. Heyde, P. van Isacker, M. Waroquier and G. Wenes and Y. Gigase, Nucl. Phys. A398 (1983) 235.

[70] R.F. Casten, Nuclear Structure from a Simple Perspective (Oxford University Press, 1990).

[71] R.R. Whitehead, A. Watt, B.J. Cole and I. Morrision, Adv. Nucl. Phys. Vol. 9 (1977) 123.

[72] B.N. Parlett, The Symmetric Eigenvalue Problem, (Prentice Hall, Englewood Cliffs NJ, 1980).

[73] B.R. Barrett, E.D. Davis, and A.F. Diallo, Phys. Lett. B295 (1992) 5.

[74] A.F. Diallo, E.D. Davis and B.R. Barrett, Ann. Phys. (N.Y.) 22 (1993) 126.

[75] S. Wolfram, Mathematica (Addison-Wesley, Redwood City, 1991).

[76] S. Kuyucak and K. Unnikrishnan, J. Phys. A, 28 (1995) 2101.

[77] S. Kuyucak and I. Morrison, Phys. Rev. C 38 (1988) 2482.

[78] S. Kuyucak and S.C. Li, Computer code IBM-1/N (ANU, 1994).

[79] S. Kuyucak and I. Morrison, Phys. Rev. C41 (1990) 1803.

[80] P.O. Lipas, P. Toivonen and D.D. Warner, Phys. Lett. B155 (1985) 295.

[81] D. Troltenier, J.P. Draayer, P.O. Hess and O. Castanos, Nucl. Phys. A 576 (1994) 351.

[82] F. Iachello, Nucl. Phys. A522 (1991) 83c.

[83] R.V.F. Janssens and T.L. Khoo, Ann. Rev. Nucl. Part. Sci. 41 (1991) 321.

[84] M.A. Lee, Nucl. Data Sheets [A158] 56 (1989) 199.

[85] M.A. Lee and R.L. Bunting, Nucl. Data Sheets [A160] 46 (1985) 187.

[86] R.G. Helmer, Nucl. Data Sheets [A162] 44 (1985) 659.

[87] E.N. Shurshikov and N.V. Timofeeva, Nucl. Data Sheets [A164] 65 (1992) 365.

[88] E.N. Shurshikov and N.V. Timofeeva, Nucl. Data Sheets [A166] 67 (1992) 45.

[89] V.S. Shirley, Nucl. Data Sheets [A168] 71 (1994) 261.

[90] C. Zhou, Nucl. Data Sheets [A170] 50 (1987) 351.

[91] G. Wang, Nucl. Data Sheets [A172] 51 (1987) 557.

[92] E. Browne, Nucl. Data Sheets [A174] 62 (1991) 1.

[93] E. Browne, Nucl. Data Sheets [A176] 60 (1990) 227.

[94] E. Browne, Nucl. Data Sheets [A178] 72 (1994) 221.

[95] M.J. Martin, Nucl. Data Sheets [A228] 49 (1986) 83.

[96] Y.A. Akovali, Nucl. Data Sheets [A230] 69 (1993) 155.

[97] M.R. Schmorak, Nucl. Data Sheets [A232, A236] 63 (1991) 139.

[98] Y.A. Akovali, Nucl. Data Sheets [A234] 71 (1994) 181.

[99] E.N. Shurshikov, Nucl. Data Sheets [A238] 53 (1988) 601.

[100] J.E. Draper *et al.*, Phys. Rev. C42 (1990) R1791, C.S. Wu *et al.*,Phys. Rev. C45 (1992) 261, J.A. Becker *et al.*, Phys. Rev. C46 (1992) 889.

[101] X. Wu *et al.*, Phys. Rev. C49 1994) 1837.

[102] M. Oshima *et al.*, Phys. Rev. C52 (1995) 3492.

[103] Y.D. Devi and V.K.B. Kota, Z. Phys. A337 (1990) 15.

[104] A. Leviatan, Z. Phys. A321 (1985) 467.

[105] I. Talmi, Simple Models of Complex Nuclei, (Contemporary Concepts in Physics, Vol 7, 1993).